Universidade Federal de Goiás
Instituto de Física

Emanuel Melo Isaac Moreira

Stability and aromaticity of small neutral and charged boron clusters: a quantum Monte Carlo study

Goiânia
2019

sistema de bibliotecas ufg

PRPG
PRÓ-REITORIA DE PÓS-GRADUAÇÃO

UFG

TERMO DE CIÊNCIA E DE AUTORIZAÇÃO PARA DISPONIBILIZAR VERSÕES ELETRÔNICAS DE TESES E DISSERTAÇÕES NA BIBLIOTECA DIGITAL DA UFG

Na qualidade de titular dos direitos de autor, autorizo a Universidade Federal de Goiás (UFG) a disponibilizar, gratuitamente, por meio da Biblioteca Digital de Teses e Dissertações (BDTD/UFG), regulamentada pela Resolução CEPEC nº 832/2007, sem ressarcimento dos direitos autorais, de acordo com a Lei nº 9610/98, o documento conforme permissões assinaladas abaixo, para fins de leitura, impressão e/ou *download*, a título de divulgação da produção científica brasileira, a partir desta data.

1. Identificação do material bibliográfico: **[ ] Dissertação** **[x] Tese**

2. Identificação da Tese ou Dissertação:

Nome completo do autor: Emanuel Melo Isaac Moreira

Título do trabalho: **Stability and aromaticity of small neutral and charged boron clusters: a quantum Monte Carlo study**

3. Informações de acesso ao documento:

Concorda com a liberação total do documento [ ] SIM [x] NÃO[1]

Havendo concordância com a disponibilização eletrônica, torna-se imprescindível o envio do(s) arquivo(s) em formato digital PDF da tese ou dissertação.

Emanuel Melo Isaac Moreira
Assinatura do(a) autor(a)[2]

Ciente e de acordo:

Assinatura do(a) orientador(a)[2]

Data: 27 / 06 / 2019

[1] Neste caso o documento será embargado por até um ano a partir da data de defesa. A extensão deste prazo suscita justificativa junto à coordenação do curso. Os dados do documento não serão disponibilizados durante o período de embargo.

Casos de embargo:
- Solicitação de registro de patente
- Submissão de artigo em revista científica
- Publicação como capítulo de livro
- Publicação da dissertação/tese em livro

[2] A assinatura deve ser escaneada.

TERMO DE CIÊNCIA E DE AUTORIZAÇÃO PARA DISPONIBILIZAR AS TESES E DISSERTAÇÕES ELETRÔNICAS NA BIBLIOTECA DIGITAL DA UFG

Na qualidade de titular dos direitos de autor, autorizo a Universidade Federal de Goiás (UFG) a disponibilizar, gratuitamente, por meio da Biblioteca Digital de Teses e Dissertações (BDTD/UFG), regulamentada pela Resolução CEPEC nº 832/2007, sem ressarcimento dos direitos autorais, de acordo com a Lei nº 9610/98, o documento conforme permissões assinaladas abaixo, para fins de leitura, impressão e/ou *download*, a título de divulgação da produção científica brasileira, a partir desta data.

1. Identificação do material bibliográfico: **[ ] Dissertação** **[x] Tese**

2. Identificação da Tese ou Dissertação

Nome completo do autor: Emanuel Melo Isaac Moreira

Título do trabalho:Stability and aromaticity of small neutral and charged boron clusters: a quantum Monte Carlo study

3. Informações de acesso ao documento:

Concorda com a liberação total do documento [x] SIM [ ] NÃO[1]

Havendo concordância com a disponibilização eletrônica, torna-se imprescindível o envio do(s) arquivo(s) em formato digital PDF da tese ou dissertação.

Emanuel Melo Isaac Moreira

Assinatura do (a) autor (a) [2]

Data: 05 /08 /2022

[1] Neste caso o documento será embargado por até um ano a partir da data de defesa. A extensão deste prazo suscita justificativa junto à coordenação do curso. Os dados do documento não serão disponibilizados durante o período de embargo.

[2] A assinatura deve ser escaneada.

Emanuel Melo Isaac Moreira

Stability and aromaticity of small neutral and charged boron clusters: a quantum Monte Carlo study

A thesis submitted to the Institute of Physics of the Federal University of Goiás as partial fulfillment of requirements for the degree of Doctorate in Physics

Research field: Theoretical and Computational Physics

Advisor: Prof. Dr. Ladir Cândido da Silva

Goiânia
2019

Ficha de identificação da obra elaborada pelo autor, através do
Programa de Geração Automática do Sistema de Bibliotecas da UFG.

Moreira, Emanuel Melo Isaac
Stability and aromaticity of small neutral and charged boron clusters: a quantum Monte Carlo study [manuscrito] / Emanuel Melo Isaac Moreira. - 2019.
131 f.: il.

Orientador: Prof. Dr. Ladir Cândido da Silva.
Tese (Doutorado) - Universidade Federal de Goiás, Instituto de Física (IF), Programa de Pós-Graduação em Física, Goiânia, 2019.
Bibliografia. Apêndice.
Inclui siglas, abreviaturas, símbolos, gráfico, tabelas, lista de figuras, lista de tabelas.

1. Electron binding energy. 2. Energy decomposition. 3. Electron correlation. 4. Aromaticity. 5. Quantum Monte Carlo. I. Silva, Ladir Cândido da, orient. II. Título.

CDU 539

UNIVERSIDADE FEDERAL DE GOIÁS

INSTITUTO DE FÍSICA

ATA DE DEFESA DE TESE

Ata Nº 49 da sessão de Defesa de Tese de Emanuel Melo Isaac Moreira que confere o título de Doutor em Física, na área de concentração em Física.

Aos 26 dias do mês de julho de 2019, a partir das 14h00min, no Anfiteatro I do Instituto de Física da UFG, realizou-se a sessão pública de Defesa de Tese intitulada “Stability and aromaticity of small neutral and charged boron clusters: a quantum Monte Carlo study”. Os trabalhos foram instalados pelo Orientador, Professor Doutor Ladir Cândido da Silva (IF/UFG) com a participação dos demais membros da Banca Examinadora: Professor Doutor Marcos Cesar de Oliveira (IFGW/UNICAMP), membro titular externo; Professor Doutor Heibbe Cristhian Benedito de Oliveira (IQ/UFG), membro titular externo; Professor Doutor Renato Pessoa Vale (IF/UFG), membro titular externo; Professor Doutor Guilherme Colherinhas de Oliveira (CEPAE/UFG), membro titular interno. Durante a arguição, os membros da banca não fizeram sugestão de alteração do título do trabalho. A Banca Examinadora reuniu-se em sessão secreta a fim de concluir o julgamento da Tese, tendo sido o candidato aprovado pelos seus membros. Proclamados os resultados pelo Professor Doutor Ladir Cândido da Silva, Presidente da Banca Examinadora, foram encerrados os trabalhos e, para constar, lavrou-se a presente ata que é assinada pelos Membros da Banca Examinadora, aos 26 dias do mês de julho de 2019.

TÍTULO SUGERIDO PELA BANCA

Documento assinado eletronicamente por **Guilherme Colherinhas De Oliveira**, **Professor do Magistério Superior**, em 26/07/2019, às 17:26, conforme horário oficial de Brasília, com fundamento no art. 6º, § 1º, do Decreto nº 8.539, de 8 de outubro de 2015.

Documento assinado eletronicamente por **Renato Pessoa Vale**, **Professor do Magistério Superior**, em 26/07/2019, às 17:27,

conforme horário oficial de Brasília, com fundamento no art. 6º, § 1º, do Decreto nº 8.539, de 8 de outubro de 2015.

Documento assinado eletronicamente por **Heibbe Cristhian Benedito De Oliveira**, **Professora do Magistério Superior**, em 26/07/2019, às 17:28, conforme horário oficial de Brasília, com fundamento no art. 6º, § 1º, do Decreto nº 8.539, de 8 de outubro de 2015.

Documento assinado eletronicamente por **Marcos Cesar de Oliveira**, **Usuário Externo**, em 26/07/2019, às 17:30, conforme horário oficial de Brasília, com fundamento no art. 6º, § 1º, do Decreto nº 8.539, de 8 de outubro de 2015.

Documento assinado eletronicamente por **Ladir Candido Da Silva**, **Professor do Magistério Superior**, em 26/07/2019, às 17:31, conforme horário oficial de Brasília, com fundamento no art. 6º, § 1º, do Decreto nº 8.539, de 8 de outubro de 2015.

A autenticidade deste documento pode ser conferida no site https://sei.ufg.br/sei/controlador_externo.php?acao=documento_conferir&id_orgao_acesso_externo=0, informando o código verificador **0783033** e o código CRC **799184C0**.

Referência: Processo nº 23070.018353/2019-56 SEI nº 0783033

I dedicate this work to my family.

Acknowledgments

I could not have completed this work without the support of many people whom I would like to thank. First of all, I thank God for His immense grace to me. I thank my family for their love, encouragement, and support. I thank my father Gil Diogo, my mother Telma Melo, my grandmother Vanda Melo, my siblings Gabriella Isaac and Diogo Elias, my girlfriend Gabriela Danelli, my brother-in-law Tiago Alves, my nephew Davi Isaac, and my niece Manuela Rosa.

I would like to thank my supervisor, Dr. Ladir Cândido da Silva, for his guidance and teachings over the last 8 years. I also thank Dr. Bráulio Gabriel for his co-guidance, and all my friends who helped me along my academic journey.

I thank CAPES financial support, the National Laboratory for Scientific Computing (LNCC/MCTI, Brazil) for providing computational resources of the SDumont supercomputers, and the Institute of Physics of the Federal University of Goiás.

"The great delusion of modernity, is that the laws of nature explain the universe for us. The laws of nature describe the universe, they describe the regularities. But they explain nothing."

– Ludwig Wittgenstein

Abstract

In this work, we investigated the electron binding energies of neutral and charged boron clusters B_n, with $n = 3$ up to $n = 13$, using a combination of the fixed-node diffusion quantum Monte Carlo (FN-DMC) method, the density functional theory, and the Hartree-Fock approximation. The electron binding energies such as the adiabatic detachment energy, vertical detachment energy, adiabatic ionization potential, and vertical ionization potential have been examined for different isomers, and the obtained values are in excellent agreement with available experimental results, which is a good indicator of the correctness of the boron clusters geometry obtained in this work. The decomposition of these electron binding energies into three physical components, namely as the electrostatic potential and exchange interaction, the relaxation energy, which includes the geometrical and orbitals relaxation, and the electronic correlation effects has allowed us to determine that the neutral boron clusters are stabilized by the electrostatic and exchange interactions, while the anionic clusters are stabilized by the electrostatic and exchange energy, the relaxation energy, and the correlation effects. We also investigated the aromaticity, of neutral and charged small boron clusters with three and four atoms, based on the electronic structure principles descriptor and the resonance energy. The FN-DMC results from the electronic structure principles of the energy, hardness, and electrophilicity have supported the aromaticity of B_3^-, B_4^-, and B_4 and partially supported the aromaticity of clusters B_3, B_3^+, and B_4^+. The obtained values for the resonance energy of clusters B_3^-, B_3, B_3^+, B_4, B_4^+, and B_4^-, are 55.1(7), 54.2(8), 33.9(7), 84(1), 67(1), and 58(1) kcal/mol, respectively. Therefore, the order of decreasing stability of the trimer is $B_3^- > B_3 > B_3^+$, while for the tetramer it is $B_4 > B_4^+ > B_4^-$, which is in agreement with the results from the molecular orbital analysis.

Key - words: Electron binding energy, energy decomposition, electron correlation, aromaticity, quantum Monte Carlo.

Resumo

Neste trabalho, investigamos as energias de ligação eletrônica dos clusters de boro neutros B_n, com $n = 3$ até $n = 13$, seus ânions e cátions, usando uma combinação dos métodos Monte Carlo quântico na aproximação dos nós fixos (FN-DMC), teoria do funcional da densidade e Hartree-Fock. As energias de ligação eletrônica como *adiabatic detachment energy*, *vertical detachment energy*, *adiabatic ionization potential* e *vertical ionization potential* foram examinadas para diferentes isômeros, e os valores obtidos estão em excelente concordância com resultados disponíveis na literatura, indicando que as geometrias dos clusters de boro, obtidas neste trabalho, estão corretas. A decomposição dessas energias de ligação eletrônica em três componentes físicas como, o potencial eletrostático e a interação de troca (*exchange*), a energia de relaxação, a qual inclui a relaxação da geometria e dos orbitais, e a correlação eletrônica, nos permitiu determinar que os clusters de boro neutros são estabilizados pelas interações eletrostática e de *exchange*, enquanto os clusters aniônicos são estabilizados pela energia eletrostática e de troca, energia de relaxação e efeitos de correlação eletrônica. Também investigamos a aromaticidade de pequenos clusters de boro com três e quatro átomos através de princípios de estrutura eletrônica e energia de ressonância. Os resultados FN-DMC aplicados aos princípios de estrutura eletrônica para a energia, dureza e eletrofilicidade suportam a aromaticidade dos clusters B_3^-, B_4^- e B_4, e parcialmente suportam a aromaticidade dos clusters B_3, B_3^+ e B_4^+. Os valores obtidos para a energia de ressonância dos clusters B_3^-, B_3, B_3^+, B_4, B_4^+ e B_4^- foram: 55.1(7), 54.2(8), 33.9(7), 84(1), 67(1), and 58(1) kcal/mol, respectivamente. Então, a ordem decrescente de estabilidade do trímero é $B_3^- > B_3 > B_3^+$, enquanto que para o tetrâmero é $B_4 > B_4^+ > B_4^-$, o que está de acordo com resultados de análise de orbitais.

Palavras - chaves: Energia de ligação eletrônica, decomposição da energia, correlação eletrônica, aromaticidade, Monte Carlo quântico.

List of Abbreviations and Acronyms

DFT – Density Functional Theory
XC – Exchange and Correlation
LDA – Local Density Approximation
GGA – Generalized Gradient Approximation
GEA – Gradient Expansion Approximation
FCI – Full Configuration Interaction
CC – Coupled Cluster
CCSD(T) – Coupled Cluster with Single, Double, and Triple excitations
HF – Hartree-Fock
CBS – Complete Basis Set
KT – Koopmans' Theorem
MC – Monte Carlo
QMC – Quantum Monte Carlo
VMC – Variational Monte Carlo
DMC – Diffusion Monte Carlo
FN-DMC – Fixed-Node Diffusion Monte Carlo
MD-DMC – Multi-Determinat Diffusion Monte Carlo
PES – Photoelectron Spectroscopy
MTOF-PES – Magnetic Time-of-Fly Photoelectron Spectroscopy
Exp. – Experimental
IP – Ionization Potential
EA – Electron Affinity
VDE – Vertical Detachment Energy
ADE – Adiabatic Detachment Energy
VIP – Vertical Ionization Potential
AIP – Adiabatic Ionization Potential
BE – Binding Energy
ABE – Atomic Binding Energy
ΔE_e – Electron binding Energy

E_a – Atomization Energy

RE – Resonance Energy

NICS – Nucleus-Independent Chemical Shifts

List of Figures

Figure 1.1: Experimental apparatus of MTOF-PES. Figure extracted from [7] 25
Figure 1.2: Schematic figure where the clusters are produced (cluster nozzle). Adapted from [57] 25
Figure 1.3: Mass gate and momentum decelerator. Adapted from [57] 26

Figure 2.1: Schematic figure of the self-consistent cycle. Adapted from [58] 42
Figure 2.2: Illustration of the VMC algorithm. Extracted from [82]. 51
Figure 2.3: Schematic figure for the branching process where (a) a walker is dead; (b) a walker keeps to the trajectory; and (c) an identical copy is made. 55
Figure 2.4: Illustration of the walker evolution in DMC algorithm. Figure extracted from [82]. 56
Figure 2.5: Fixed-node approximation for a simple one-dimensional wave function. Figure adapted from [79]. 62

Figure 3.1: Illustrative diagram of potential representing different types of electron affinities. 73
Figure 3.2: Illustrative diagram of potential representing different types of ionization potentials. 74
Figure 3.3: Size-dependence of the electron correlation per electron, in eV, for the neutral (black circles), anionic (red square), and cationic (blue up triangle) lowest-energy boron clusters. Values obtained from FN-DMC and HF-CBS calculations. 77
Figure 3.4: Size-dependence of the atomic binding energy per atom, in eV, for the neutral (black circles), anionic (red square), and cationic (blue up triangle) lowest-energy boron clusters. Values obtained from FN-DMC calculations. 79
Figure 3.5: Ground-state geometric structures of trimer boron clusters, obtained at B3LYP/6-311+G* 79
Figure 3.6: Ground-state geometries of the boron clusters with four atoms, obtained at B3LYP/6-311+G* 82
Figure 3.7: Ground-state geometries of the boron clusters with five atoms, obtained at B3LYP/6-311+G* 84

Figure 3.8: Ground-state geometries of the hexaatomic boron clusters, obtained at B3LYP/6-311+G* . . . 86
Figure 3.9: Ground-state geometries of the hepta-atomic boron clusters, obtained at B3LYP/6-311+G* . . . 89
Figure 3.10: Ground-state geometries of the octa-atomic boron clusters, obtained at B3LYP/6-311+G*. . . . 92
Figure 3.11: Ground-state geometries of the nona-atomic boron clusters, obtained at B3LYP/6-311+G*. . . . 95
Figure 3.12: Ground-state geometries of the 10-atomic boron clusters, obtained at B3LYP/6-311+G*. . . . 97
Figure 3.13: Ground-state geometries of the 11-atomic boron clusters, obtained at B3LYP/6-311+G*. . . . 100
Figure 3.14: Ground-state geometries of the 12-atomic boron clusters, obtained at B3LYP/6-311+G*. . . . 102
Figure 3.15: Ground-state geometries of the 13-atomic boron clusters, obtained at B3LYP/6-311+G*. . . . 104
Figure 3.16: Size-dependence of the Adiabatic Detachment Energy (ADE in eV). Values obtained from FN-DMC calculations (black circles), and experimental results (red square) for comparison from Refs. [14, 15, 19, 27–30, 37]. . . . 107
Figure 3.17: Size-dependence of the Vertical Detachment Energy (VDE in eV). Values obtained from FN-DMC calculations (black circles), and experimental results (red square) for comparison from Refs. [14, 15, 19, 27–30, 37]. . . . 107
Figure 3.18: Size-dependence of the Adiabatic Ionization Potential (AIP in eV). Values obtained from FN-DMC calculations (black circles), and theoretical results (red square for CCSD(T) and up triangle for G3B3) for comparison from Ref. [95]. . . . 108
Figure 3.19: Size-dependence of the Vertical Ionization Potential (VIP in eV). Values obtained from FN-DMC calculations (black circles). . . . 108
Figure 3.20: Cyclic (left) and linear (right) lowest energy structures of the neutral with three and four atoms boron clusters. The indicated bond lengths are in ångstrom (Å). 110
Figure 3.21: Cyclic (left) and linear (right) lowest energy structures of the anionic with three and four atoms boron clusters. The indicated bond lengths are in ångstrom (Å). 110
Figure 3.22: Cyclic (left) and linear (right) lowest energy structures of the cationic with three and four atoms boron clusters. The indicated bond lengths are in ångstrom (Å). . . . 110

List of Tables

Table 3.1: Energy, in a.u., for the atom and dimer of boron. M represents the spin multiplicity. The number in parentheses indicates the statistical uncertainty in the last shown digit. 70

Table 3.2: Total FN-DMC energy, in a.u., for the atom and dimers and the atomization energy E_a, in eV, for the dimers. M represents the spin multiplicity of the system and R_0 is the bond length in Å. The number in parentheses indicates the statistical uncertainty in the last shown digit. 70

Table 3.3: FN-DMC results for the atomic binding energy per atom, in eV, for the lowest-energy boron clusters, and G3B3 results [34, 95] for comparison. Statistical error in the last decimal place is indicated in the parentheses. 78

Table 3.4: Total energy, in a.u., at HF-CBS, DFT (B3LYP/6-311+G*) and FN-DMC, and spin multiplicity M for the ground-state trimer boron clusters. Statistical error in the last decimal place is indicated in the parentheses. 80

Table 3.5: The ADE, VDE, AIP, and VIP values for the anionic and neutral trimer boron clusters and comparison with the experimental results; the energies are in eV. . 80

Table 3.6: Decomposition of the ADE, VDE, AIP, and VIP of the trimer boron clusters. Statistical error in the last decimal place is indicated in the parentheses. All energies are in eV. 81

Table 3.7: Total energy, in a.u., at HF-CBS, DFT (B3LYP/6-311+G*) and FN-DMC, and spin multiplicity M for the ground-state four-atomic boron clusters. Statistical error in the last decimal place is indicated in the parentheses. 82

Table 3.8: The ADE, VDE, AIP, and VIP values for the anionic and neutral tetramer boron clusters and comparison with the experimental results; the energies are in eV. 82

Table 3.9: Decomposition of the ADE, VDE, AIP, and VIP of the tetramer boron clusters. Statistical error in the last decimal place is indicated in the parentheses. All energies are in eV. 83

Table 3.10: Total energy, in a.u., at HF-CBS, DFT (B3LYP/6-311+G*) and FN-DMC, and spin multiplicity M for the ground-state of the penta-atomic boron clusters. Statistical error in the last decimal place is indicated in the parentheses. . . . 84

Table 3.11: The ADE, VDE, AIP, and VIP values for the anionic and neutral penta-atomic boron clusters and comparison with the experimental results; the energies are in eV. . . . 84
Table 3.12: Decomposition of the ADE, VDE, AIP, and VIP of the penta-atomic boron clusters. Statistical error in the last decimal place is indicated in the parentheses. All energies are in eV. . . . 85
Table 3.13: Total energy, in a.u., at HF-CBS, DFT (B3LYP/6-311+G*) and FN-DMC, and spin multiplicity M for the ground-state of the hexaatomic boron clusters. Statistical error in the last decimal place is indicated in the parentheses. . . . 87
Table 3.14: The ADE, VDE, AIP, and VIP values for the anionic and neutral hexaatomic boron clusters and comparison with the experimental results; the energies are in eV. . . . 87
Table 3.15: Decomposition of the ADE, VDE, AIP, and VIP of the hexa-atomic boron clusters. Statistical error in the last decimal place is indicated in the parentheses. All energies are in eV. . . . 88
Table 3.16: Total energy, in a.u., at HF-CBS, DFT (B3LYP/6-311+G*) and FN-DMC, and spin multiplicity M for the ground-state of the hepta-atomic boron clusters. Statistical error in the last decimal place is indicated in the parentheses. . . . 90
Table 3.17: The ADE, VDE, AIP, and VIP values for the anionic and neutral hepta-atomic boron clusters and comparison with the experimental results; the energies are in eV. . . . 90
Table 3.18: Decomposition of the ADE, VDE, AIP, and VIP of the hepta-atomic boron clusters. Statistical error in the last decimal place is indicated in the parentheses. All energies are in eV. . . . 91
Table 3.19: Total energy, in a.u., at HF-CBS, DFT (B3LYP/6-311+G*) and FN-DMC, and spin multiplicity M for the ground-state of the octa-atomic boron clusters. Statistical error in the last decimal place is indicated in the parentheses. . . . 93
Table 3.20: The ADE, VDE, AIP, and VIP values for the anionic and neutral octa-atomic boron clusters and comparison with the experimental results; the energies are in eV. . . . 93
Table 3.21: Decomposition of the ADE, VDE, AIP, and VIP of the octa-atomic boron clusters. Statistical error in the last decimal place is indicated in the parentheses. All energies are in eV. . . . 94
Table 3.22: Total energy, in a.u., at HF-CBS, DFT (B3LYP/6-311+G*) and FN-DMC, and spin multiplicity M for the ground-state of the nona-atomic boron clusters. Statistical error in the last decimal place is indicated in the parentheses. . . . 96
Table 3.23: The ADE, VDE, AIP, and VIP values for the anionic and neutral nona-atomic boron clusters and comparison with the experimental results; the energies are in eV. . . . 96

Table 3.24: Decomposition of the ADE, VDE, AIP, and VIP of the nona-atomic boron clusters. Statistical error in the last decimal place is indicated in the parentheses. All energies are in eV. 96
Table 3.25: Total energy, in a.u., at HF-CBS, DFT (B3LYP/6-311+G*) and FN-DMC, and spin multiplicity M for the ground-state of the 10-atomic boron clusters. Statistical error in the last decimal place is indicated in the parentheses. . . . 98
Table 3.26: The ADE, VDE, AIP, and VIP values for the anionic and neutral 10-atomic boron clusters and comparison with the experimental results; the energies are in eV. 98
Table 3.27: Decomposition of the ADE, VDE, AIP, and VIP of the 10-atomic boron clusters. Statistical error in the last decimal place is indicated in the parentheses. All energies are in eV. 99
Table 3.28: Total energy, in a.u., at HF-CBS, DFT (B3LYP/6-311+G*) and FN-DMC, and spin multiplicity M for the ground-state of the 11-atomic boron clusters. Statistical error in the last decimal place is indicated in the parentheses. . . . 100
Table 3.29: The ADE, VDE, AIP, and VIP values for the anionic and neutral 11-atomic boron clusters and comparison with the experimental results; the energies are in eV. 100
Table 3.30: Decomposition of the ADE, VDE, AIP, and VIP of the 11-atomic boron clusters. Statistical error in the last decimal place is indicated in the parentheses. All energies are in eV. 101
Table 3.31: Total energy, in a.u., at HF-CBS, DFT (B3LYP/6-311+G*) and FN-DMC, and spin multiplicity M for the ground-state of the 12-atomic boron clusters. Statistical error in the last decimal place is indicated in the parentheses. . . . 102
Table 3.32: The ADE, VDE, AIP, and VIP values for the anionic and neutral 12-atomic boron clusters and comparison with the experimental results; the energies are in eV. 102
Table 3.33: Decomposition of the ADE, VDE, AIP, and VIP of the 12-atomic boron clusters. Statistical error in the last decimal place is indicated in the parentheses. All energies are in eV. 103
Table 3.34: Total energy, in a.u., at HF-CBS, DFT (B3LYP/6-311+G*) and FN-DMC, and spin multiplicity M for the ground-state 13-atomic boron clusters. Statistical error in the last decimal place is indicated in the parentheses. 105
Table 3.35: The ADE, VDE, AIP, and VIP values for the anionic and neutral 13-atomic boron clusters and comparison with the experimental results; the energies are in eV. 105
Table 3.36: Decomposition of the ADE, VDE, AIP, and VIP of the 13-atomic boron clusters. Statistical error in the last decimal place is indicated in the parentheses. All energies are in eV. 106

Table 3.37: The ground-state energies (in a.u.) from HF-CBS, DFT and FN-DMC calculations for the boron clusters with three an four atoms ($n = 3$ and 4). The digits in parentheses are estimated standard errors in the last decimal places. 111

Table 3.38: The total energy (E), hardness (η), electrophilicity (ω), and $A_{\rm aro}(A \equiv E, \eta, \omega)$ of the cyclic and linear isomers B_3^-, B_4^-, B_3, B_4, B_3^+, and B_4^+ clusters. The energy is in a.u., whereas the hardness and electrophilicity are given in eV. . . 113

Table 3.39: Total energy in a.u. and E_a in eV for the boron atom, dimer, trimer, and tetramer. The total energies of the trimers and tetramers (presented in Table3.2) are shown again here to facilitate the readability of this table. The number in parentheses indicates the statistical uncertainty in the last shown digit. 114

Table 3.40: The resonance energies (REs) fo the trimer and tetramer neutral, anionic, and cationic boron clusters. All energies are in kcal/mol. 115

Contents

Chapter 1: Introduction **18**

1.1 Clusters: An Overview 18

1.2 Boron Clusters 20

1.3 Aromaticity in Boron Clusters 22

1.4 Some Experimental Aspects in Cluster Science 24

1.4.1 Photoelectron Spectroscopy and Electron Binding Energy. 26

Chapter 2: Theoretical Methods **28**

2.1 The Hartree-Fock method 33

2.1.1 Koopmans' Theorem 36

2.2 Density Functional Theory 36

2.2.1 The Exchange-Correlation Functional Approximation 41

2.3 Quantum Monte Carlo Methods 43

2.3.1 Monte Carlo Integration 43

2.3.2 Random walks and Markov Chains 45

2.3.3 The Metropolis method 47

2.3.4 The Generalized Metropolis Method 48

2.3.5 Variational Quantum Monte Carlo 49

2.3.5.1 The u, χ and f terms in the Jastrow factor 52

2.3.6 Diffusion Quantum Monte Carlo 53

2.3.6.1 Integral Form of Schrödinger Equation: Green's function formalism 56

2.3.7 Simple Diffusion Monte Carlo 58

2.3.8 Estimating the Ground-state Energy 63

2.3.9 The DMC Algorithm 64

Chapter 3: Results and Discussion **67**

3.1 Computational Details 67

3.2 The atom and the dimer of boron: neutrals, anions and cations 69

3.3 Study of the electronic properties of neutral boron clusters B_n ($n = 3$–13), its anions and cations 71

3.3.1 Electron Affinity and Ionization Potential 71

3.3.2 Decomposition of the electron binding energies . . . 74
3.3.3 Overall considerations . . . 76
3.3.4 B_3, B_3^- and B_3^+ . . . 79
3.3.5 B_4, B_4^- and B_4^+ . . . 81
3.3.6 B_5, B_5^- and B_5^+ . . . 83
3.3.7 B_6, B_6^- and B_6^+ . . . 85
3.3.8 B_7, B_7^- and B_7^+ . . . 89
3.3.9 B_8, B_8^- and B_8^+ . . . 92
3.3.10 B_9, B_9^- and B_9^+ . . . 95
3.3.11 B_{10}, B_{10}^- and B_{10}^+ . . . 97
3.3.12 B_{11}, B_{11}^- and B_{11}^+ . . . 99
3.3.13 B_{12}, B_{12}^- and B_{12}^+ . . . 101
3.3.14 B_{13}, B_{13}^- and B_{13}^+ . . . 103
3.4 Aromaticity of B_3 and B_4, its anions and cations . . . 109
3.4.1 Aromaticity from the electronic structure principles . . . 110
3.4.2 Aromaticity based on the resonance energy . . . 113

Chapter 4: Conclusions and Future Perspectives . . . 117

APPENDICES 119

Appendix A: The Quantum Variational Principle . . . 120

Appendix B: The Koopmans' Theorem . . . 122

Appendix C: Cartesian Coordinates of Clusters B_n ($n = 3 - 13$) . . . 124

CHAPTER 1

Introduction

Clusters: An Overview

In Physics and Chemistry, clusters are an aggregate of particles (atoms or molecules) of a countable number ($2-10^n$, where n can be as high as 6 or 7) [1]. This state of matter can be considered as a bridge between individuals atoms and bulk materials. In this sense, clusters are sometimes called the building blocks of the material world. One reason that this state of matter is of great interest in the scientific community is that it can possess electronic, magnetic and optical features that are very distinct from its respective bulk phase. As noted in reference [2], "Clusters of nonmagnetic elements become magnetic, semiconducting materials exhibit metallic properties, metallic systems become semiconducting, the color of particles change with size, noble metals become reactive, and brittle materials become malleable"[1].

Clusters have some remarkable features that make them differ from bulk materials. One of the most interesting features is the variation of its properties with the number and type of particles, N, that constitute them. While the properties of bulks remain unchanged if some atoms or molecules are added or removed from its structure, the properties of clusters can vary widely and, in some cases, non-monotonic. For example, structural and electronic properties of clusters, such as the coordination number[2], the average binding energy per atom, the HOMO-LUMO[3] gap, can vary significantly with the number of atoms in the system. Another important difference between clusters and bulks is the most stable geometric structure that configures the ground-state of each of these

1. Some examples of these features in clusters can be found in Refs. [3–6].
2. The coordination number of an atom is the number of atoms bonded to this reference atom.
3. HOMO is an acronym for Highest Occupied Molecular orbital and LUMO is an acronym for Lowest Unoccupied Molecular orbital.

state of matter. Most of the bulk materials have a periodic crystalline structure while clusters, in majority, do not have a periodic structure. Many of them have polyhedral shapes that can not grow periodically. An issue which is not well understood and is still under debate in cluster and materials science is the mechanism behind the structure's growth from a polyhedral cluster to periodic bulk. Thus, the study of clusters are of fundamental interest due to their own intrinsic properties and because of the central position that they occupy between molecular and condensed matter science [1].

As pointed out by Johnston [1], the progress in cluster science follows closely on the development of new experimental apparatus and techniques. However, the experimental study of clusters still presents some problems associated with fundamental questions such as the generation of intense size-selected cluster beams, the determination of the geometry of the clusters, the determination of physical and chemical properties related to the electronic structure of the clusters, and so forth. Despite these problems, nowadays there are a variety of techniques that have been applied to the investigation of clusters, mainly regarding their electronic structure, which is one of the most important questions in clusters research [7]. One powerful technique, which has been used to provide very accurate results for the electronic structure of clusters, is Photoelectron Spectroscopy. Nowadays, this technique is applied in combination with theoretical and computational methods to the investigation of clusters. Further, in the text, we present a section where we discuss some experimental aspects in cluster science.

In this context, theoretical and computational methods are of extreme importance in helping to determinate the most stable structure of the cluster and to interpret the experimental data. One of the most commonly used theoretical methods to study the physical-chemical properties of clusters is Density Functional Theory (DFT). Nevertheless, it is well known that DFT, due to the approximation in the exchange-correlation (XC) energy[4], usually cannot predict results with chemical accuracy, failing for some cases (but being successful for others), in the description of physical quantities of clusters [8]. Other methods, such as Full Configuration Interaction (FCI) and Coupled-Cluster (CC), which accurately includes electron correlation effects, can provide very accurate results for clusters but, these methods are very limited by the system size, requiring a considerable computational effort. For FCI, the computational effort scales as factorial $N!$ and for CC as N^5 to N^7, N is the number of electrons. The quantum Monte Carlo method (QMC), the primary method employed in this work, solves the many-body Schrödinger equation stochastically, with a better computational cost-benefit, which scales as N^2 to N^3 depending on the quantities of interest [9], to obtain results that include electron

4. This approximation is discussed in more details in section 2.2.1.

correlation effects for clusters. The Quantum Monte Carlo (QMC) methods have a weak dependence on the basis set, in comparison to the methods cited above, but requires high accuracy for the numerical orbitals that define the nodal structure. The electronic energy obtained within QMC methods can recover about 90% of the correlation energy within the fixed-node approximation[5] in a single determinant picture. Calculations using QMC methods, including multideterminant wave functions, have shown that it is possible to recover 100% of the electron correlation for some particular systems[6] [10, 11]. Therefore, QMC provides an efficient tool to obtain very accurate results for the electronic energy and can be used as a benchmark for other approaches and experimental data.

Boron Clusters

The boron atom has a small covalent radius[7] and its electronic distribution is $1s^2 2s^2 2p^1$, which characterizes the boron as an electron-deficient material due to the number of valence electrons ($2s^2 2p^1$) is lower than the number of stable orbitals in valence shell (s, p_x, p_y, p_z). The boron element, as well as carbon, has a property know as catenation, i.e., boron can build molecules of unlimited size by covalently bonding to itself [12]. In most of its compounds, boron undergoes sp^2 hybridization, leaving an empty atomic orbital ($2p_z$), which still configures boron as electron-deficient. This electron-deficiency characterizes the covalent chemical bonds in boron compound [13, 14], and understanding this type of interaction is very important to elucidate chemical bonding theory in clusters, as pointed out by Zhai *et al.* [15]. Those authors state: "boron clusters represent the lightest covalently bound species and understanding the electronic and atomic structures in these systems is important for the development of a unified chemical bonding theory for all covalently bound molecules".

There are a wide variety of potential technological applications for boron-based-materials due to their large capacity for structural arrangements in any dimensionality, as is the case of applications in medicine, pharmacology, non-linear optics, and polymer science [12]. Therefore, there exist several types of synthesized systems of zero-, one-, and two-dimensional boron nanomaterials such as nanocluster, nanotubes, atomic chains and monolayer crystalline sheets called borophene [16–18]. These recently found boron

5. This approximation, which is required for the treatment of fermionic systems in quantum Monte Carlo calculations, is discussed in section 2.3.7.
6. Of course, this type of calculations demands a larger computational effort. In this work, we use only single determinant calculations.
7. The covalent radius is the half the distance between the nuclei of two atoms of the same element. If compared with all elements in the periodic table, boron is the eighth element with the smallest covalent radius. The covalent radius of boron is 85 pm.

nanomaterials encourage further investigation of the small size boron clusters to determine their fundamental physical and chemical properties, since such clusters may serve as building blocks [19] to create and design new classes of clusters assembled materials with new functionalities and features.

Experimentally, Anderson and coworkers were the pioneers, in 1988, of the study of small boron clusters [20–22]. They generated cationic boron clusters by laser vaporization to analyze their mass distribution, and they concluded that the boron clusters, up to 13 atoms, would prefer to form three-dimensional structures. The first computational studies started in 1994 with a series of articles by Boustani [23–26], where he predicted, as opposed to Anderson and coworkers, that planar or quasi-planar small boron clusters are more stable than the three-dimensional ones. Around the year 2002, Wang and coworkers, in a series of studies using Photoelectron Spectroscopy (PES) and computational quantum chemistry calculations [14,15,19,27–30], confirmed the prediction of Boustani (that the most stable structures of small boron clusters are planar or quasi-planar). They compared experimental PES results, for the electron binding energy of anionic boron clusters B_n^-, with theoretical results obtained computationally for the lowest energy isomers. These experimental results, combined with quantum chemistry calculations for small boron clusters, have caught the attention of the scientific community, bringing a significant advance in this field in recent decades. A wide variety of properties of boron clusters have been discussed, and among them we highlight: thermochemistry and electronic structure, chemical bond analysis, structural determination, structural evolution and Aufbau principle[8] for boron clusters, ionization potential, and cationic structures, planarity and quasi-planarity in terms of aromaticity, resonance energy, and other features of these systems [13,31–36]. Very recently, Wang's group [37–41] combined photoelectron spectroscopy and quantum chemistry methods to characterize the structural and electronic properties of several sizes of boron clusters, showing that the research on boron clusters is still active and very fertile.

Although, as mentioned above, there are a variety of experimental and theoretical studies that explore various aspects of boron clusters, some physical and chemical properties of such systems are not fully understood at the electronic level. Furthermore, as far as we know, there is no discussion in the literature about the roles played by the electrostatic and exchange interactions, the electronic effects, and the orbital relaxation energy in the electron binding energies of small boron clusters, at a sophisticated level, such as quantum Monte Carlo. These electron binding energies are known as *Vertical*

8. The Aufbau principle, for this case of boron clusters, describe how boron atoms are progressively added into a key boron cluster element to form boron sheets and boron nanotubes.

Detachment Energy (VDE), *Adiabatic Detachment Energy* (ADE), *Vertical Ionization Potential* (VIP), and *Adiabatic Ionization Potential* (AIP), and they are fundamental quantities that are experimentally accessible[9] for boron clusters. These fundamental quantities carry information about the size-dependent stability of the system and may also provide thermochemical values that are important for the understanding of the nature of the cluster formation.

In general, the structural and electronic properties of clusters are experimentally difficult to determine. Therefore, theoretical and computational modeling becomes important. In this work, we combine *ab initio* calculations with quantum Monte Carlo methods to study the stability in boron clusters, B_n with $n = 3$–13, its anions and cations, and investigate the role played by the electron correlation energy, the electrostatic and exchange interactions and the orbitals relaxation energy, in the electronic structure of such systems. Very recently, quantum Monte Carlo studies on the energetics of small metallic clusters have shown the importance of the electron correlation energy in the determination of the binding energy, the dissociation energy, and the stability of several metallic clusters [42–45]. It is reasonable to expect that the effects of electron correlation would play an important role in the stability and the properties of small boron clusters. To analyze the electronic structure we decomposed the electron binding energies into three physical components by using a procedure developed by Kaplan and coworkers [46–48]. This procedure is very useful to provide information about the nature of the electron binding energy in different clusters. By using this procedure, we were able to give a better understanding of the electron binding in boron clusters.

Aromaticity in Boron Clusters

The aromaticity is a concept that was initially introduced, in 1865 by August Kekulé [49], to explain the peculiar stability and low reactivity of benzene and its derivatives in organic chemistry. Although the term “aromaticity” is employed quite frequently in scientific literature, this concept does not have a precise definition. The lack of a precise definition of aromaticity is because such quantity has no well-founded physical basis and it is not a directly observable property. In other words, the aromaticity is a virtual quantity, rather than a physical observable [50]. Although aromaticity is an imprecise concept, as mentioned above, it is a consensus in the literature that aromatic structures manifest some typical features such as the electron delocalization in the structure, high structural symmetry, the tendency in the equalization of the

9. For the case of VDE and ADE of anions.

bond length, low reactivity and magnetic features [50–52]. In an attempt to provide a better understanding of the concept of aromaticity, we present, as follows, two qualitative definitions of aromaticity that may cover various aspects of this concept. One definition is, "An aromatic molecule is one in which electrons are free to cycle around circular arrangements of atoms connected via identical bonds which are resonance hybrids of single and double bonds. It displays enhanced chemical stability compared to similar nonaromatic molecules and possesses a significant magnetic field, a planar structure, and $(4n + 2, n \geq 0)$ π-electrons in a single ring. On the other hand, an antiaromatic molecule contains $4n$ $(n \neq 0)$ π-electrons in a cyclic planar, or nearly planar, system of alternating single and double bonds" [53], and the other is, "Aromaticity is a manifestation of electron delocalization in closed circuits, either in two or in three dimensions. This results in energy lowering, often quite substantial, and a variety of unusual chemical and physical properties. These include a tendency toward bond length equalization, unusual reactivity, and characteristic spectroscopy features. Since aromaticity is related to induce ring currents, magnetic properties are particularly important for its detection and evaluation" [50].

Initially, the concept of aromaticity was restricted to organic molecules; however, with an advance in experimental techniques to create novel molecules and clusters, the idea of aromaticity has been applied far beyond organic chemistry [51]. Boldyrev and Wang [54] were the first to report experimental and theoretical evidences of aromaticity an all-metal systems. They created and studied the aromaticity of a series of bimetallic clusters, with chemical composition MAl_2^- (M= Li, Na or Cu), with photoelectron spectroscopy and *ab initio* calculations. This extension of the concept of aromaticity for inorganic systems attracted attention in the scientific community, and among the major candidates to be explored were boron clusters, in particular, because these systems present planarity, which is a typical feature in aromatic systems.

A series of experimental and theoretical studies that explore the aromaticity/antiaromaticity of small boron clusters, via different computational methods and different perspectives, have been reported in the literature. Tai *et al.* [34], using Coupled-Cluster and G3B3 calculations, analyzed the aromaticity of boron clusters based on the resonance energy, Zhai *et al.* [14], with PES experimental data and *ab initio* calculations explored the aromaticity and the planarity of boron clusters using molecular orbital analysis and Hückel's rule, while Zubarev and Boldyrev [31], using *ab initio* calculations, studied the aromaticity in boron clusters by chemical bond analysis and Nuclear Independent Chemical Shift (NICS). In addition to these works mentioned above, a considerable number of theoretical and experimental studies focusing the aromaticity/antiaromaticity of boron clusters have been reported in the literature [15, 19, 27–30, 32, 55, 56]. Although, as we mentioned, there are experimental and theoretical studies confirming the aromatic characteristic of boron-based clusters, these features are not fully understood at the electronic

level. In this work, we explore the aromaticity of some small boron clusters (B_3, B_3^-, B_3^+, B_4, B_4^- e B_4^+) at the electronic level by using quantum Monte Carlo methods and *ab initio* calculations. We quantify the aromaticity of these boron clusters using two criteria based on the electronic structure principles descriptor and resonance energy.

Next, we present a brief section where we discuss the physical principles and the techniques involved in experiments with clusters. We understand that a comprehension of the experimental aspects involved in study of clusters can provide us a more accurate and correct interpretation of the results obtained via computational methods.

Some Experimental Aspects in Cluster Science

Progress in cluster science has reached the point that experimental methods have been developed that allow the production, selection, and detection of clusters. In this section, we succinctly discuss a type of experimental apparatus used to perform experiments with boron clusters [19], as well as the physical principles involved in this experiment. This apparatus is known as Magnetic-Bottle Time-of-Fly Photoelectron Spectroscopy (MTOF-PES), equipped with a laser vaporization cluster source [7,57]. It is a powerful technique that provides information about the electronic structure of clusters.

Figure 1.1 shows a schematic representation of the experimental apparatus. This apparatus is composed of a pulsed laser vaporization cluster source, a Time-of-Flight (TOF) mass spectrometer, a mass gate (where the clusters of interest are selected), a momentum decelerator and a magnetic bottle time-of-fly (MTOF) photoelectron analyzer.

To generate a cluster ensemble, a directed pulsating laser (1) hits a target disk (2), which is composed of an element of interest[10]. By ablation[11], plasma from the element that composes the disk is formed inside a small nozzle orifice, see Figure 1.2. Two valves are used to insert helium gas, which mixes with and cools the laser-induced plasma, producing clusters. In this process, both neutral and charged clusters are produced. The cluster/Helium mixture undergoes a supersonic expansion with the objective of cooling it, even more, causing the small clusters to lose much of the vibrational and rotational energy. This expansion promotes the condensation of the clusters in such a way that it is possible to separate them from the mixture and form a collimated beam into the ion extraction chamber (3). In the ion extraction chamber, the negative clusters are extracted by a high voltage pulse and then subjected to a TOF mass spectrometer, for mass analysis. Basically, in a time-of-flight (TOF) mass spectrometer the ions are accelerated by an electric field

10.In the case of the production of boron clusters, a disk target made of enriched ^{10}B isotope in the presence of a helium gas carrier is used [19].
11.Ablation, in this case, is the removal of particles from the surface of an object by vaporization.

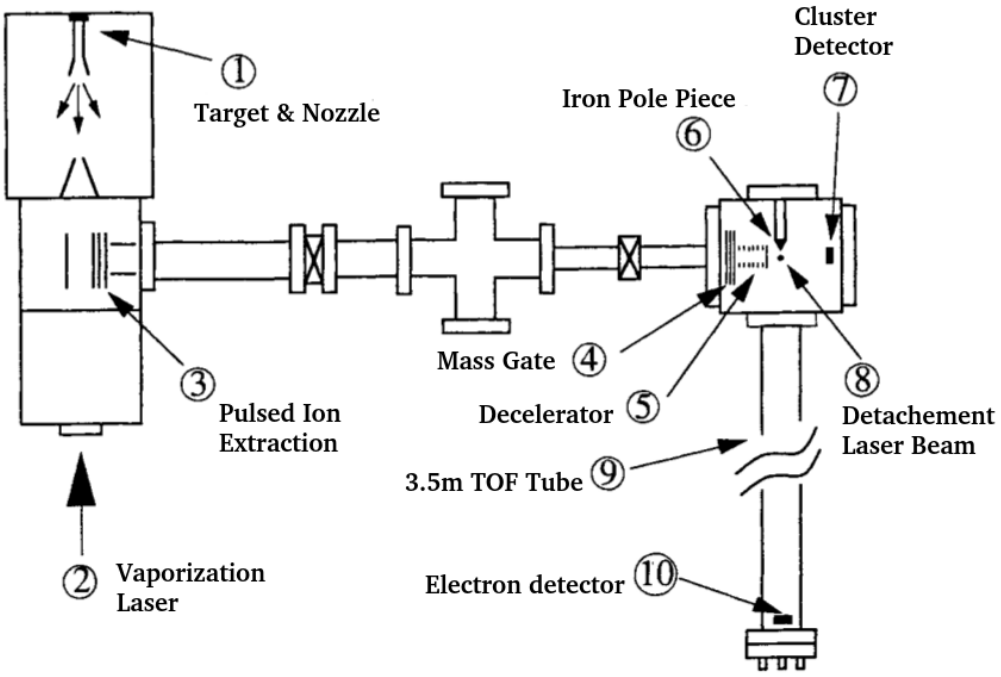

Figure 1.1: Experimental apparatus of MTOF-PES. Figure extracted from [7]

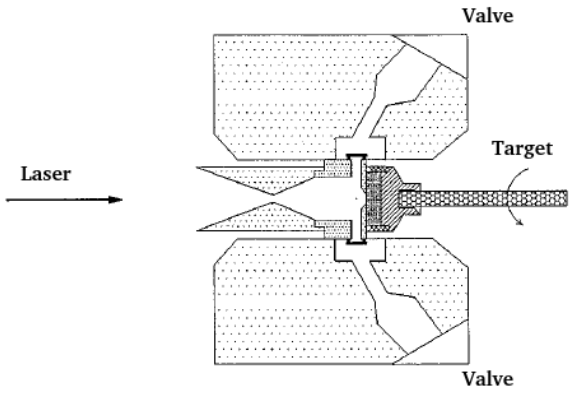

Figure 1.2: Schematic figure where the clusters are produced (cluster nozzle). Adapted from [57]

and is measured the time the ions spent to reach a detector at a known distance (the time of flight). Once the electric field magnitude, the distance traveled by the ion, and the time of flight are know, the ion's mass-to-charge ratio can be determined, and thus, the mass distribution of the clusters that compose the beam can be analyzed. After the clusters have been subjected to the TOF mass spectrometer, they pass through a mass gate[12] (4), and then they are decelerated by a momentum decelerator (5). Figure 1.3 shows the mass gate and the momentum decelerator.

The mass gate is composed of three grids. The first and the third grid are

12.The mass gate selects the clusters of interest that are allowed to enter the interaction zone.

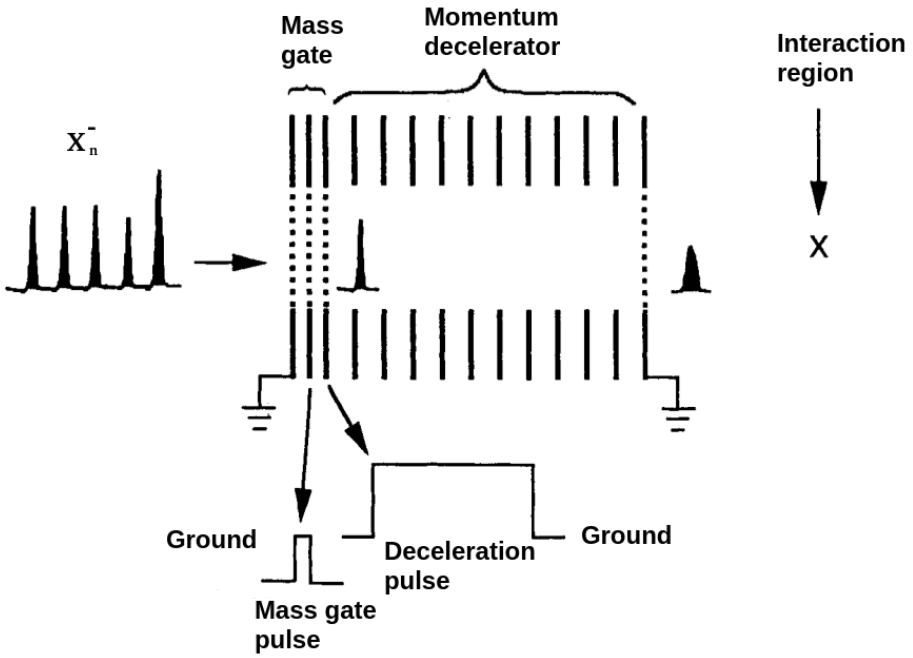

Figure 1.3: Mass gate and momentum decelerator. Adapted from [57]

grounded, and the second grid is at a high voltage so that no negative clusters can pass through the mass gate and enter the interaction zone. Once the cluster of interest arrives at the first grid, the second grid is adjusted to grounded for a short period, allowing the desired clusters to pass unaffected. After being selected, the clusters are decelerated by a pulse of positive high voltage. When decelerated, the ionic clusters acquire a low distribution of kinetic energy so the that effect of broadening of spectral lines, due to the Doppler effect, does not interfere in the resolution of the photoelectronic spectroscopy. Finally, the clusters enter an ultra-vacuum region where, by laser (8), electrons are removed from its electronic structure. By a magnetic field, the electrons are guided to an MTOF tube (9), and at the end of this tube are located an electron detector is located (10). The formed clusters, after the removal of electrons, are detected in a cluster detector (7). The electron TOF spectra are converted to kinetic energy distribution. Thus, with this kinetic distribution and the photon energies of the laser, it is possible to determine the electron binding energy of the cluster.

Photoelectron Spectroscopy and Electron Binding Energy.

The physical phenomenon that photoelectron spectroscopy techniques are based on is similar to the photoelectric effect. A target ion R^- is hit by a light beam, which has a frequency ν and energy $E = h\nu$. The valence electron of the ion absorbs the energy from the light beam, and it can be ejected from the atom if this energy is greater than the

minimal energy[13] necessary to break the electron bond with the ion. This energy is known as the electron binding energy. Typically, in PES experiments, a laser with frequency ν_0 ($\nu_0 > \nu_L$) hits an ion sample, and an electron detector monitors the electrons that are ejected. This ejected electron has a kinetic energy distribution KE that can be determined by the data from the electron detector.

The following reaction can represent the process of the emission of an electron from one ion,

$$R^- + h\nu_0 \rightarrow R + e^-(KE), \tag{1.1}$$

where R represents a neutral structure formed after the removal of one electron from the anion R^-, and $e^-(KE)$ is the kinetic energy of the ejected valence electron. By the conservation of energy, the energy from the laser must be equal to the electron binding energy (BE) added to the kinetic energy distribution of the valence electrons,

$$BE = h\nu_0 - KE. \tag{1.2}$$

Thus, this electron binding energy can be interpreted as the electron affinity of a neutral structure,

$$EA(R) = h\nu_0 - KE. \tag{1.3}$$

Although the physical theory of such PES experiments may seem quite simple, their execution is very complicated and complex. However, in the last few years, a significant advance in experimental techniques has enabled the execution of experiments that provide results that elucidate the understanding of this interesting and peculiar phase of matter. That shows a promising future in the area, calling the attention of scientists from various fields of science and engineering.

In the next section, we discuss the theoretical methods that our work is based on. We discuss the Hartree-Fock method, the Density Functional Theory, and the quantum Monte Carlo methods used in this work.

13.The minimal energy required to remove the electron from the valence shell of the cluster is related to a limit frequency ν_L.

CHAPTER 2

Theoretical Methods

In this section, we discuss the electronic problem, the Born-Oppenheimer approximation, and the variational principle [58,60,61]. We also define some useful concepts and discuss the theoretical methods that are the basis of our work, which are the Hartree-Fock method, Density Functional Theory, and quantum Monte Carlo methods, emphasizing the main concepts of each theory.

Our primary interest is to find an approximate solution of the non-relativistic time-independent Schrödinger equation for a system constituted of N electrons and M nuclei [58, 60, 61],

$$\hat{H}|\psi\rangle = E|\psi\rangle, \tag{2.1}$$

which can be written in a position-space representation as

$$\hat{H}\psi(\mathbf{r}, \mathbf{d}) = E\psi(\mathbf{r}, \mathbf{d}), \tag{2.2}$$

where $\hat{H}$ is the total non-relativistic Hamiltonian operator for a system composed for nuclei and electrons described by a set of nuclear coordinates $\mathbf{d}$ and a set of electronic coordinates $\mathbf{r}$, respectively. In atomic units, the Hamiltonian for N electrons and M nuclei is given by

$$\hat{H} = -\sum_{i=1}^{N} \frac{1}{2}\nabla_i^2 - \sum_{A=1}^{M} \frac{1}{2M_A}\nabla_A^2 - \sum_{i=1}^{N}\sum_{A=1}^{M} \frac{Z_A}{r_{iA}} + \sum_{i=1}^{N}\sum_{j>i}^{N} \frac{1}{r_{ij}} + \sum_{A=1}^{M}\sum_{B>A}^{M} \frac{Z_A Z_B}{d_{AB}}, \tag{2.3}$$

where, $r_{iA} = |\mathbf{r}_{iA}| = |\mathbf{r}_i - \mathbf{d}_A|, r_{ij} = |\mathbf{r}_i - \mathbf{r}_j|, d_{AB} = |\mathbf{d}_A - \mathbf{d}_B|$, M_A is the ratio of the mass of nucleus A to the mass of an electron, and Z_A is the charge of a nucleus A.

The first term in equation 2.3 is the kinetic energy operator of the electrons; the second one is the kinetic energy operator of the nuclei; the third is the operator that represents Coulomb interaction between the electrons and nuclei; and the fourth and fifth terms are the electron-electron repulsion and nuclei-nuclei repulsion operator, respectively.

The equation 2.3 can be written in a compact way as

$$\hat{H} = \hat{T}_e(\mathbf{r}) + \hat{T}_N(\mathbf{d}) + \hat{V}_{Ne}(\mathbf{d},\mathbf{r}) + \hat{V}_{NN}(\mathbf{d}) + \hat{V}_{ee}(\mathbf{r}). \tag{2.4}$$

The term $\hat{V}_{Ne}(\mathbf{d},\mathbf{r})$ prevents us from separating the Hamiltonian $\hat{H}$ into nuclear and electronic parts, which would allow us to write the wave function of the system as a product of nuclear and electronic functions. Within the Born-Oppenheimer approximation [58,60,62] we can uncouple the electronic part from the nuclear one. The first hypothesis of this approximation is based in the fact that the nucleus is much more massive than the electrons, so the nucleus does not follow the fast change of the electrons, and we can consider that the nuclei are approximately fixed with respect to the movement of the electrons. Then, we consider that the electrons of the system are moving in a field due to a set of fixed nuclei. Within this approximation, the second term in equation 2.4, which corresponds to the kinetic energy of the nuclei, can be neglected. The term $\hat{V}_{Ne}(\mathbf{d},\mathbf{r})$ will depend parametrically on nuclear coordinations $\mathbf{d}$, in the sense that we can determine $\hat{V}_{Ne}(\mathbf{d},\mathbf{r})$ for particulars nuclear positions, and the repulsion term between the nuclei can be considered to be constant, not acting in the eigenfunction. Within these considerations, we write the Hamiltonian in equation 2.4, for $M_A \to \infty$, as [58,60],

$$\hat{H} = \hat{T}_e(\mathbf{r}) + \hat{V}_{Ne}(\mathbf{d},\mathbf{r}) + \hat{V}_{NN}(\mathbf{d}) + \hat{V}_{ee}(\mathbf{r}). \tag{2.5}$$

Therefore, the total Hamiltonian, $\hat{H}$, can be written as

$$\hat{H} = \hat{H}_{ele}(\mathbf{r},\mathbf{d}) + \hat{V}_{NN}(\mathbf{d}) \tag{2.6}$$

where

$$\hat{H}_{ele}(\mathbf{r},\mathbf{d}) = \hat{T}_e(\mathbf{r}) + \hat{V}_{Ne}(\mathbf{d},\mathbf{r}) + \hat{V}_{ee}(\mathbf{r}), \tag{2.7}$$

is the electronic Hamiltonian of the system. Because $\hat{V}_{Ne}(\mathbf{d},\mathbf{r})$ depends parametrically on the nuclear coordinates $\mathbf{d}$, the electronic Hamiltonian, $\hat{H}_{ele}(\mathbf{r},\mathbf{d})$, will also have the same parametrically dependency. Thus, we use our problem to find an approximate solution for the electronic Schrödinger-type equation,

$$\hat{H}_{ele}\Phi_m(\mathbf{r},\mathbf{d}) = \varepsilon_{ele}(\mathbf{d})\Phi_m(\mathbf{r},\mathbf{d}), \tag{2.8}$$

where $\Phi_m(\mathbf{r},\mathbf{d})$ is the electronic wave function, which defines an electronic state for particular nuclear positions, and ε_{ele} is the respective electronic energy, which also depends parametrically on the nuclear positions. In the total energy, relative to the total Hamiltonian of the system, one should include the nucleus-nucleus repulsion term,

considered constant,

$$E_m(\mathbf{d}) = \varepsilon_m(\mathbf{d}) + \sum_{A=1}^{M}\sum_{B>A}^{M}\frac{Z_A Z_B}{d_{AB}}. \tag{2.9}$$

We can write the wave function $\psi(\mathbf{r},\mathbf{d})$ as an expansion in the complete set of the electronic functions, which are eigenfunctions of the electronic Hamiltonian $\hat{H}_{ele}$, as

$$\psi(\mathbf{r},\mathbf{d}) = \sum_m \chi_m(\mathbf{d})\Phi_m(\mathbf{r},\mathbf{d}), \tag{2.10}$$

where $\chi_m(\mathbf{d})$ are the coefficients of the expansion, which depends explicit on the nuclear coordinates. Inserting 2.10 into equation 2.2 we obtain

$$\left(\hat{T}_N(\mathbf{d}) + \hat{H}_{ele}(\mathbf{r},\mathbf{d}) + \hat{V}_{NN}(\mathbf{d})\right)\sum_m \chi_m(\mathbf{d})\Phi_m(\mathbf{r},\mathbf{d}) = E\sum_m \chi_m(\mathbf{d})\Phi_m(\mathbf{r},\mathbf{d}), \tag{2.11}$$

which can be written, using equation 2.8 and 2.9, as

$$\sum_m \left(\hat{T}(\mathbf{d}) + E_m(\mathbf{d})\right)\chi_m(\mathbf{d})\Phi_m(\mathbf{r},\mathbf{d}) = E\sum_m \chi_m(\mathbf{d})\Phi_m(\mathbf{r},\mathbf{d}). \tag{2.12}$$

Multiplying equation 2.12 from left by $\Phi_m^*(\mathbf{r},\mathbf{d})$ and integrating over the electron coordinates we obtain [58]

$$\left(\hat{T}(\mathbf{d}) + E_n(\mathbf{d})\right)\chi_n(\mathbf{d}) = E\chi_n(\mathbf{d}) + \sum_m C_{nm}(\mathbf{d},\nabla)\chi_m(\mathbf{d}), \tag{2.13}$$

where the term C_{nm} is written as [58],

$$C_{nm}(\mathbf{d},\nabla) = \sum_{A=1}^{M}\frac{1}{M_A}(\mathrm{X}_{nm}^{(A)}\nabla_A + \mathrm{Y}_{nm}^{(A)}), \tag{2.14}$$

with

$$\mathrm{X}_{nm}^{(A)} = \int \Phi_n^*(\mathbf{r},\mathbf{d})\nabla_A\Phi_m(\mathbf{r},\mathbf{d})d\mathbf{r}, \tag{2.15}$$

and

$$\mathrm{Y}_{nm}^{(A)} = \frac{1}{2}\int \Phi_n^*(\mathbf{r},\mathbf{d})\nabla_A^2\Phi_m(\mathbf{r},\mathbf{d})d\mathbf{r}. \tag{2.16}$$

We see from equation 2.13 that, if C_{nm} is neglected, we obtain an Schrödinger equation for the nuclear movement [58],

$$\hat{H}_{nuc}\chi_n(\mathbf{d}) = E\chi_n(\mathbf{d}), \tag{2.17}$$

where

$$\hat{H}_{nuc}(\mathbf{d}) = \hat{T}_N(\mathbf{d}) + E_n(\mathbf{d}), \tag{2.18}$$

which means that the nuclei move in a potential energy surface $E_n(\mathbf{d})$, which is a solution

of the electronic problem 2.8 and 2.9. The off-diagonal elements of X_{nm} and Y_{nm} are the non-adiabatic coupling elements, and the approximation known as adiabatic, consider that all off-diagonal elements are neglected, thus, the total wave function is restricted to one electronic surface, and the total wave function is given by $\psi(\mathbf{r},\mathbf{d}) = \chi_m(\mathbf{d})\Phi_m(\mathbf{r},\mathbf{d})$ [58,59]. The original formulation of the Born-Oppenheimer approximation [58, 62] consider that all elements of X_{nm} and Y_{nm} are null, thus, as a consequence, within this approximation, we can separate the original Schrödinger equation 2.1 into one electronic equation and one equation for the nuclear movement, where the latter occurs in an effective potential which is the electronic energy $E_m(\mathbf{d})$. Thus, within the Born-Oppenheimer approximation we can write the electronic and nuclear equations, respectively, as

$$[\hat{T}_e + \hat{V}_e + \hat{V}_{Ne} + \hat{V}_{NN}]\Phi_\mu(\mathbf{r},\mathbf{d}) = E_\mu(\mathbf{d})\Phi_\mu(\mathbf{r},\mathbf{d}), \tag{2.19}$$

and

$$[\hat{T}_N + E_\mu(\mathbf{d})]\chi_{\mu\nu}(\mathbf{d}) = E_{\mu\nu}\chi_{\mu\nu}(\mathbf{d}). \tag{2.20}$$

For a complete description of the electron it is necessary to specify its spin. We do this in the context of the non-relativistic theory by introducing two spin function α and β, corresponding to spin up and spin down, respectively [60]. These spin functions are complete and orthonormal,

$$\langle\alpha|\alpha\rangle = \langle\beta|\beta\rangle = 1, \tag{2.21}$$

and

$$\langle\alpha|\beta\rangle = \langle\beta|\alpha\rangle = 0. \tag{2.22}$$

Thus, the wave function for an N electron system will be write as

$$\Phi(\mathbf{x}_1,\mathbf{x}_2,\ldots,\mathbf{x}_N), \tag{2.23}$$

where $\mathbf{x}$ denote, in a compact way, the spatial coordinates and the spin of an electron.

Because we are treating a fermionic system, the wave function must satisfy the antisymmetry principle, which requires that "a many-electron wave function must be antisymmetric with respect to the interchange of the coordinate $\mathbf{x}$ (both space and spin) of any two electrons" [60],

$$\Phi(\mathbf{x}_1,\ldots,\mathbf{x}_i,\ldots,\mathbf{x}_j,\ldots,\mathbf{x}_N) = -\Phi(\mathbf{x}_1,\ldots,\mathbf{x}_j,\ldots,\mathbf{x}_i,\ldots,\mathbf{x}_N). \tag{2.24}$$

Now, we will define the functions known as spin-orbitals as well as the spatial orbitals for a single particle. A spatial orbital $\phi(\mathbf{r})$ is a function of the position vector $\mathbf{r}$, which describes the spatial distribution of an electron such that $|\phi(\mathbf{r})|^2$ is the probability

density of finding an electron in a volume element $d\mathbf{r}$ surrounding $\mathbf{r}$. We assume that the spatial orbitals form an orthonormal set

$$\langle \phi_i | \phi_j \rangle = \delta_{ij}. \tag{2.25}$$

If the set of spatial orbitals $\{\phi_i\}$ were complete we could exactly expand any arbitrary function $f(\mathbf{r})$ as,

$$f(\mathbf{r}) = \sum_{i=1}^{\infty} a_i \phi_i(\mathbf{r}), \tag{2.26}$$

but, in practice, we will never have a complete set, but only a finite set.

The spin-orbital of a single electron is a wave function that describes both its spatial distribution and spin. We write the spin-orbital as a product of spatial orbital $\phi(\mathbf{r}_1)$ with the spin function, which can be $\alpha(1)$ or $\beta(1)$. For each spatial function, one can form two different spin-orbitals, one with spin up and other with spin down,

$$\chi(\mathbf{x}_1) = \begin{cases} \phi(\mathbf{r}_1)\alpha(1) \\ \phi(\mathbf{r}_1)\beta(1) \end{cases} . \tag{2.27}$$

Because the spatial orbitals and the spin functions are orthonormal, the spin-orbitals will also be,

$$\langle \chi_i | \chi_j \rangle = \delta_{ij}. \tag{2.28}$$

In quantum mechanics, the variational principle [58,60,61], which will be used in all the theoretical methods discussed in this section, ensures that, for a given trial wave function, Ψ, the average value of the energy (the expectation value of the Hamiltonian) is an upper boundary to the exact ground-state energy of the system E_0,

$$\frac{\langle \Psi | \hat{H} | \Psi \rangle}{\langle \Psi | \Psi \rangle} \geq \frac{\langle \Phi | \hat{H} | \Phi \rangle}{\langle \Phi | \Phi \rangle} = E_0. \tag{2.29}$$

Here, we consider that the functions Ψ and Φ (the exact wave function) may not be normalized. This principle is very important in molecular modeling since it guarantees a way, from a trial wave function, to approach the exact wave function of the system by minimizing the functional

$$E[\Psi] = \frac{\langle \Psi | \hat{H} | \Psi \rangle}{\langle \Psi | \Psi \rangle}. \tag{2.30}$$

In appendix A we present a proof of the variational principle.

From the considerations discussed above, we present now the main concepts of the theoretical methods used in this work. Initially, we discuss the Hartree-Fock method (HF), Density Functional Theory (DFT), and quantum Monte Carlo (QMC) methods.

The Hartree-Fock method

To satisfy the antisymmetry principle of the wave function, the HF method [60] use a determinant, called the Slater determinant[63], to describe the atomic system. For an N-electron system the Slater determinant is given by

$$\Psi = \frac{1}{\sqrt{N!}} \begin{vmatrix} \chi_1(\mathbf{x}_1) & \chi_2(\mathbf{x}_1) & \dots & \chi_N(\mathbf{x}_1) \\ \chi_1(\mathbf{x}_2) & \chi_2(\mathbf{x}_2) & \dots & \chi_N(\mathbf{x}_2) \\ \vdots & \vdots & & \vdots \\ \chi_1(\mathbf{x}_N) & \chi_2(\mathbf{x}_N) & \dots & \chi_N(\mathbf{x}_N) \end{vmatrix}, \tag{2.31}$$

where the factor $\frac{1}{\sqrt{N!}}$ is a normalization factor.

Using the Slater determinant to calculate the expected value of the Hamiltonian we can write the energy of the system as [64]

$$\langle \Psi | H | \Psi \rangle = E = \sum_{a=1}^{N} \langle a|h|a\rangle + \frac{1}{2}\sum_{a=1}^{N}\sum_{b=1}^{N} \langle ab|ab\rangle - \langle ab|ba\rangle, \tag{2.32}$$

where the indexes a and b represents the spin-orbitals χ_a and χ_b, respectively, and h is the core Hamiltonian, given by

$$h(\mathbf{x}_1) = -\frac{1}{2}\nabla^2{}_1 - \sum_{A=1}^{M} \frac{1}{r_{1A}}. \tag{2.33}$$

The HF method consists of combining the variational principle with the assumption that the wave function which describes the system is a Slater determinant. Therefore, the best wave function that describes the system will be the one that minimizes the expected value of the Hamiltonian. Because the Slater determinant is written in terms of spin-orbitals, we can write the energy as a functional of the molecular spin-orbitals, according to equation 2.32,

$$E[\chi] = \sum_{a=1}^{N} \langle \chi_a|h|\chi_a\rangle + \frac{1}{2}\sum_{a=1}^{N}\sum_{b=1}^{N} \langle \chi_a\chi_b|\chi_a\chi_b\rangle - \langle \chi_a\chi_b|\chi_b\chi_a\rangle. \tag{2.34}$$

We should minimize $E[\chi]$ subject to the condition of orthonormality of spin-orbitals, $\langle \chi_a|\chi_b\rangle - \delta_{ab} = 0$. To do this, we use the method of Lagrange multipliers and write a

functional $\mathcal{L}[\chi]$, given by

$$\mathcal{L}[\chi] = \sum_{a=1}^{N}\langle\chi_a|h|\chi_a\rangle + \frac{1}{2}\sum_{a=1}^{N}\sum_{b=1}^{N}\langle\chi_a\chi_b|\chi_a\chi_b\rangle - \langle\chi_a\chi_b|\chi_b\chi_a\rangle - \sum_{a=1}^{N}\sum_{b=1}^{N}\epsilon_{ba}\{\ \langle\chi_a|\chi_b\rangle - \delta_{ab}\}\ , \tag{2.35}$$

where ϵ_{ba} are constants called Lagrange undetermined multiplier. Minimizing this functional we obtain the HF equation [60],

$$f|\chi_a\rangle = \epsilon_a|\chi_a\rangle, \tag{2.36}$$

where ϵ_a is the energy eigenvalue of the orbital a and f is the Fock operator defined as [60],

$$f(\mathbf{x}_1) = h(\mathbf{x}_1) + \sum_{b=1}^{N}[\mathcal{J}_b(\mathbf{x}_1) - \mathcal{K}_b(\mathbf{x}_1)]. \tag{2.37}$$

The operators $\mathcal{J}$ and $\mathcal{K}$ are the Coulomb and exchange operators, respectively, defined as [60],

$$\mathcal{J}_b(\mathbf{x}_1)\chi_a(\mathbf{x}_1) = \left[\int d\mathbf{x}_2\chi_b^*(\mathbf{x}_2)\frac{1}{r_{12}}\chi_b(\mathbf{x}_2)\right]\chi_a(\mathbf{x}_1), \tag{2.38}$$

and

$$\mathcal{K}_b(\mathbf{x}_1)\chi_a(\mathbf{x}_1) = \left[\int d\mathbf{x}_2\chi_b^*(\mathbf{x}_2)\frac{1}{r_{12}}\chi_a(\mathbf{x}_2)\right]\chi_b(\mathbf{x}_1), \tag{2.39}$$

The unique set of spin-orbitals obtained from a solution of the equation 2.36 is called canonical spin-orbitals. We should note that the Fock operator depends on the solutions of the HF equation, the spin-orbitals. Furthermore, there is one equation for each spin-orbital, which depends on the other spin-orbitals through the Fock operator. Therefore, these equations must be solved in a coupled and iterative way (through successive approximations). The $\chi's$ obtained as solutions of the HF equations must be the same $\chi's$ that constitute the Fock operator. That characterizes the HF method as a self-consistent method. HF equation 2.36 describes a system from a formal perspective in terms of a set of general spin-orbitals $\{\chi_i \quad |i = 1, 2, ..., N\}$. However, to obtain solutions to the HF equation, we should be more specific about the form of spin-orbitals. There are two types of spin-orbitals: the restricted spin-orbitals, which are constrained to have the same spatial function for α and β spin functions, and the unrestricted spin-orbitals, which have different spatial functions for α and β spin functions. Here, to illustrate the HF method, we consider the restricted spin-orbitals [65] in the case that the system has a closed shell, which means that the system has an even number of electrons and two

electrons occupy each orbital, one with spin up and the other with spin down,

$$\chi_i(\mathbf{x}) = \begin{cases} \phi_j(\mathbf{r})\alpha(\omega) \\ \phi_j(\mathbf{r})\beta(\omega) \end{cases} . \tag{2.40}$$

Within these considerations for restricted HF we obtain a closed-shell spatial Hartree-Fock equation

$$f(\mathbf{r}_1)\phi_p(\mathbf{r}_1) = \epsilon_p\phi_p(\mathbf{r}_1), \tag{2.41}$$

and the closed-shell Hartree-Fock energy

$$E = 2\sum_{p=1}^{N/2}\langle p|h|p\rangle + \sum_{p,q=1}^{N/2} 2\langle pq|pq\rangle - \langle pq|qp\rangle, \tag{2.42}$$

where

$$f(\mathbf{r}_1) = h(r_1) + \sum_{q=1}^{N/2} 2\mathcal{J}_q(\mathbf{r}_1) - \mathcal{K}_q(\mathbf{r}_1) \tag{2.43}$$

is the closed-shell Fock operator, and $\mathcal{J}_q(\mathbf{r}_1)$ and $\mathcal{K}_q(\mathbf{r}_1)$ are the closed-shell Coulomb and exchange operators, respectively, given by [60],

$$\mathcal{J}_q(\mathbf{r}_1)\phi_p(\mathbf{r}_1) = \int \phi_q^*(\mathbf{r}_2)\frac{1}{r_{12}}\phi_q(\mathbf{r}_2)d\mathbf{r}_2\phi_p(\mathbf{r}_1), \tag{2.44}$$

$$\mathcal{K}_q(\mathbf{r}_1)\phi_p(\mathbf{r}_1) = \int \phi_q^*(\mathbf{r}_2)\frac{1}{r_{12}}\phi_p(\mathbf{r}_2)d\mathbf{r}_2\phi_q(\mathbf{r}_1). \tag{2.45}$$

After eliminating the spin dependency, through the considerations of restricted closed-shell Hartree-Fock, the problem becomes that of solving a spatial differential equation. For a small systems, the restricted closed-shell HF equations can be solved numerically, but for larger systems with many electrons, the solution becomes impracticable. One possible solution to this problem is expanding the spatial part of spin-orbitals in terms of a set of K known basis functions $\{g_\nu(\mathbf{r})|\nu = 1, 2..., K\}$,

$$\phi_p(\mathbf{r}) = \sum_{\nu=1}^{K} C_{\nu p}g_\nu(\mathbf{r}), \tag{2.46}$$

where $C_{\nu p}$ are coefficients of the linear expansion of the spatial orbitals.

Replacing equation 2.46 in equation 2.41 we obtain the so-called Hartree-Fock-Roothaan equations [65], which in matrix form is written as,

$$\mathbf{FC} = \mathbf{SC}\epsilon, \tag{2.47}$$

where $\mathbf{S}$ is a $K \times K$ matrix known as the overlap matrix and $\mathbf{F}$ is a $K \times K$ matrix known

as the Fock matrix, which are formed by the following elements [60]

$$S_{\mu\nu} = \int d\mathbf{r}_1 g^*_\mu(\mathbf{r}_1) g_\nu(\mathbf{r}_1), \qquad F_{\mu\nu} = \int d\mathbf{r}_1 g^*_\mu(\mathbf{r}_1) f(\mathbf{r}_1) g_\nu(\mathbf{r}_1). \tag{2.48}$$

In equation 2.47, $\mathbf{C}$ is a $K \times K$ matrix of the expansion coefficients $C_{\nu p}$ and ϵ is a diagonal matrix of the orbitals energies. This equation must be solved in an iterative way and one can use the Self Consistent Field procedure [60] as an algorithm to obtain the solutions.

Koopmans' Theorem

Koopmans' theorem [66], which arises in the HF context, gives us a physical interpretation for the ionization potential (IP) and the electron affinity (EA) in terms of the spin-orbitals of the system, which are considered to be "frozen", i.e., when removing or adding an electron in a system, the orbitals remain the same. This theorem, formulated by Tjalling Koopmans, can be stated as follows [60].

Koopmans' Theorem: Given an N-electron Hartree-Fock single determinant $|^N\Psi_0\rangle$ with occupied and virtual spin-orbitals energies ϵ_a and ϵ_r, then the ionization potential to produce an $(N-1)$-electron single determinant $|^{N-1}\Psi_a\rangle$ with identical spin-orbitals, obtained by removing an electron from spin-orbital χ_a, and the electron affinity to produce an $(N+1)$-electron single determinant $|^{N+1}\Psi^r\rangle$ with identical spin-orbital, obtained by adding an electron to spin-orbital χ_r, are just $-\epsilon_a$ and $-\epsilon_r$, respectively.

Koopmans' theorem can be expressed mathematically as

$$IP = E_a(N-1) - E_0(N) = -\epsilon_a, \tag{2.49}$$

$$EA = E_0(N) - E_r(N+1) = -\epsilon_r. \tag{2.50}$$

Because Koopmans' theorem is obtained at HF level, the ionization potential and the electron affinity obtained by this theorem, only have electrostatic and exchange contributions. This theorem will be very useful in our work in characterizing the electronic binding energy in the studied boron clusters. In appendix B, we present a proof for Koopmans' Theorem.

Density Functional Theory

Density Functional Theory (DFT) [58, 67, 68] is a method that also starts from the idea of solving the non-relativistic time-independent Schrödinger equation for an N-

electrons system within the Born-Oppenheimer approximation, where the Hamiltonian operator is given by the equation 2.5. The first term of this Hamiltonian is the kinetic energy operator $\hat{T}_e$; the second is the operator that represents the external potential over the electrons due to the nuclei, $\hat{V}_{Ne}$, which can be written as

$$\hat{V}_{Ne} = \sum_{i=1}^{N} v(\mathbf{r}_i), \tag{2.51}$$

where

$$v(\mathbf{r}_i) = \sum_{A=1}^{M} \frac{Z_A}{|\mathbf{r}_i - \mathbf{d}_A|}, \tag{2.52}$$

and the third term is the electron-electron repulsion operator $\hat{V}_{ee}$.

The ground-state electron density is defined as

$$\rho_0(\mathbf{r}) = \langle\Phi| \sum_{i=1}^{N} \delta(\mathbf{r} - \mathbf{r}_i)|\Phi\rangle, \tag{2.53}$$

where $|\Phi\rangle$ is the ground-state wave function, and the total energy of the ground-state of the system is given by $E_0 = \langle\Phi|H|\Phi\rangle$. We can write the ground-state energy in terms of the kinetic energy, the external potential and the electron-electron repulsion operators as

$$\begin{aligned} E_0 &= \langle\Phi|\hat{T}_e + \hat{V}_{Ne} + \hat{V}_{ee}|\Phi\rangle = \langle\Phi|\hat{T}_e + \hat{V}_{ee}|\Phi\rangle + \langle\Phi|\hat{V}_{Ne}|\Phi\rangle \\ &= \langle\Phi|\hat{T}_e + \hat{V}_{ee}|\Phi\rangle + \sum_{i=1}^{N} \int d^3r_1 \ldots \int d^3r_N \Phi^*(\mathbf{r}_1, \mathbf{r}_2, \ldots \mathbf{r}_N) v(\mathbf{r}_i) \Phi(\mathbf{r}_1, \mathbf{r}_2, \ldots \mathbf{r}_N) \\ &= \langle\Phi|\hat{T}_e + \hat{V}_{ee}|\Phi\rangle + \int \rho(\mathbf{r}) v(\mathbf{r}) d\mathbf{r}. \end{aligned} \tag{2.54}$$

Therefore, N and $v(\mathbf{r})$ completely define the properties of the system for the ground-state.

The DFT method is based on two theorems that were introduced by Hohemberg and Kohn (HK) [69], which can be stated as follows:

Theorem 1 *The external potential $v(\mathbf{r})$ is a unique functional of the electron density up to an arbitrary constant.*

To prove this theorem, let us consider the following situation: let $|\Phi\rangle$ be the ground-state wave function of a given system, characterized by a Hamiltonian $\hat{H}$ ($\hat{H} = \hat{T}_e + \hat{V}_{Ne} + \hat{V}_{ee}$) with an external potential $v(\mathbf{r})$. Now, suppose that there is another external potential $v'(\mathbf{r})$ that leads to a Hamiltonian $\hat{H}'$ ($\hat{H}' = \hat{T}_e + \hat{V}'_{Ne} + \hat{V}_{ee}$) and to a ground-state $|\Phi'\rangle$. Let us assume, by hypothesis, that the two potentials, $v(\mathbf{r})$ and $v'(\mathbf{r})$, leads to the same electron density $\rho(\mathbf{r})$. Here we are considering only non-degenerate states, but the proof of this theorem can be extended to the case of degenerate states.

By the variational theorem we have

$$E = \langle\Phi|\hat{H}|\Phi\rangle < \langle\Phi'|\hat{H}|\Phi'\rangle, \tag{2.55}$$

and

$$E' = \langle\Phi'|\hat{H}'|\Phi'\rangle < \langle\Phi|\hat{H}'|\Phi\rangle. \tag{2.56}$$

Therefore, writing $\hat{H} = \hat{H}' + \hat{V}_{Ne} - \hat{V}'_{Ne}$ we obtain the following inequality,

$$\langle\Phi|\hat{H}|\Phi\rangle < \langle\Phi'|\hat{H}|\Phi'\rangle = \langle\Phi'|\hat{H}'|\Phi'\rangle + \langle\Phi'|\hat{V}_{Ne} - \hat{V}'_{Ne}|\Phi'\rangle, \tag{2.57}$$

which, as shown in 2.54, we can write as,

$$E < E' + \int [v(\mathbf{r}) - v'(\mathbf{r})]\rho(\mathbf{r})d^3r. \tag{2.58}$$

Using the same as procedure above, for $\langle\Phi'|\hat{H}'|\Phi'\rangle$, we obtain,

$$E' < E + \int [v'(\mathbf{r}) - v(\mathbf{r})]\rho(\mathbf{r})d^3r. \tag{2.59}$$

Adding 2.58 to 2.59 we obtain the following absurd result,

$$E + E' < E' + E. \tag{2.60}$$

Thus, we conclude by *reductio ad absurdum* that different external potentials cannot be related to the same electron density, which defines the uniqueness of $\rho(\mathbf{r})$. Hence, the ground-state wave function is a unique functional of the ground-state electron density of the system,

$$|\Phi\rangle = |\Phi[\rho_0]\rangle, \tag{2.61}$$

which implies that the expectation value of any physical observable, designated by the operator $\hat{O}$, is also a functional of $\rho(\mathbf{r})$,

$$O_0 = \langle\Phi[\rho_0]|\hat{O}|\Phi[\rho_0]\rangle = O[\rho_0]. \tag{2.62}$$

Therefore, the ground-state energy of the system is a unique functional of the ground-state electron density

$$E_{v,0} = E_v[\rho_0] = \langle\Psi[\rho_0]|\hat{H}|\Psi[\rho_0]\rangle, \tag{2.63}$$

where we use the index v to make explicit the energy dependency with the external potential.

Theorem 2 *The ground-state energy of the system $E[\rho]$ is minimal for the exact*

electron density $\rho(\boldsymbol{r})$.

According the equation 2.54, we can write the energy functional for a given state $|\Psi\rangle$ in terms of the electron density $\rho(\mathbf{r})$ as,

$$E[\rho] = \langle\Psi|\hat{T}_e + \hat{V}_{ee}|\Psi\rangle + \langle\Psi|\hat{V}_{Ne}|\Psi\rangle, \tag{2.64}$$

where we define the universal functional,

$$F[\rho] = \langle\Psi|\hat{T}_e + \hat{V}_{ee}|\Psi\rangle, \tag{2.65}$$

which is a valid functional for any Coulomb system. It is independent of the external potential, unlike the term $\langle\Psi|\hat{V}_{Ne}|\Psi\rangle$, which depends on the system in question.

Similarly, to the ground-state of the system, we have,

$$E[\rho_0] = F[\rho_0] + \langle\Phi|\hat{V}_{Ne}|\Phi\rangle, \tag{2.66}$$

and the variational principle ensures that,

$$E[\rho_0] < E[\rho]. \tag{2.67}$$

Here, we are considering that the electron density is v-representable, which means that any electron density is determined by some external potential. In other words, the second theorem of Hohemberg and Khon tells us that any trial electron density $\tilde{\rho}(\mathbf{r})$, with $\tilde{\rho}(\mathbf{r}) \geq 0$ and $\int \tilde{\rho}(\mathbf{r})d\mathbf{r} = N$, gives us an energy value greater than or equal to the exact ground-state energy of the system,

$$E[\tilde{\rho}] \geq E[\rho_0] = E_0.$$

The approximation $\tilde{\rho}(\mathbf{r})$ defines its own external potential $\tilde{v}$, Hamiltonian $\tilde{\hat{H}}$, and wave function $|\tilde{\Psi}\rangle$, where the latter can be used as a trial wave function to a particular problem of interest with the external potential $v(\mathbf{r})$. Thus, we have,

$$E_0 = E_v[\rho_0] = F[\rho_0] + \int \rho_0(\mathbf{r})v(\mathbf{r})d\mathbf{r} \leq E_v[\tilde{\rho}] = F[\tilde{\rho}] + \int \tilde{\rho}(\mathbf{r})v(\mathbf{r})d\mathbf{r}. \tag{2.68}$$

The universal functional $F[\rho]$ can be written in terms of the Coulomb electron-electron repulsion as,

$$F[\rho] = \frac{1}{2}\iint \frac{\rho(\mathbf{r})\rho(\mathbf{r}')}{|r - r'|}d\mathbf{r}d\mathbf{r}' + G[\rho], \tag{2.69}$$

where $G[\rho]$ as well as $F[\rho]$ is a universal functional of $\rho(\mathbf{r})$. Thus, the energy functional

can be written as,

$$E_v[\rho] = \frac{1}{2}\iint \frac{\rho(\mathbf{r})\rho(\mathbf{r}')}{|r-r'|}d\mathbf{r}d\mathbf{r}' + G[\rho] + \int \rho(\mathbf{r})v(\mathbf{r})d\mathbf{r}. \tag{2.70}$$

We need to propose an approximation to $G[\rho]$, and a way of doing this, according to Khon and Sham [70], is by writing

$$G[\rho] \equiv T_s[\rho] + E_{xc}[\rho], \tag{2.71}$$

where $T_s[\rho]$ is the kinetic energy functional of a system of non-interacting electrons, which has the same electron density $\rho(\mathbf{r})$ of an interacting system, and $E_{xc}[\rho]$ is the exchange-correlation energy of an interacting system with electron density $\rho(\mathbf{r})$, which also includes the residual part of the kinetic energy, $T[\rho] - T_s[\rho]$, where $T[\rho]$ is the exact kinetic energy of an interacting electrons system.

Due to the variational principle, we want to minimize the energy functional subject to the constraint $\int \rho(\mathbf{r})d\mathbf{r} = N$. We do this with the method of Lagrange multipliers, by writing,

$$\delta\left\{ E_v[\rho] - \mu\left[\int \rho(\mathbf{r})d\mathbf{r} - N\right]\right\} = 0, \tag{2.72}$$

where μ is the Lagrange multiplier.

Using the equations 2.70 and 2.71 we can write

$$E_v[\rho] = \int \rho(\mathbf{r})v(\mathbf{r})d\mathbf{r} + T_s[\rho] + E_{xc}[\rho] + \frac{1}{2}\iint \frac{\rho(\mathbf{r})\rho(\mathbf{r}')}{|\mathbf{r}-\mathbf{r}'|}d\mathbf{r}d\mathbf{r}', \tag{2.73}$$

and with equation 2.72 we obtain

$$\int \delta\rho(\mathbf{r})\left[v(\mathbf{r}) + \frac{\delta T_s[\rho]}{\delta\rho} + \int \frac{\rho(\mathbf{r}')}{|\mathbf{r}-\mathbf{r}'|}d\mathbf{r}' + \frac{\delta E_{xc}[\rho]}{\delta\rho} - \mu\right]d\mathbf{r} = 0. \tag{2.74}$$

Writing,

$$V_{KS}(\mathbf{r}) = v(\mathbf{r}) + \int \frac{\rho'(\mathbf{r}')}{|\mathbf{r}-\mathbf{r}'|}d\mathbf{r}' + v_{xc}[\rho], \tag{2.75}$$

where $v_{xc}[\rho]$ is the exchange-correlation potential term,

$$\frac{\delta E_{xc}[\rho]}{\delta\rho} = v_{xc}[\rho], \tag{2.76}$$

we obtain the following equation,

$$\frac{\delta T_s[\rho]}{\delta\rho} + V_{KS}(\mathbf{r}) = \mu, \tag{2.77}$$

which is an equation for a non-interacting electrons system moving in the given external potential V_{KS}, know as Khon-Sham potential.

According to Khon and Sham [70], it is possible to use a reference non-interacting electron system for which the Hamiltonian is,

$$H^{KS} = -\frac{1}{2}\nabla^2 + V_{KS}(\mathbf{r}), \tag{2.78}$$

and solve the one-particle Schrödinger equation,

$$\left(-\frac{1}{2}\nabla^2 + V_{KS} \right) \Psi_i^{KS} = \epsilon_i \Psi_i^{KS}, \tag{2.79}$$

to obtain ρ. The connection between the hypothetical system and the real one can be established by choosing an external potential such that the electron density of the non-interacting system (ρ_s) approaches the real electron density ρ,

$$\rho_s(\mathbf{r}) = \sum_i^N |\Psi_i^{KS}(\mathbf{r})|^2 \approx \rho(\mathbf{r}), \tag{2.80}$$

where N is the number of electrons. The kinetic energy can be obtained by

$$T_s[\rho] = \sum_i^N \langle \Psi_i | -\frac{1}{2}\nabla^2 | \Psi_i \rangle. \tag{2.81}$$

These equations (2.75, 2.76, 2.79 and 2.80), known as Khon-Sham equations, have to be solved self-consistently [68, 70] to obtain the electron density and hence the physical observable of interest. One begins with an assumed $\rho(\mathbf{r})$, constructs $V_{KS}(\mathbf{r})$ from 2.75 and $v_{xc}[\rho]$ from 2.76, and finds a new $\rho(\mathbf{r})$ from 2.79 and 2.80. This procedure is repeated until the convergence criteria are reached. In Figure 2.1 we show a commonly adopted self-consistent schematic cycle. However, to construct $V_{KS}(\mathbf{r})$ we must choose *a priori* the exchange-correlation functional E_{xc}. There is a large variety of approximations for the exchange-correlation term and we briefly discuss some of this approximations below.

The Exchange-Correlation Functional Approximation

One of the most important types of approximation in the exchange-correlation functional, E_{xc}, is Local Density Approximation (LDA) [64, 68, 71]. The LDA is based on the homogeneous gas theory and consider that the exchange-correlation energy per electron in a non-homogeneous electron gas with local density $\rho(\mathbf{r})$, such as in an atom, is equal to the exchange-correlation in a homogeneous electron gas, which has the same local density $\rho(\mathbf{r})$ as the non-homogeneous electron gas. It is also considered that the exchange-correlation functional, in the LDA approximation, can be split into two terms,

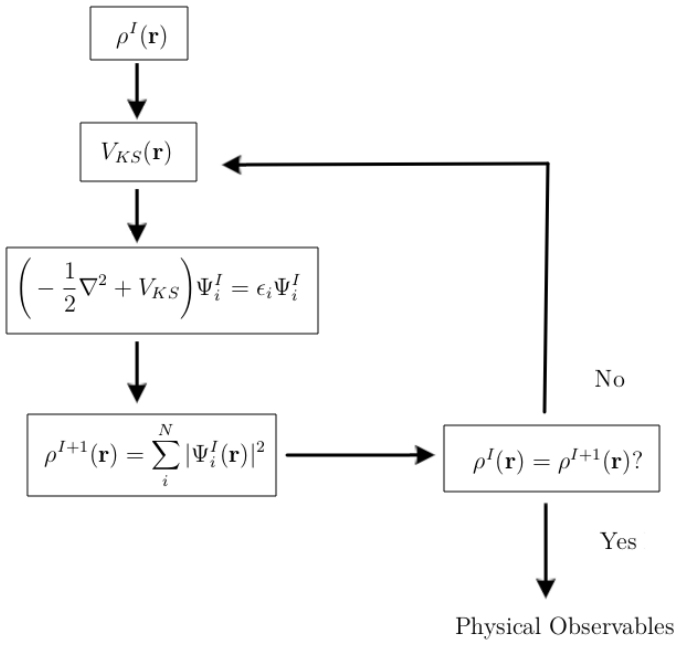

Figure 2.1: Schematic figure of the self-consistent cycle. Adapted from [58]

the exchange and the correlation contributions,

$$E_{xc}[\rho] = E_x[\rho] + E_c[\rho], \tag{2.82}$$

where the exchange functional $E_x[\rho]$ is written as the exchange energy of a gas in the Thomas-Fermi-Dirac model [64, 71],

$$E_x^{LDA}[\rho] = -\frac{3}{4}\left(\frac{3}{\pi}\right)^{1/3}\int \rho^{4/3}(\mathbf{r})d\mathbf{r}. \tag{2.83}$$

For the correlation functional there is no explicit expression, however, and based on results of highly accurate numerical quantum Monte Carlo simulations of the homogeneous electron gas, available from the work of Ceperley and Alder [72], analytical expressions could be obtained for the correlation functional, which are parametrizations of these data. There is a vast variety of works about the $E_c[\rho]$ term. We cite here two functionals for the correlation term, which are probably the most used in the LDA approximation, the functional developed by Vosko, Wilk, and Nusair [73], known as the VWN functional, and the functional designed by Perdew and Wang [74], known as the PW functional.

Another approximation to $E_{xc}[\rho]$ is based in the idea of using information not only of the electron density $\rho(\mathbf{r})$ but also of the electron density gradient $\nabla\rho(\mathbf{r})$, to account for the non-homogeneity of the true electron system. The first attempt to take into account the electron density gradient was done trying to include it as a Taylor expansion, where the first term of the expansion would be interpreted as the LDA approximation. This

approximation, known as Gradient Expansion Approximation (GEA) [68, 71], was not very successful reproducing results that were even worse than the LDA approximation to real systems. In this context, of the representation of the non-homogeneity of the real systems by the electron density gradient, another approximation arises, known as the Generalized Gradient Approximation (GGA) [64, 68, 71], which considers the exchange-correlation functional as being expressed in the following way,

$$E_{xc}^{GGA}[\rho] = \int f(\rho(\mathbf{r}), \nabla\rho(\mathbf{r}))d\mathbf{r}. \tag{2.84}$$

Depending on the methods employed to construct the function $f(\rho, \nabla\rho)$ one can obtain different GGA exchange-correlation functionals. Among the most used GGA-type functionals, there is the BLYP functional (denoting the combination of Becke's exchange functional [75] with the correlation functional of Lee, Yang, and Parr [76]), which were obtained by fitting empirical parameters of molecules, and the PBE functional, proposed by Perdew, Burke, and Ernzerhof [77], which do not use empirical parameters.

Another class of functionals, know as hybrid functionals [68, 71], are constructed in such a way as to combine the exact exchange Hartree-Fock energy with the exchange-correlation from DFT, which is the case of exchange functional B3 (Becke's three-parameters) [78]. The combination of the exchange functional B3 with the correlation functional LYP forms one of the most popular hybrid functional, the B3LYP functional, which is used in this work and has the following functional form [68],

$$E_{xc}^{\mathrm{B3LYP}} = E_x^{\mathrm{LDA}} + a(E_x^{\mathrm{HF}} - E_x^{\mathrm{LDA}}) + b(E_x^{\mathrm{GGA}} - E_x^{\mathrm{LDA}}) + E_c^{\mathrm{LDA}} + c(E_c^{\mathrm{GGA}} - E_c^{\mathrm{LDA}}), \tag{2.85}$$

where a, b, and c are parameters with the values 0.20, 0.72, and 0.81, respectively. E_x^{LDA} is the exchange functional in the LDA approximation, E_x^{HF} is the Hartree-Fock exchange functional, E_x^{GGA} is Becke's exchange functional, E_c^{LDA} is the VWN correlation functional and E_c^{GGA} is the LYP correlation functional.

Quantum Monte Carlo Methods

In this section, we present the quantum Monte Carlo methods [64, 79], which are a set of techniques that apply the Monte Carlo method to calculate the quantum properties of a many body system.

Monte Carlo Integration

A classical application of the Monte Carlo method is the solution of multidimensional definite integrals with complicated boundary conditions. An approximate manner

to evaluate a one-dimensional definite integral,

$$I = \int_a^b f(x)dx, \tag{2.86}$$

is through a fragmentation, in N rectangles of base Δx, of the area below the curve defined by $f(x)$. Thus, the definite integral can be written as,

$$I = \int_a^b f(x)dx \cong \sum_{i=1}^{N} f(x_i)\Delta x, \tag{2.87}$$

and Δx can be calculated in terms of the integration limits as,

$$\Delta x = (b-a)/N. \tag{2.88}$$

Thus, equation 2.87 can be written as follows,

$$I = \int_a^b f(x)dx \cong \frac{(b-a)}{N}\sum_{i=1}^{N} f(x_i) = (b-a)\cdot\langle f(x)\rangle. \tag{2.89}$$

The best result for the integral is obtained in the limit that N tends to infinity; thus, the integral is estimated as

$$I = \lim_{N\to\infty}\frac{(b-a)}{N}\sum_{i=1}^{N} f(x_i). \tag{2.90}$$

The estimated integral is an arithmetic average of the function $f(x)$ for equally spaced values of x_i. However, to evaluate the average of $f(x)$, it is not necessary that the values of x_i be equally spaced. To determine the area below the curve, the Monte Carlo integration [79] uses points x_i that are randomly drawn between a and b, but this strategy is not always efficient, since the random numbers generated can represent points that are not relevant to the average, which increases the calculation time and the associated error. To handle this sampling issue, one uses the *importance sampling* method. The idea is to use a function $w(x)$ defined over the domain $[a, b]$, such that the behavior of the function $w(x)$ is similar to the $f(x)$. Furthermore, let us suppose that we can generate pseudo random variates from the normalized function $p(x)$, where

$$p(x) = \frac{w(x)}{\int_a^b w(x)dx} \tag{2.91}$$

is a probability density function over $[a, b]$ [79]. Thus, we can write the integral 2.86 as

$$I = \int_a^b \frac{f(x)}{p(x)} p(x)dx = \int_a^b g(x)p(x)dx$$
$$\approx \frac{1}{N}\sum_{i=1}^{N} g(x_i)_{p(x)} = \langle g(x)\rangle_{p(x)}, \tag{2.92}$$

where we defined the function $g \equiv f/p$. This approximation is valid in the limit of $N \to \infty$, and since the points $\{x_i\}$ are a random sequence of numbers generated from $p(x)$ (in our notation we use the subscript $p(x)$ to indicate that $g(x)$ is sampled by the probability density function $p(x)$). Now, the random numbers generated by $p(x)$ will have higher density where $f(x)$ is large and lower density where $f(x)$ is small, to the extent that $w(x) \approx f(x)$. The advantage of importance sampling is that, because $w(x)$ has similar behavior to $f(x)$, the function $g(x) = f(x)/p(x)$ is smoother than the original $f(x)$, which reduces the statistical error in the evaluation of the integral.

Random walks and Markov Chains

To give an idea of the concepts such random walks, Markov chains, and the Metropolis method, which are fundamental in quantum Monte Carlo methods, we follow the discussions in reference [79]. In the Monte Carlo method, one of the most powerful tools is the *random walk* [79], which can be used to generate the most desired distributions. In a random walk we define a mathematical entity called a *walker* [79], whose attributes completely determines the state of the system in question. This walker move in an appropriate state space by a combination of deterministic and random displacements from its previous position. The sequence of steps of the walker from one position to another forms a *chain*.

Let us consider a system of N possible states, denoted by $S_1, S_2, \ldots, S_N$, and at a discrete point in time i we have the state $x^{(i)}$, e.g. if the system is in the state S_j at the time i then $x^{(i)} = S_j$. Thus, the sequence of $x^{(i)}$ from time zero to the end of the walk forms a chain. If the state-state transition probabilities are independent of time and history, i.e., the transition probability from one state to another depends only on the current state of the system, then, the chain is called *Markov chain* [79, 80]. We define the probability of the system changing from state S_j to S_k in one time step as [79],

$$P_{kj} \equiv P(x^{(i+1)} = S_k \leftarrow x^{(i)} = S_j). \tag{2.93}$$

The $\mathbf{P}$ matrix must be normalized, i.e., the rows of this matrix sum to unity, which ensures that in a transition the system will be in one of its N allowed states.

Let $p_k^{(i)}$ be the probability that the system is in the state S_k at time i. Then, the

probability-space density may be represented as the column vector,

$$\mathbf{p}^{(i)} = \begin{bmatrix} p_1^{(i)} \\ p_2^{(i)} \\ \vdots \\ p_N^{(i)} \end{bmatrix}, \tag{2.94}$$

with normalization,

$$\sum_k^N p_k^{(i)} = 1. \tag{2.95}$$

At each point in time the system can move from S_j to S_k with probability P_{kj}, and the probability distribution will evolve as [79],

$$p_k^{(i+1)} = \sum_j P_{kj} p_j^{(i)}, \tag{2.96}$$

which can be written in matrix form as,

$$\mathbf{p}^{(i+1)} = \mathbf{P}\mathbf{p}^{(i)}. \tag{2.97}$$

The system will evolve from the initial distribution as follows: $\mathbf{p}^{(1)} = \mathbf{P}\mathbf{p}^{(0)}$; and then $\mathbf{p}^{(2)} = \mathbf{P}\mathbf{p}^{(1)} = \mathbf{P}\mathbf{P}\mathbf{p}^{(0)}$ and so on. After m steps $\mathbf{p}^{(m)}$ is related to $\mathbf{p}^{(0)}$ by

$$\mathbf{p}^{(m)} = \mathbf{P}^m \mathbf{p}^{(0)}, \tag{2.98}$$

and for a sufficiently long time M, $|\mathbf{p}^{(M+1)} - \mathbf{p}^{(M)}| \to 0$. So, there must be an equilibrium probability distribution $\mathbf{p}^*$ defined by [79]

$$\mathbf{p}^* = \mathbf{P}\mathbf{p}^*. \tag{2.99}$$

A necessary condition for the system to reach equilibrium is ergodicity [79], i.e., in the limit of an infinite system, the spatial averages are equal to the temporal averages. For a process to be ergodic, it is necessary that all possible states must have a nonzero probability of being visited.

Generalizing to continuous variables, where both space and time are considered to be continuous, the probability of moving from the point x at time t to y at time $t+\Delta t$ is denoted by $G(y, x; \Delta t)$, which is the continuous variable analogous to P_{kj}. We will denote by $f(x, t)$ the probability density of a particle being at x at time t. Thus, the equations for the continuous case, analogous to the discrete case, are [79],

$$f(y, t + \Delta t) = \int f(x, t) G(y, x; \Delta t) dx, \tag{2.100}$$

and

$$f(y, t + m\Delta t) = \int f(x, t)G(y, x; m\Delta t)dx. \tag{2.101}$$

In an equilibrium situation, we should have,

$$f^*(y) = \int f^*(x)G(y, x; t)dx. \tag{2.102}$$

One can solve equation 2.100 iteratively and produce continuous distribution $f^*(y)$. Thus, we see that the distribution f^* can arise from a Markov process governed by a transition probability G. An efficient method to accomplish the procedure discussed above, which is a fundamental technique in Monte Carlo methods, is the Metropolis method [79], introduced originally by Metropolis *et al.* [81]; since then, this algorithm has been widely used in Statistical Mechanics and quantum Monte Carlo simulations.

The Metropolis method

Consider a discrete N-state system with equilibrium probabilities $\mathbf{p}^*$. Let the state of maximum probability be S_i, thus $p_i^* = \max(\mathbf{p}^*)$. We define the probability of moving from this most probable state S_i to any other state, say S_k, as $A_{ki} = p_k^*/p_i^*$, and similarly the probability of moving from the second most probable state S_j to any other state S_k (with $k \neq i$) is $A_{kj} = p_k^*/p_j^*$. Thus, we see that these transition probabilities obey the relationship $A_{kj} \cdot A_{ji} = A_{ki}$, which means that the probability of moving from i to k is the same regardless of path. With this choice of A_{ij}, we can construct the matrix $\mathbf{A}$. In the construction of the matrix $\mathbf{A}$, there is no problem with the elements of type A_{ji}, because $p_i^* \geq p_j^*$, but, the matrix elements that represent moves to higher probabilities, the elements A_{ij}, will be set to unity, because $p_i/p_j > 1$. This choice of matrix $\mathbf{A}$ produces the equilibrium distribution [79]. Thus, if we order the states in ascending probability ($p_1^* \leq p_2^* \leq \cdots$) the matrix $\mathbf{A}$ will have elements of type p_j^*/p_i^* as its upper triangle and 1 elsewhere.

Let us consider, for a very large ensemble, that ν_i and ν_j are the current populations of states S_i and S_j, respectively, and $p_i^* > p_j^*$. Then, all the ν_j walkers at S_j may move to S_i since, as discussed above, $A_{ij} = p_i^*/p_j^* = 1$. There is also an average number of walkers that move in the reverse direction, from S_i to S_j. This number of walkers can be expressed as $\nu_i \cdot p_j^*/p_i^* = \nu_i \cdot A_{ji}$. Thus, the net change in the population between S_i and S_j is,

$$\delta\nu_j = \nu_i \frac{p_j^*}{p_i^*} - \nu_j. \tag{2.103}$$

We can see from the equation 2.103 that, if the current population of the ensemble is $\nu_i/\nu_j = p_i^*/p_j^*$, then $\delta\nu_j = 0$ and the system reached equilibrium. If $\nu_i/\nu_j > p_i^*/p_j^*$, then $\delta\nu_j > 0$, and the population S_j increases, driving the inequality toward equality and

equilibrium is reached, similarly if $\nu_i/\nu_j < p_i^*/p_j^*$, $\delta\nu_j < 0$, then the population of S_j decreases, driving the system to equilibrium. Thus, this choice of matrix $\mathbf{A}$ correctly drives the system to a stable equilibrium distribution [79].

These considerations can be generalized for continuous variables by adding time and spatial continuous variables. The acceptance probabilities, of moving a walker from $\mathbf{x}$ at time t to $\mathbf{y}$ at time $t + \Delta t$, may be written as [79]

$$A(\mathbf{x}, \mathbf{y}; \Delta t) = min\left(\frac{p^*(\mathbf{y}, t + \Delta t)}{p^*(\mathbf{x}, t + \Delta t)}, 1\right), \tag{2.104}$$

to account for cases in which the ratio of the probabilities p's are greater or less than 1.

The Generalized Metropolis Method

In the Metropolis method, discussed in the previous section, each walker moves from one state to another with uniform probability. In the Generalized Metropolis method [79], each attempt to move from state i to j has a probability T_{ji} and this move has an acceptance probability B_{ji}, which is chosen to produce the equilibrium distribution $\mathbf{p}^*$. The average number of walkers population moving from j to i is $\nu_j \cdot T_{ij} \cdot B_{ij}$. Similarly, the average number moving from i to j is $\nu_i \cdot T_{ji} \cdot B_{ji}$, thus, the net population at point j from point i is,

$$\delta\nu_j = T_{ji}B_{ji}\nu_i - T_{ij}B_{ij}\nu_j. \tag{2.105}$$

At the equilibrium, the average net population must be zero, $\delta\nu_j = 0$, thus, the equation 2.105 can be written as,

$$\frac{\nu_j}{\nu_i} = \frac{T_{ji}}{T_{ij}}\frac{B_{ji}}{B_{ij}}. \tag{2.106}$$

We know that at equilibrium $\nu_j/\nu_i = p_j^*/p_i^*$, therefore, given $\mathbf{T}$ the matrix $\mathbf{B}$ must satisfy

$$\frac{B_{ji}}{B_{ij}} = \frac{p_j^*}{p_i^*}\frac{T_{ij}}{T_{ji}}. \tag{2.107}$$

Equation 2.107 is called the detailed balance condition.

A good choice of B_{ij} which satisfies 2.107 is the following [79],

$$B_{ji} = min\left(1, \frac{T_{ij}p_j^*}{T_{ji}p_i^*}\right). \tag{2.108}$$

For the continuous case 2.108 becomes [79],

$$B(\mathbf{y}, \mathbf{x}; \Delta t) = min\left(1, \frac{G(\mathbf{x}, \mathbf{y}; \Delta t)\mathbf{p}^*(\mathbf{y})}{G(\mathbf{y}, \mathbf{x}; \Delta t)\mathbf{p}^*(\mathbf{x})}\right). \tag{2.109}$$

A difficulty in this method is knowing the transition function $G(\mathbf{y}, \mathbf{x}; \Delta t)$ that generates

$\mathbf{p}^*$. Once the transition function that generates a probability density function close to $\mathbf{p}^*$ is known, the generalized Metropolis method is of very great use, as we will see in the next section, where we discuss the application of the Monte Carlo methods to solve a quantum many-body problem.

Variational Quantum Monte Carlo

The variational quantum Monte Carlo method (VMC) [79,82,88] is based on the variational principle and the Monte Carlo method for the evaluation of integrals using importance sampling based on the Metropolis algorithm. We are interested in solving equation 2.2, and the starting point is the choice of a trial wave function $|\Psi_T[\eta]\rangle$, which depends on a set of parameters $[\eta]$ that are optimized to find a minimum for the total energy of the system.

The expected value of the Hamiltonian of the N-electrons system is given by [79],

$$\langle \hat{H} \rangle = \frac{\int \Psi_T^*([\eta], \mathbf{R}) \hat{H} \Psi_T([\eta], \mathbf{R}) d\mathbf{R}}{\int \Psi_T^*([\eta], \mathbf{R}) \Psi_T([\eta], \mathbf{R}) d\mathbf{R}}, \tag{2.110}$$

where $\mathbf{R} = (\mathbf{r}_1, \mathbf{r}_2, \ldots, \mathbf{r}_N)$ is a $3N$-dimensional vector specifying the coordinates of the N electrons of the system. A particular value of $\mathbf{R}$ is sometimes called a walker, a configuration, or a psip in the QMC literature [82]. Multiplying and dividing equation 2.110 by $\Psi_T([\eta], \mathbf{R})$, we can write the expected value as,

$$\langle \hat{H} \rangle = \frac{\int |\Psi_T([\eta], \mathbf{R})|^2 E_L([\eta], \mathbf{R}) d\mathbf{R}}{\int |\Psi_T([\eta], \mathbf{R})|^2 d\mathbf{R}}, \tag{2.111}$$

where $E_L([\eta], \mathbf{R})$ is the local energy defined as

$$E_L([\eta], \mathbf{R}) = \frac{\hat{H} \Psi_T([\eta], \mathbf{R})}{\Psi_T([\eta], \mathbf{R})}. \tag{2.112}$$

It is a convenient way to write the expected value because we obtain an integral that is a weighted average,

$$E[\Psi_T(\eta, \mathbf{R})] = \frac{\int E_L([\eta], \mathbf{R}) |\Psi_T([\eta], \mathbf{R})|^2 d\mathbf{R}}{\int |\Psi_T([\eta], \mathbf{R})|^2 d\mathbf{R}} = \langle E_L \rangle_{\Psi^2}, \tag{2.113}$$

where the weight is the normalized probability density function of the electrons,

$$\frac{|\Psi_T([\eta], \mathbf{R})|^2}{\int |\Psi_T([\eta], \mathbf{R})|^2 d\mathbf{R}}. \tag{2.114}$$

In equation 2.113, $\langle E_L \rangle_{\Psi^2}$ denotes the average of E_L with respect to the distribution $|\Psi|^2$. Another purpose of writing the expected value of the Hamiltonian in terms of the local

energy E_L is that the local energy has the property of being a constant when $\Psi_T(\eta, \mathbf{R})$ is an eigenfunction of $\hat{H}$. Since $\hat{H}\Psi_T = E_T\Psi_T$ we have

$$E_L = \frac{\hat{H}\Psi_T}{\Psi_T} = \frac{E_T}{\Psi_T}\Psi_T = E_T. \tag{2.115}$$

It is significant because the variance of local energy can be zero. In practice, the trial wave function rarely will be an eigenfunction of the Hamiltonian. Despite this, the more Ψ_T approaches to the exact wave function of the system the less variance E_L will have. Therefore, one can note that the integral

$$\langle \hat{H} \rangle = E[\Psi] = \int \left(\frac{\hat{H}\Psi_T([\eta], \mathbf{R})}{\Psi_T([\eta], \mathbf{R})} \right) \left(\frac{|\Psi_T([\eta], \mathbf{R})|^2}{\int |\Psi_T([\eta], \mathbf{r})|^2 d\mathbf{R}} \right) d\mathbf{R}, \tag{2.116}$$

can be evaluated by the Monte Carlo method with the Metropolis importance sampling technique. Thus, the Monte Carlo estimated energy is given by

$$E[\Psi] = \langle E_L \rangle_{\Psi^2} = \lim_{M \to \infty} \frac{1}{M} \sum_{i=1}^{M} E_L(\mathbf{R}_i), \tag{2.117}$$

where the Monte Carlo sample points $\mathbf{R}_i$ are drawn from the distribution Ψ^2, and the variance of the mean value is

$$\sigma^2(E[\Psi]) = \frac{\langle E_L^2 \rangle_{\Psi^2} - \langle E_L \rangle_{\Psi^2}^2}{M - 1}. \tag{2.118}$$

A method proposed by Umrigar *et al.* [83] guarantees that the trial wave function optimization can be accomplished by the minimization of the local energy variance, given by equation 2.118. This method is based on the argument that in the limit of the wave function approach of the ground-state, the variance will approach zero.

The probabilities density controls the process of mapping the coordinate space, and an efficient algorithm for mapping regions of coordinate space significantly, to evaluate the integral by Monte Carlo importance sampling, is the Metropolis algorithm [81], discussed in the previous sections. The Metropolis algorithm decides if the system will accept or reject a transition from a configuration $\mathbf{R}$ to $\mathbf{R}'$ according to the probability,

$$P(\mathbf{R} \to \mathbf{R}') = \min\left(1, \frac{w(\mathbf{R}')}{w(\mathbf{R})}\right), \tag{2.119}$$

in which $w(\mathbf{R})$ is the probability density given by,

$$w(\mathbf{R}) = \frac{|\Psi_T([\eta], \mathbf{R})|^2}{\int |\Psi_T([\eta], \mathbf{R})|^2 d\mathbf{R}}. \tag{2.120}$$

A typical VMC algorithm is as follows [64, 84]:

1. Generate an initial configuration of random positions for the electrons.

2. Propose a move from $\mathbf{R}$ to $\mathbf{R}'$.

3. Calculate the probability ratio $w(\mathbf{R}')/w(\mathbf{R})$, where $w(\mathbf{R})$ is given by 2.120.

4. Accept or reject the move according to Metropolis probability, given by 2.119.

5. If the move is accepted update the electron position and then calculate the local energy. If the move is rejected keep the electron position and then calculate the local energy.

6. Repeat configuration moves until sufficient data is accumulated.

Figure 2.2, extracted from [82], illustrates the VMC algorithm.

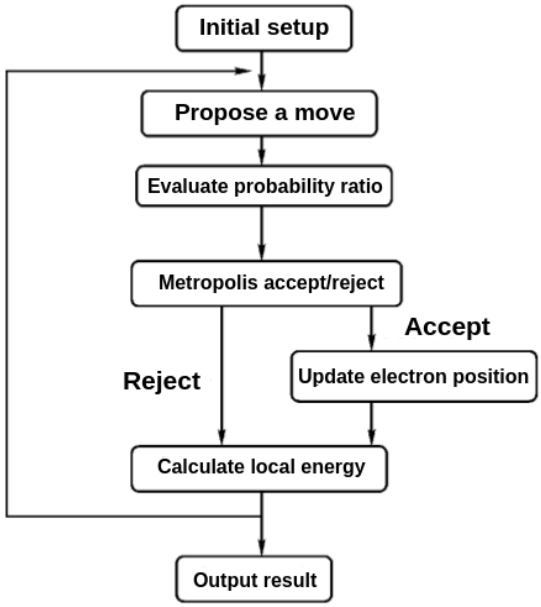

Figure 2.2: Illustration of the VMC algorithm. Extracted from [82].

The accuracy in the VMC method will depend on how close the trial wave function is to the exact ground-state wave function of the system. Because we are dealing with a fermionic system, we can consider the trial wave function as a combination of Slater determinants and an electron correlation factor. In VMC, the trial wave function is the Slater-Jastrow wave function, which can be written as

$$\Psi_T(\{\mathbf{r}_i\},\{\mathbf{r}_I\}) = D_\uparrow(\phi_i)D_\downarrow(\phi_i)e^{J(\{\mathbf{r}_i\},\{\mathbf{r}_I\})}, \tag{2.121}$$

where $\{\mathbf{r}_i\}$ and $\{\mathbf{r}_I\}$ denote the electron and ion coordinates, respectively, e^J is the correlation factor, where $J(\{\mathbf{r}_i\},\{\mathbf{r}_I\})$ is the Jastrow term [85,86], $D_\uparrow$ is a determinant of spin-up single particle orbitals ϕ's and $D_\downarrow$ is a determinant of spin-down single particle orbitals.

The Jastrow factor is the sum of three terms: the homogeneous and isotropic electron-electron terms $u(r_{ij})$, the isotropic electron-nucleus terms $\chi_I(r_{iI})$ centered on the

nuclei and the isotropic electron-electron-nucleus term $f_I(r_{Ii}, r_{Ij}, r_{ij})$ also centered on the nuclei. The form of the Jastrow factor is,

$$J(\{\mathbf{r}_i\},\{\mathbf{r}_I\}) = \sum_{i=1}^{N-1}\sum_{j=i+1}^{N} u(r_{ij}) + \sum_{I=1}^{N_{ions}}\sum_{i=1}^{N}\chi_I(r_{iI}) + \sum_{I=1}^{N_{ions}}\sum_{i=1}^{N-1}\sum_{j=i+1}^{N} f_I(r_{Ii}, r_{Ij}, r_{ij}). \quad (2.122)$$

The Slater-Jastrow wave function must satisfy cusp conditions, known as Kato cusp conditions [85–87]. The cusp conditions determine the behavior of the many body wave function when two electrons or a nucleus and an electron coincide in space. The cusp conditions derive from the requirement that the divergence in the local kinetic energy at a coalescence point cancels the divergence in the local potential energy. The cusp condition, imposed on the Slater-Jastrow wave function, lead to the following conditions in the Jastrow factor [85]:

$$\left(\frac{\partial J}{\partial r_{ij}}\right)_{\substack{r_{ij}=0\\ r_i=r_j}} = \frac{1}{2}, \quad (2.123)$$

for the case in which two electrons of opposite spin, i and j, approach one another,

$$\left(\frac{\partial J}{\partial r_{ij}}\right)_{\substack{r_{ij}=0\\ r_i=r_j}} = \frac{1}{4}, \quad (2.124)$$

for the case in which two electrons of the same spin, i and j, approach each other, and

$$\left(\frac{\partial J}{\partial r_i}\right)_{\substack{r_i=0\\ r_{ij}=r_j}} = -Z. \quad (2.125)$$

when an electron i approaches a nucleus of atomic number Z. In these considerations r_{ij}, r_i and r_j are treated as independent variables.

The u, χ and f terms in the Jastrow factor

We present the expansion form of the terms u, χ, and f [85, 86] utilized in the construction of the Jastrow factor in this work. The u term consists of a complete power expansion in r_{ij} up to order $r_{ij}^{C+N_u}$, which satisfies the cusp condition at $r_{ij} = 0$. The u term has continuous derivatives at the cutoff length L_u and goes to zero at $L_u = r_{ij}$. The form of u term is

$$u(r_{ij}) = (r_{ij} - L_u)^C \times \Theta(L_u - r_{ij}) \times \left(\alpha_0 + \left[\frac{\Gamma_{ij}}{(-L_u)^C} + \frac{\alpha_0 C}{L_u}\right] r_{ij} + \sum_{l=2}^{N_u} \alpha_l r_{ij}^l\right), \quad (2.126)$$

where Θ is the Heaviside funtion, $\Gamma_{ij} = 1/2$ in case of the electrons i and j are antiparallel and $\Gamma_{ij} = 1/4$ in the case of parallel spins. In the u term, C is a constant that determines the behavior of the cutoff length.

The χ term has the following form

$$\chi_I(r_{iI}) = (r_{iI} - L_{\chi I})^C \times \Theta(L_{\chi I} - r_{iI}) \times \left(\beta_{0I} + \left[\frac{-Z_I}{(-L_{\chi I})^C} + \frac{\beta_{0I} C}{L_{\chi I}} \right] r_{iI} + \sum_{m=2}^{N_\chi} \beta_{mI} r_{iI}^m \right). \quad (2.127)$$

In this expression, the term involving the ionic charge Z_I enforces the electron-nucleus cusp conditions and $L_{\chi I}$ is the cutoff length. When I and J are equivalents ions it may be assumed that $\beta_{mI} = \beta_{mJ}$.

The form of f is

$$f_I(r_{iI}, r_{iJ}, r_{ij}) = (r_{iI} - L_{fI})^C (r_{jI} - L_{fJ})^C \Theta(L_{fI} - r_{iI}) \Theta(L_{fI} - r_{jI}) \sum_{l=0}^{N_{fI}^{eN}} \sum_{m=0}^{N_{fI}^{eN}} \sum_{n=0}^{N_{fI}^{ee}} \gamma_{lmnI} r_{iI}^l r_{jI}^m r_{ij}^n. \quad (2.128)$$

This term is an expansion of a function of r_{ij}, r_{iI} and r_{jI} that goes smoothly to zero when either r_{iI} or r_{iJ} reach the cutoff length. If ions are equivalents, then, it is demanded that $\gamma_{lmnI} = \gamma_{lmnJ}$, and to ensures the Jastrow factor is symmetrical under electron exchange it is required that $\gamma_{lmnI} = \gamma_{mlnI}$ $\forall$ I, m, l, n. The f term does not interfere with the cusp conditions. The condition that f has no electron-electron and electron-nucleus cusp is

$$\left(\frac{\partial f}{\partial r_{ij}} \right)_{\substack{r_{ij} = 0 \\ r_{iI} = r_{jI}}} = 0 \quad (2.129)$$

and

$$\left(\frac{\partial f}{\partial r_{ij}} \right)_{\substack{r_{iI} = 0 \\ r_{ij} = r_{jI}}} = 0, \quad (2.130)$$

which implies some restrictions in the γ term.

The α, β and γ terms that appear in equations 2.126, 2.127 and 2.128, respectively, are variational parameters that are adjusted during the VMC simulation in order to obtain the wave function and hence, the energy, the closest to the exact ground-state.

The correlation energy represents a small part of the total energy of clusters. However, it plays a significant role in the electron binding energy and other electronic properties of such systems. Thus, the Jastrow factor becomes important to correct the wave function, to correctly analyze the electronic properties of clusters.

Diffusion Quantum Monte Carlo

The Diffusion Quantum Monte Carlo method (DMC) [79, 82, 88] solves the time-dependent Schrödinger equation for an imaginary time $\tau \equiv it$. The idea of DMC is to explore the similarities between the imaginary time Schrödinger equation and the generalized diffusion equation.

The time-dependent Schrödinger equation, in atomic units, and its solution are given, respectively, by,

$$i\frac{\partial|\Psi,t\rangle}{\partial t} = \hat{H}|\Psi,t\rangle, \tag{2.131}$$

and

$$|\Psi,t\rangle = e^{i\hat{H}t}|\Psi,0\rangle. \tag{2.132}$$

Writing the Schrödinger equation in the position representation and making the change $it \to \tau$, we obtain

$$\frac{\partial\Psi(\mathbf{R},\tau)}{\partial\tau} = \hat{H}\Psi(\mathbf{R},\tau), \tag{2.133}$$

where the Hamiltonian $\hat{H}$ is given, in atomic units, by

$$\hat{H} = -\frac{1}{2}\nabla^2 + \hat{V}(\mathbf{R}). \tag{2.134}$$

Equation 2.133 is similar to a diffusion equation, of the type

$$-\frac{\partial C}{\partial t} = D\nabla^2 C + kC. \tag{2.135}$$

Exploring this analogy we can write the imaginary-time Schrödinger equation, with the Hamiltonian given by 2.134, as a diffusion equation,

$$\frac{\partial\Psi(\mathbf{R},\tau)}{\partial\tau} = D\nabla^2\Psi(\mathbf{R},\tau) - \hat{V}(\mathbf{R})\Psi(\mathbf{R},\tau), \tag{2.136}$$

where $D = \frac{1}{2}$ is a diffusion constant.

An important modification in equation 2.136 is the change $\hat{V}(\mathbf{R}) \to \{\hat{V}(\mathbf{R}) - E_T\}$. Thus, this equation and its solution can be written as,

$$\frac{\partial\Psi(\mathbf{R},\tau)}{\partial\tau} = D\nabla^2\Psi(\mathbf{R},\tau) - \{\hat{V}(\mathbf{R}) - E_T\}\Psi(\mathbf{R},\tau), \tag{2.137}$$

$$\Psi(\mathbf{R},\tau) = e^{-\tau(\hat{H}-E_T)}\Psi(\mathbf{R},0). \tag{2.138}$$

We identify equation 2.137 as a diffusion equation associated with the kinetic term, and a branching equation associated with the potential energy term,

$$\frac{\partial\Psi(\mathbf{R},\tau)}{\partial\tau} = \underbrace{D\nabla^2\Psi(\mathbf{R},\tau)}_{\text{Diffusion}} - \underbrace{\{\hat{V}(\mathbf{R}) - E_T\}\Psi(\mathbf{R},\tau)}_{\text{Branching}}. \tag{2.139}$$

In equation 2.139, if the term $\{\hat{V}(\mathbf{R}) - E_T\}\Psi(\mathbf{R},\tau)$ were absent, we would have a general diffusion equation which could be simulated by a random walker process. On the other hand, if the term $D\nabla^2\Psi(\mathbf{R},\tau)$ were absent, we would have a branching equation, which would be simulated by process of birth/death of the configurations weighted by

the potential energy. Figure 2.3 schematically represents the process involved in the diffusion/branching simulations. An advantage in diffusion Monte Carlo techniques,which will be discussed later, is that both processes, within an approximation, can be simulated separately. Figure 2.4, extracted from [82], illustrates the DMC process for the case of a single particle moving in a one-dimensional potential well. An initial configuration of walkers samples the initial distribution, and as the imaginary-time propagation proceeds, in regions of high potential energy, the walkers occasionally disappear, and in regions around the minimum potential the walkers proliferate, until the distribution converges towards the ground-state.

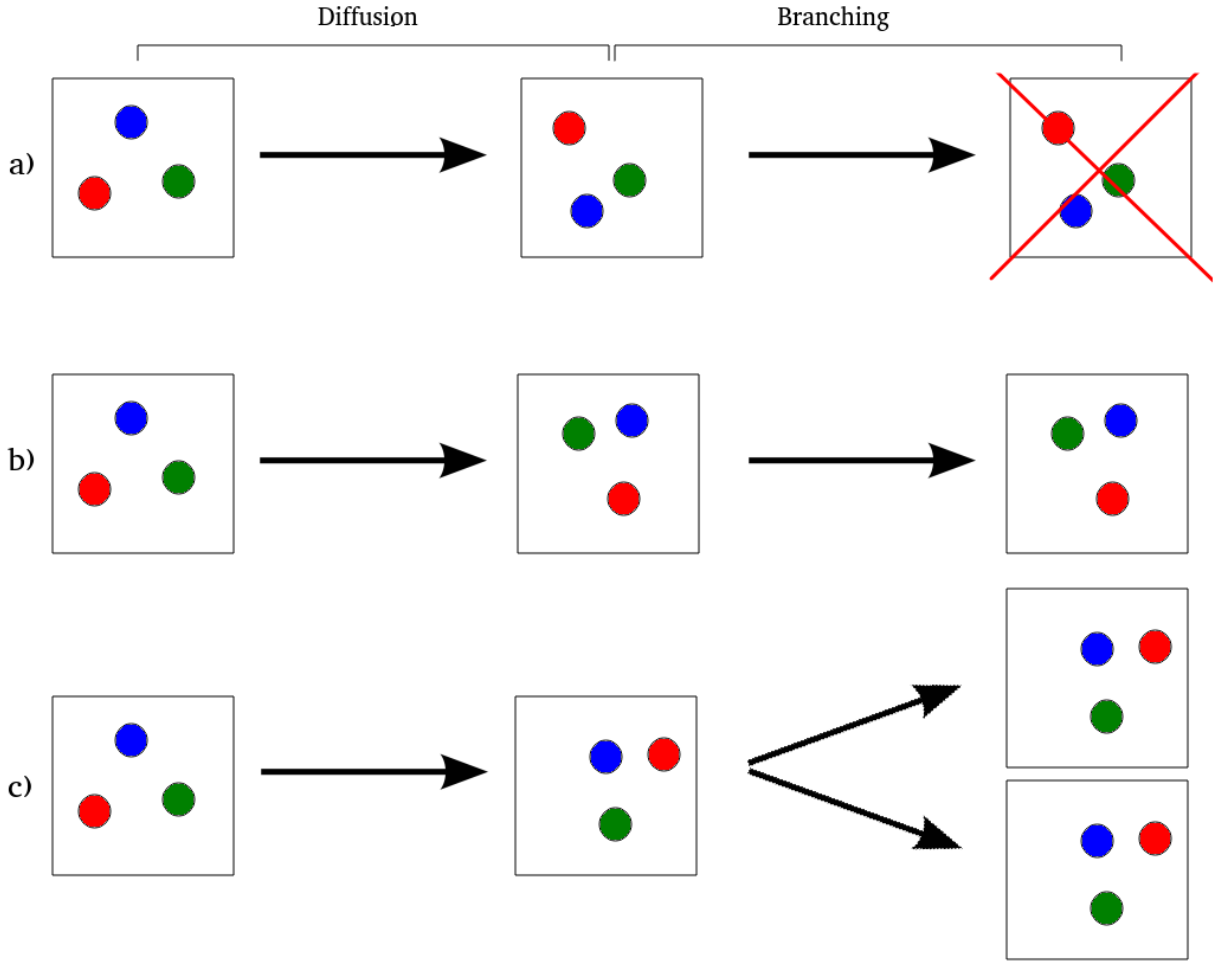

Figure 2.3: Schematic figure for the branching process where (a) a walker is dead; (b) a walker keeps to the trajectory; and (c) an identical copy is made.

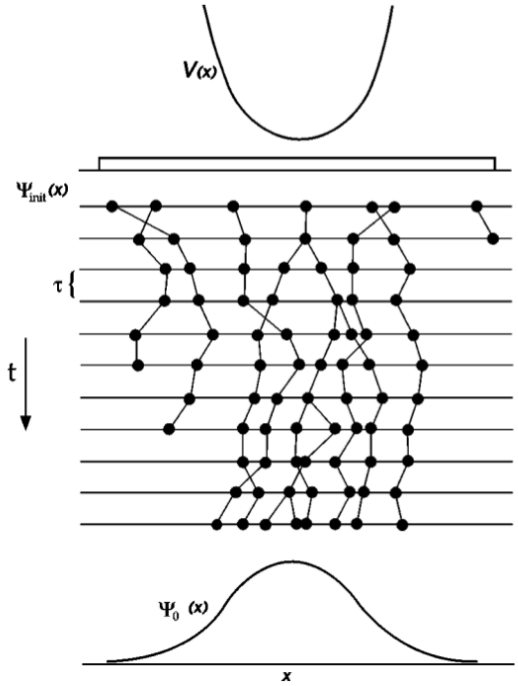

Figure 2.4: Illustration of the walker evolution in DMC algorithm. Figure extracted from [82].

Because the MC method is a technique that evaluates integrals, to solve the Schrödinger equation, we must transform it into an integral equation. We discuss this in the next section using Green's function formalism [79].

Integral Form of Schrödinger Equation: Green's function formalism

To transform the time-independent Schrödinger equation 2.1, for the ground-state, into an integral equation, we operate from the left by the inverse Hamiltonian operator $\hat{H}^{-1}$, obtaining,

$$|\Psi_0\rangle = E_0 \hat{H}^{-1} |\Psi_0\rangle. \tag{2.140}$$

Introducing a complete set of position states $\int_{-\infty}^{\infty} |\mathbf{R}\rangle\langle\mathbf{R}| d\mathbf{R}$ between H^{-1} and $|\Psi_0\rangle$, and multiplying from the left by $\langle\mathbf{R}'|$, we obtain

$$\langle\mathbf{R}'|\Psi_0\rangle = E_0 \int_{-\infty}^{\infty} \langle\mathbf{R}'|\hat{H}^{-1}|\mathbf{R}\rangle\langle\mathbf{R}|\Psi_0\rangle d\mathbf{R}, \tag{2.141}$$

where we define the Green's function associated with the Hamiltonian as

$$G(\mathbf{R}', \mathbf{R}) \equiv \langle\mathbf{R}'|\hat{H}^{-1}|\mathbf{R}\rangle. \tag{2.142}$$

Thus, equation 2.141 can be written, in the position representation, as

$$\Psi_0(\mathbf{R}') = E_0 \int_{-\infty}^{\infty} G(\mathbf{R}', \mathbf{R}) \Psi_0(\mathbf{R}) d\mathbf{R}. \tag{2.143}$$

The equation 2.143 may be solved iteratively by choosing an initial state $\Psi^{(0)}$ and a trial energy E_T which approximates to Ψ_0 and E_0, respectively, by n an step series,

$$\Psi^{n+1}(\mathbf{R}') = E_T \int_{-\infty}^{\infty} G(\mathbf{R}', \mathbf{R})\Psi^{(n)}(\mathbf{R})d\mathbf{R}. \tag{2.144}$$

One difficulty is to know exactly the function $G(\mathbf{R}', \mathbf{R})$. Although *a priori*, we do not know the specific form of Green's function $G(\mathbf{R}', \mathbf{R})$, we can highlight some of its properties. The Green's function of a Hermitian operator is symmetric. Then, because the function $G(\mathbf{R}', \mathbf{R})$ is Green's function associated with the Hamiltonian, it will be symmetric. Furthermore, in the Monte Carlo method, the Green's function must be positive everywhere and normalizable, so that we can interpret $G(\mathbf{R}', \mathbf{R})$ as the transition probability from $\mathbf{R}$ to $\mathbf{R}'$ in the random walk process. Thus, the equation 2.143 can be interpreted as: for each point $\mathbf{R}'$ the wave function is composed of a sum over all other points $\mathbf{R}$ weighted by the probability of a particle moving from $\mathbf{R}$ to $\mathbf{R}'$, and is normalized by E_0.

Because Green's function was constructed for the time-independent Schrödinger equation, this function is also time-independent. Let us explore Green's function for the time-dependent Schrödinger equation. We can express the solution of the time-dependent Schrödinger equation 2.138 as an expansion in terms of the eigenfunctions and eigenvalues of the Hamiltonian, $H\psi_k = E_k\psi_k$,

$$\Psi(\mathbf{R}, \tau) = \sum_{k=0}^{\infty} C_k\psi_k(\mathbf{R})e^{-(E_k - E_T)\tau}. \tag{2.145}$$

For a sufficient large imaginary time τ the excited states will be eliminated and only the ground-state ψ_0 will contribute to the wave function. Also, we can eliminate the temporal dependency choosing $E_T = E_0$,

$$\Psi(\mathbf{R}, \tau) = C_0\psi_0 + \sum_{k=1}^{\infty} C_k\psi_k(\mathbf{R})e^{-(E_k - E_0)\tau}, \tag{2.146}$$

Thus, as $\tau \to \infty$ the wave function goes to the stationary ground-state,

$$\lim_{\tau\to\infty} \Psi(\mathbf{R}, \tau) = C_0\psi_0. \tag{2.147}$$

In the same way as we write the integral form of the time-independent Schrödinger equation, we can write an integral form for the imaginary-time Schrödinger equation [79],

$$\Psi(\mathbf{R}', \tau_2) = \int G(\mathbf{R}', \tau_2; \mathbf{R}, \tau_1)\Psi(\mathbf{R}, \tau_1)d\mathbf{R}. \tag{2.148}$$

The Green's function satisfies the same Schrödinger equation as the wave function Ψ,

$$-\frac{\partial\Psi(\mathbf{R},\tau)}{\partial\tau} = (\hat{H} - E_T)\Psi(\mathbf{R},\tau), \tag{2.149}$$

$$-\frac{\partial G(\mathbf{R}',\tau_2;\mathbf{R},\tau_1)}{\partial\tau_2} = (\hat{H} - E_T)G(\mathbf{R}',\tau_2;\mathbf{R},\tau_1). \tag{2.150}$$

We can write the solution of equation 2.149, by introducing the two times, τ_1 and τ_2, as

$$|\Psi(\tau_2)\rangle = e^{-(\hat{H}-E_T)(\tau_2-\tau_1)}|\Psi(\tau_1)\rangle, \tag{2.151}$$

where $e^{-(\hat{H}-E_T)(\tau_2-\tau_1)}$ is the time evolution operator for $\hat{H} - E_T$. One can verify this solution by substitution into equation 2.149. We can obtain the time-dependent Green's function by inserting a complete set $\int_{-\infty}^{\infty}|\mathbf{R}\rangle\langle\mathbf{R}|d\mathbf{R}$ between the time evolution operator and the state $|\Psi(\tau_1)\rangle$, and multiply on the left by $\langle\mathbf{R}'|$,

$$\Psi(\mathbf{R}',\tau_2) = \int\langle\mathbf{R}'|e^{-(\hat{H}-E_T)(\tau_2-\tau_1)}|\mathbf{R}\rangle\Psi(\mathbf{R},\tau_1)d\mathbf{R}. \tag{2.152}$$

Comparing 2.148 with 2.152 we obtain the following expression for Green's function,

$$G(\mathbf{R}',\tau_2;\mathbf{R},\tau_1) = \langle\mathbf{R}'|e^{-(\hat{H}-E_T)(\tau_2-\tau_1)}|\mathbf{R}\rangle. \tag{2.153}$$

Green's function depends only on the difference $\tau_2 - \tau_1 \equiv \delta\tau$, hence, we can write,

$$\Psi(\mathbf{R}',\tau+\delta\tau) = \int G(\mathbf{R}',\mathbf{R};\delta\tau)\Psi(\mathbf{R},\tau)d\mathbf{R}. \tag{2.154}$$

The interpretation for the time-dependent Green's function is the same as for the time-independent case. This equation must be solved iteratively but the fact that we do not know the analytical form of Green's function does not allow us to solve it. In the next section, we discuss an approximation within the DMC method, called *Short time approximation*, which will enable us to obtain an approximate analytical form for Green's function.

Simple Diffusion Monte Carlo

Based on the mathematical tools discussed above, we focus our discussion on how to solve the initially proposed equation, imaginary-time-dependent Schrödinger equation 2.137. As previously discussed, without the second term on the right side, equation 2.137 becomes the usual diffusion equation; on the other hand, ignoring the first term on the right side, equation 2.137 becomes a branching/rate equation. Both equations can be simulated separately by Monte Carlo methods, but these equations are coupled. To obtain an explicit expression for Green's function, we can factorize the time propagator $e^{-(H-E_T)\tau}$

using the Trotter-Suzuki formula [89, 90] as

$$e^{-(T+V-E_T)\tau} \approx e^{-T\tau}e^{-(V-E_T)\tau}, \tag{2.155}$$

which is accurate for $\tau \to 0$ [79, 82]. Thus, we can write an approximation for the function $G(\mathbf{R}', \mathbf{R}, \tau)$ as,

$$G(\mathbf{R}', \mathbf{R}, \tau) \approx G_{diff}(\mathbf{R}', \mathbf{R}, \tau)G_B(\mathbf{R}', \mathbf{R}, \tau). \tag{2.156}$$

We identify G_{diff} as Green's function for a classical diffusion equation and G_B as Green's function for a rate equation. The diffusion Green's function satisfies the diffusion equation

$$-\frac{\partial G_{diff}(\mathbf{R}', \mathbf{R}; \tau)}{\partial \tau} = D\nabla^2 G_{diff}(\mathbf{R}', \mathbf{R}; \tau), \tag{2.157}$$

and its solution is a Gaussian distribution,

$$G_{diff}(\mathbf{R}', \mathbf{R}, \tau) = (4\pi D\tau)^{-3N/2} e^{-(\mathbf{R}'-\mathbf{R})^2/4D\tau}. \tag{2.158}$$

This part of the transition probability, in the Monte Carlo iteration of equation 2.154, can be simulated by spreading random walkers according to a Gaussian distribution.

The function G_B satisfies a rate equation,

$$-\frac{\partial G_B(\mathbf{R}', \mathbf{R}, \tau)}{\partial \tau} = (E_T - V)G_B(\mathbf{R}', \mathbf{R}, \tau), \tag{2.159}$$

and its solution is,

$$G_B(\mathbf{R}', \mathbf{R}, \tau) = e^{-(\frac{1}{2}[V(\mathbf{R})+V(\mathbf{R}')]-E_T)\tau}. \tag{2.160}$$

This part can be simulated by a process of creation or destruction of walkers with probability G_B.

We can see, from equation 2.146, that the initial distribution of walkers will converge to the ground-state when $\tau \to \infty$. On the other hand, the analytical Green's function is accurate when $\tau \to 0$. To satisfy both conditions, we divide the time τ into a large number of small time steps, $\delta\tau$, in each iteration step,

$$\begin{aligned} e^{-(H-E_T)\tau} &= e^{-(H-E_T)n\delta\tau} \\ &= e^{-(H-E_T)\delta\tau}e^{-(H-E_T)\delta\tau}e^{-(H-E_T)\delta\tau}\cdots, \end{aligned} \tag{2.161}$$

and one can achieve a long time by applying the short-time propagator many times. This approximation is known as short time approximation. It is expected that in a sufficiently small time steps regime, the behavior of the DMC energy is linear with the time step. Thus, we can extrapolate the DMC energy for a zero time step by a linear polynomial fit. This zero time step extrapolation provides us very accurate results for the energy and

hence other properties of the system.

Even with the short time approximation, the results for the simulations are very unstable, being able to diverge or present considerably high standard deviations [79]. We can use the Monte Carlo technique of importance sampling to obtain greater stability in DMC simulations. We write a distribution function $f(\mathbf{R},\tau) = \Phi(\mathbf{R})\Psi(\mathbf{R},\tau)$ where $\Phi(\mathbf{R})$ is an associated wave function used to bias the random walkers to regions with a higher probability to produce the desired distribution. This function $\Phi(\mathbf{R})$ is constructed based on any available knowledge of Ψ_0, and can be generated by a standard methods such as HF and DFT. One can use VMC calculations for the optimization of parameters in $\Phi(\mathbf{R})$. For a large τ, the density function f will converge to

$$f(\mathbf{R},\tau\to\infty) \equiv f_\infty(\mathbf{R}) = \Phi(\mathbf{R})\Psi_0(\mathbf{R}). \tag{2.162}$$

If we multiply equation 2.137 by $\Phi(\mathbf{R})$ we can rewrite this equation in terms of the density function $f(\mathbf{R},\tau)$ as,

$$\frac{\partial\Phi(\mathbf{R})\Psi(\mathbf{R},\tau)}{\partial\tau} = D\Phi(\mathbf{R})\nabla^2\Psi(\mathbf{R},\tau) - \{\hat{V}(\mathbf{R}) - E_T\}\Phi(\mathbf{R})\Psi(\mathbf{R},\tau). \tag{2.163}$$

Using the identity

$$\nabla^2(\Phi\Psi) = (\nabla^2\Phi)\Psi + 2\nabla\Phi\cdot\nabla\Psi + \Psi(\nabla^2\Phi), \tag{2.164}$$

we can write equation 2.163 as

$$\begin{aligned}\frac{\partial f(\mathbf{R},\tau)}{\partial\tau} =& D\nabla^2 f(\mathbf{R},\tau) - 2D\nabla\Phi(\mathbf{R})\cdot\nabla\Psi(\mathbf{R},\tau) - D\Psi(\mathbf{R},\tau)\nabla^2\Phi(\mathbf{R}) + \\ &- \hat{V}(\mathbf{R})\Phi(\mathbf{R})\Psi(\mathbf{R},\tau) + E_T\Phi(\mathbf{R})\Psi(\mathbf{R},\tau).\end{aligned} \tag{2.165}$$

Rearranging terms and adding $(-D\Psi(\mathbf{R},\tau)\nabla^2\Phi(\mathbf{R}) + D\Psi(\mathbf{R},\tau)\nabla^2\Phi(\mathbf{R}))$ to the equation 2.165 we obtain

$$\begin{aligned}\frac{\partial f(\mathbf{R},\tau)}{\partial\tau} =& D\nabla^2 f(\mathbf{R},\tau) - 2D\nabla\Phi(\mathbf{R})\cdot\nabla\Psi(\mathbf{R},\tau) - 2D\Psi(\mathbf{R},\tau)\nabla^2\Phi(\mathbf{R}) + \\ &+ \left\{\frac{D\nabla^2\Phi(\mathbf{R}) - \hat{V}(\mathbf{R})\Phi(\mathbf{R})}{\Phi(\mathbf{R})}\right\}\Phi(\mathbf{R})\Psi(\mathbf{R},\tau) + E_T\Phi(\mathbf{R})\Psi(\mathbf{R},\tau).\end{aligned} \tag{2.166}$$

Using the Hamiltonian defined as

$$\hat{H} = -D\nabla^2 + \hat{V}, \tag{2.167}$$

the local energy defined as

$$E_L = \frac{\hat{H}\Phi(\mathbf{R})}{\Phi(\mathbf{R})}, \tag{2.168}$$

and the identity

$$\nabla \cdot (\Psi \nabla \Phi) = \Psi \nabla^2 \Phi + \nabla \Psi \cdot \nabla \Phi, \tag{2.169}$$

we can obtain [79, 82, 88],

$$\frac{\partial f(\mathbf{R},\tau)}{\partial \tau} = D\nabla^2 f(\mathbf{R},\tau) - D\nabla \cdot \{f(\mathbf{R},\tau)\mathbf{F}_Q(\mathbf{R})\} + \{E_T - E_L(\mathbf{R})\}f(\mathbf{R},\tau), \tag{2.170}$$

where

$$\mathbf{F}_Q(\mathbf{R}) = \frac{2\nabla\Phi(\mathbf{R})}{\Phi(\mathbf{R})} \tag{2.171}$$

is a vector field known as quantum force.

With importance sampling, we obtain an equation for the distribution f that is similar to equation 2.139, but with an additional term. Equation 2.170 is composed of a diffusion term for a density function, a branching term that is now proportional to $\{E_T - E_L(\mathbf{R})\}$, rather than $\{E_T - \hat{V}(\mathbf{R})\}$, which has the advantage of avoiding the singularities of V, and a drift term that modifies the diffusion,

$$\frac{\partial f(\mathbf{R},\tau)}{\partial \tau} = \underbrace{D\nabla^2 f(\mathbf{R},\tau)}_{\text{Diffusion}} - \underbrace{D\nabla \cdot \{f(\mathbf{R},\tau)\mathbf{F}_Q(\mathbf{R})\}}_{\text{Drift}} + \underbrace{\{E_T - E_L(\mathbf{R})\}f(\mathbf{R},\tau)}_{\text{Branching}}. \tag{2.172}$$

The drift term acts to impose a drift velocity on the diffusion, similar to the way in which particles undergoing Brownian motion are affected by an external field. In regions of low probability, where $\Phi(\mathbf{R})$ is small, the force $\mathbf{F}_Q(\mathbf{R})$ is large and, hence, any random walkers reaching regions where Φ^2 is small are driven away. Thus, the advantage of importance sampling, over equation 2.139, is that the diffusion process is guided by $\Phi(\mathbf{R})$, through the force $\mathbf{F}_Q(\mathbf{R})$, so the configuration space will be sampled with regions where $\Phi(\mathbf{R})$ is large.

Importance sampling changes the form of Green's functions, thus, the new Greens's functions are written as the following form [79],

$$\tilde{G}_{diff}(\mathbf{R}',\mathbf{R},\delta\tau) = (4\pi D\delta\tau)^{-3N/2} e^{-(\mathbf{R}-\mathbf{R}'-D\delta\tau\mathbf{F}_Q(\mathbf{R}'))^2/4D\delta\tau}, \tag{2.173}$$

and

$$\tilde{G}_B(\mathbf{R}',\mathbf{R},\delta\tau) = e^{-(\frac{1}{2}[E_L(\mathbf{R})+E_L(\mathbf{R}')]-E_T)\delta\tau}. \tag{2.174}$$

Therefore, the acceptance of the move of the walker from $\mathbf{R}$ to $\mathbf{R}'$, with Metropolis

probability, is given by,

$$A(\mathbf{R}', \mathbf{R}; \delta\tau) = min\left(1, \frac{|\Phi(\mathbf{R}')|^2}{|\Phi(\mathbf{R})|^2} \frac{\tilde{G}(\mathbf{R}, \mathbf{R}', \delta\tau)}{\tilde{G}(\mathbf{R}', \mathbf{R}, \delta\tau)}\right). \tag{2.175}$$

With these modifications we can write the time evolution of $f(\mathbf{R}, \tau)$ as

$$f(\mathbf{R}', \tau + \delta\tau) = \int \tilde{G}(\mathbf{R}', \mathbf{R}, \delta\tau) f(\mathbf{R}, \tau) d\mathbf{R}, \tag{2.176}$$

where, with the Trotter decomposition,

$$\tilde{G}(\mathbf{R}', \mathbf{R}, \delta\tau) \approx \tilde{G}_{diff}(\mathbf{R}', \mathbf{R}, \delta\tau) \tilde{G}_B(\mathbf{R}', \mathbf{R}, \delta\tau). \tag{2.177}$$

Another important approximation in Diffusion Monte Carlo, which is necessary due to the nature of Fermi statistics, is the fixed-node approximation [72, 79, 82, 88], which was proposed initially by Anderson [91]. The central point of the necessity of this approximation is that, with importance sampling, the exact wave function of the system is represented by a density of walkers, and this density fails to represent antisymmetric states. The density function f, in equation 2.170, can not represent an antisymmetric state because it is composed of wave functions that have both negative and positive regions, and the density f has the implicit boundary condition $f(\mathbf{R}, \tau) = \Phi(\mathbf{R})\Psi(\mathbf{R}, \tau) \geq 0$. The condition $\Phi(\mathbf{R})\Psi(\mathbf{R}, \tau) \geq 0$ can be enforced by fixing the nodes of $\Psi(\mathbf{R}, \tau)$ to be those of $\Phi(\mathbf{R})$, and rejecting the move of a walker that attempts to cross a node of $\Phi(\mathbf{R})$ [79]. Figure 2.5 illustrates the fixed-node approximation for a one-dimensional wave function. The asymptotic solution of equation 2.170, within the fixed-node approximation, can be expressed as,

$$f_\infty(\mathbf{R}) = \Phi(\mathbf{R})\Psi_0^{fn}(\mathbf{R}), \tag{2.178}$$

where Ψ_0^{fn} is an approximation of the exact Fermi ground-state Ψ_0^F.

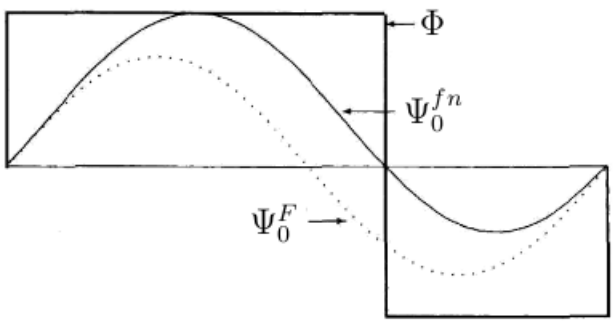

Figure 2.5: Fixed-node approximation for a simple one-dimensional wave function. Figure adapted from [79].

Estimating the Ground-state Energy

In this work, all physical and chemical discussion, about the studied system, is in terms of the ground-state energy of the system. Moreover, in variational and diffusion Monte Carlo simulations, the ground-state energy is the principal quantity to be achieved. In this section, we discuss how the ground-state energy can be estimated in the DMC simulations. We focus on two different approaches to determine the energy, the growth estimator, which is based on the analyses of the growth of the walkers population, and the local energy estimator, which uses the local energy average to estimate E_0 [79].

We can see, from equation 2.145, that after all excited states are eliminated, the remaining time dependence of the wave function is $e^{-(E_0-E_T)\tau}$. From this behavior, the growth of the walker population can be expressed as [79],

$$N(\tau+\delta\tau) = e^{-(E_0-E_T)\delta\tau}N(\tau), \tag{2.179}$$

where $N(\tau)$ represents the walkers population at time τ and can be written, exploring the normalization of $f(\mathbf{R},\tau)$, as

$$N(\tau) = \int f(\mathbf{R},\tau)d\mathbf{R}. \tag{2.180}$$

For sufficiently large sample points of Monte Carlo, the ground-state energy can be estimated by the growth energy E_g. The growth energy can be obtained from the equation 2.179 by considering the population of an initial time τ_1 and a later time τ_2 as,

$$E_g = E_T + \frac{1}{\tau_2-\tau_1}\ln\frac{N(\tau_1)}{N(\tau_2)}. \tag{2.181}$$

The ground-state energy can be estimated by the average of the growth energy taken over the course of the walk, $E_0 = \langle E_g\rangle$. This way of estimating the ground-state energy can present some difficulties because the population can vary widely during a simulation, resulting in a large value for the mean standard deviation. Another approach uses the local energy E_L to estimate the ground-state energy. In VMC, we obtain the total energy by the average of the local energy, which is weighted by the trial wave function, $E[\Psi] = \langle E_L\rangle_{\Psi^2}$. In DMC simulations, the average is weighted by the density function in the limit of a

sufficiently long time step, in the following way,

$$\begin{aligned}\langle E_L\rangle_f =& \frac{\int f_\infty(\mathbf{R})E_L(\mathbf{R})}{\int f_\infty(\mathbf{R})d\mathbf{R}} \\ =& \frac{\int \Phi(\mathbf{R})\Psi_0(\mathbf{R})\left[\frac{\hat{H}\Phi(\mathbf{R})}{\Phi(\mathbf{R})}\right]d\mathbf{R}}{\int \Phi(\mathbf{R})\Psi_0(\mathbf{R})d\mathbf{R}} \\ =& \frac{\int \Psi_0(\mathbf{R})\hat{H}\Phi(\mathbf{R})d\mathbf{R}}{\int \Phi(\mathbf{R})\Psi_0(\mathbf{R})d\mathbf{R}} \\ =& E_0. \end{aligned} \tag{2.182}$$

Thus, we can express the DMC average of the local energy as

$$\langle E_L\rangle_f = \lim_{M\to\infty}\frac{1}{M}\sum_{i=1}^{M} E_L(\mathbf{R}_i). \tag{2.183}$$

This average will be exact to the extent that the density distribution $f_\infty(\mathbf{R})$ is exact. The accuracy of f depends on how exact the Green's function $\tilde{G}$ is, see equations 2.176 and 2.177 . Therefore, the average of the local energy will have a statistical error due to the finite number of Monte Carlo time steps. One can eliminate this time step bias by evaluation $\langle E_L\rangle_f$ as a function of $\delta\tau$ and then extrapolate to $\delta\tau = 0$.

The DMC Algorithm

In this section we present the main steps of an algorithm for diffusion Monte Carlo, based on references [64, 92].

Before the simulation begins, one must choose a good $\Phi(\mathbf{R})$, which can be obtained, for example, by VMC calculations. The initial probability density $f(\mathbf{R}, 0)$ must also be chosen. Usually, a good choice for the initial probability density is $f(\mathbf{R}, 0) = |\Phi(\mathbf{R})|^2$. Once these initial quantities have been defined, the algorithm is:

1. Initialize a set of N_c configurations of coordinates $\mathbf{R}$, with the electrons in each configuration distributed with a probability density $f(\mathbf{R}, 0)$.

2. Choose a value of E_T that should approximate the energy of the studied system. This value can be estimated by a previous variational Monte Carlo simulation.

3. Pick a configuration and calculate the local energy of this configuration $E_L(\mathbf{R})$.

4. Each electron of this configuration will move, one at a time, by letting them diffuse according to the transition probability $\tilde{G}_{diff}(\mathbf{R}', \mathbf{R}, \tau)$. If the current electron is the jth electron in the configuration, it is moved according to

$$\mathbf{x}_j' = \mathbf{x}_j + D\tau\mathbf{F}_Q(\mathbf{x}_j) + \chi, \tag{2.184}$$

where $\mathbf{x}_j$ is the jth component of $\mathbf{R}$ and represents the three-dimensional coordinate of the electron being moved. χ is a random number generated by a Gaussian distribution with a mean of zero and a variance of $2D\tau$, D is the diffusion constant associated with the Schrödinger equation and $\mathbf{F}_Q$ is a vector field, given by 2.171, which favors the electron displacement to regions with greater probability.

5. After electron j is moved, according to equation 2.184, accept the move with a probability

$$P(\mathbf{R} \to \mathbf{R}') = \frac{|\Phi(\mathbf{R}')|^2 \tilde{G}(\mathbf{R}', \mathbf{R}, \tau)}{|\Phi(\mathbf{R})|^2 \tilde{G}(\mathbf{R}, \mathbf{R}', \tau)}, \tag{2.185}$$

where $\tilde{G}(\mathbf{R}', \mathbf{R}, \tau)$ is given by 2.177. If the transition probability $P(\mathbf{R} \to \mathbf{R}')$ is greater than a random number ξ, generated by a uniform distribution between 0 and 1, then, the move is accepted, the old coordinate discarded and the new coordinate kept. If the transition probability is less than ξ, then, the new coordinate is discarded and the old coordinate kept.

6. Repeat the steps *4* and *5* until all electrons in the current configuration have been moved once. Calculate $E_L(\mathbf{R}')$ and other quantities of interest.

7. Calculate Green's function associated with the branching process, given by equation 2.174. This Green's function dictates the process of creation and destruction of electronic configurations. If the configuration obtained through the electronic displacements represents a decrease in the local energy of the system, then multiply the number of configurations in this region of space; otherwise, this configuration is destroyed. Therefore, the number of copies that will be generated is given by

$$M_B = \text{int}(\tilde{G}_B + \xi). \tag{2.186}$$

If $M_B = 1$, one keeps the configuration, if $M_B = 0$, one rejects the configuration, and if $M_B \neq 0$, weight $E_L(\mathbf{R}')$ and other quantities by $\tilde{G}_B$.

8. Pick a new configuration and repeat steps *3* to *7*, until reaching the total number of configurations.

9. Calculate the average $\langle E_L(\mathbf{R}') \rangle$ as an estimator of the ground-state energy. This average is weighted by the distribution f_∞, see equation 2.182.

10. Use the cumulative of $\langle E_L \rangle$ to update the trial energy E_T according to

$$(E_T)_{\text{new}} = \frac{1}{2}[(E_T)_{\text{old}} + \langle E_L \rangle]. \tag{2.187}$$

11. "Renormalize" the number of configurations to the initial number N_c by either randomly eliminating or copying from the existing list of configurations.

12. Repeat steps *3* to *11* until there is no systematic trend reflected in the averages of $\langle E_L \rangle$ and other quantities. At this stage, steady state has been reached, and all traces of the initial conditions are gone.

13. Reset all cumulative averages and repeat steps *3* to *11* until the variance in $\langle E_L(\mathbf{R}')\rangle$ has reached the desired level.

Now that we have discussed the theoretical and computational methods used in this work, we turn our discussion to the analysis of the results obtained. In the next section, we present the computational details of our simulations, discuss the theoretical methods for the analysis of results, and discuss the results themselves.

CHAPTER 3

Results and Discussion

Computational Details

In this section, we describe the overall procedure to obtain the ground-state energy of the studied boron clusters, and the computational and technical details of each method used in this work.

We used the Hartree-Fock (HF), density functional theory (DFT) and quantum Monte Carlo (QMC) simulations to investigate the electron properties of small neutral and charged boron clusters. The starting point of this work was determining the atomic structures of all boron clusters. We performed the optimization of the atomic structures by using DFT/B3LYP calculations, where the orbitals were expanded in a set of Gaussian functions introduced by Pople [93], with the addition of diffused and polarized functions, the 6-311+G* basis set, as implemented in the Gaussian program [94]. A brief detail about functional B3LYP is discussed in section 2.2.1. The procedure to obtain the optimized ground-state structures is as follows. Based on previous works in literature [19,31,32,34], we obtained a set of atomic spatial coordinates with different multiplicities for each neutral cluster, B_n with $n = 2$ up to $n = 13$. The Gaussian program was employed to optimize initial geometry in order to obtain the ground-state geometry of the neutral cluster. Once the neutral cluster geometry has been obtained, we add an electron[1] to the neutral cluster and again allowed the program to optimize the new structure, to obtain the anionic cluster, B_n^-. Similarly, to obtain the cationic cluster, B_n^+, we remove an electron from the neutral cluster and optimize the structure, following the same procedure. With this procedure of optimization we obtained a set of neutral, anionic and cationic lowest-energy boron clusters, B_n with $n = 2$ up to 13, that are in agreement with the best results for the

1. The addition/removal of one electron in the cluster is done by setting the number of electrons, and the multiplicities, in an input file of the program.

geometry of the ground-state in literature [15, 19, 27–32, 34, 35, 95], at DFT level. We also obtained other structures of interest by adding or removing an electron from a referential cluster and, in this case, preserving the geometric structure of the referential cluster. For example, consider a reference anionic cluster B_n^- and that an electron is removed from its valence shell, forming a neutral cluster. If the neutral structure preserves the geometry of the anionic cluster, then, the resulting cluster is denoted by $B_n^{0,-}$, which can be read as, the neutral cluster with the anionic geometry. If an electron is detached from a neutral cluster B_n and its geometry is preserved we, thus, obtain the cluster $B_n^{+,0}$ (the cationic cluster with the neutral geometry). Other unrelaxed structures are possible, such as, $B_n^{-,0}$, $B_n^{2-,-}$, $B_n^{0,+}$, $B_n^{2+,+}$, and so forth. These structures are relevant in this work for the case that we want to analyze the binding energy in a specific process, where, when the structures loss or receive an electron, they do not have sufficient time to relax their geometry. This kind of process is further discussed in the text. This procedure described above was employed for all cyclic structures and for some linear structures of interest.

Once the geometric structures and the molecular orbitals of all boron clusters are determined from DFT, we use them as input data for the quantum Monte Carlo calculations. We performed all-electron QMC simulations using the CASINO code [86, 96]. We used the variational Monte Carlo (VMC) method to find an optimized correlated many-body trial wave function of the Slater-Jastrow type, which has the form,

$$\Psi_T(\{\mathbf{r}_i\},\{\mathbf{r}_I\}) = D_\uparrow(\phi_i)D_\downarrow(\phi_i)e^{J(\{\mathbf{r}_i\},\{\mathbf{r}_I\})} \tag{3.1}$$

where $D_\uparrow$ and $D_\downarrow$ are Slater determinants formed by single-particle spin-up and spin-down orbitals, respectively, which are extracted from the DFT calculations, and J is the Jastrow factor, which describe the correlation between the electrons. The Jastrow term, given by 2.122, was developed by Drummond-Towler-Needs [85] and is implemented in CASINO code. The correlation factor includes electron-electron, electron-core, and electron-electron-core correlation terms, and its expansion coefficients are variationally optimized by minimizing the variance of the VMC energy [83, 97]. In VMC calculations we used about 74 variational parameters, where 16 parameters are of $u(r_{ij})$-type, 6 of $\chi_I(r_{iI})$-type and 52 of $f_I(r_{Ii}, r_{Ij}, r_{ij})$-type. More details about the trial wave function Ψ_T and the analytical form of the terms u, χ and f, are discussed in sections 2.3.5 and 2.3.5.1, respectively.

Subsequently, diffusion Monte Carlo (DMC) simulations were performed so as to remove most of the remaining variational bias. In this method, the optimized trial wave function is used as a guide wave function for the importance sampling approach and an imaginary time operator $e^{-\tau H}$ is repeatedly used within the short-time approximation so as to propagate the trial wave function to the long time limit ($\tau \to \infty$), to eliminate the higher states, and thus to converge to the ground-state [92]. We also employed the

fixed-node[82] DMC (FN-DMC) approximation in which the nodes of the DMC solution are considered to be the nodes of the trial wave function. For all the studied systems, we performed the DMC calculations of energy for a series of three runs with time steps of 0.01, 0.005 and 0.001 a.u. in order to extrapolate linearly to a zero time step. For all employed time steps, we obtained an acceptance ratio greater than 98%. We used 20000 DMC moves to equilibrium of the system and 40000 or more DMC moves to accumulation of the averages. A check in the number of equilibrium moves showed that the number of 20000 is sufficient for the studied systems, and from that stage one can accumulate data for the average of the energy.

In this work we used the Hartree-Fock method, as implemented in the Gaussian09 program to obtain the HF energy for the purpose of analyzing the electron correlation energy of the studied systems. In order to obtain an accurate HF energy, necessary to estimate the correct electron correlation energy, we made an extrapolation of the HF energy for the case of a complete basis set limit. From the optimized structures obtained at DFT level, we made single points calculation at HF level, i.e., the geometric structures obtained at DFT level are maintained in HF calculations. To extrapolate the energy to the complete basis set (CBS) in the valence shell, we used the basis sets developed by Dunning [98] and coworkers, which are aug-cc-PVDZ, aug-cc-PVTZ, aug-cc-PVQZ and aug-cc-PV5Z. For each boron cluster we calculated the HF energy for each of the four basis sets, and the extrapolations were made by fitting the HF energy with an exponential form $Y(i) = Y_{CBS} + Ae^{-Bi}$, where Y_{CBS} is the energy to the limit of a complete basis set in the valence shell, and $i = 1, 2, 3, 4$ stand for DZ, TZ, QZ and 5Z, respectively.

After specifying the computational and technical details of our work, we turn our discussion to the physical and chemical properties of the studied boron clusters.

The atom and the dimer of boron: neutrals, anions and cations

Initially, we present our results for the total energy, at HF-CBS and FN-DMC level, of the boron atom and dimer and compare these with the best results available in literature. Subsequently, we present our results for the charged clusters as well as results for the atomization energy of the dimers, which is the energy related to the bond of the structure.

Table 3.1 shows the values of the total energy for the atom and dimer, obtained with HF-CBS, and FN-DMC for zero time step extrapolation. We compare our results with available data in literature for the exact energy, accurate HF calculations, and for advanced quantum Monte Carlo with multideterminant expansions in the Slater-Jastrow wave function (MD-DMC).

Table 3.1: Energy, in a.u., for the atom and dimer of boron. M represents the spin multiplicity. The number in parentheses indicates the statistical uncertainty in the last shown digit.

	M	HF	HF-CBS[a]	MD-DMC	FN-DMC[a]	E_{exact}
B	2	−24.529061[b]	−24.5334	−24.65359(4)[d]	−24.6405(2)	−24.65391[e]
B_2	3	−49.09088[c]	−49.0953	−49.4137(2)[d]	−49.3837(3)	−49.415(2)[c]

[a]Our work. Values extracted from references [b]Ref.[10], [c]Ref.[99], [d]Ref.[11] and [e]Ref.[100]

Our single determinant FN-DMC total energy shows a good agreement with available results. When compared to the exact estimated energy and the MD-DMC energy of Morales *et al.* [11], our FN-DMC results show a discrepancy of 0.4 eV for the atom and 0.8 eV for the dimer. Morales [11] reports that the extrapolated MD-DMC energy recover more than 99.7% of the correlation energy for the atom and the dimer of boron. Our FN-DMC energy recover about 85% of the electron correlation energy for the atom and 89% for the dimer. For the estimation of the percentage of the electron correlation recovered we are considering that the exact correlation energy is defined as, $|E_{\text{exact}} - E_{\text{HF}}|$, and the estimated correlation energy in this work is defined as, $|E_{\text{FN-DMC}} - E_{\text{HF-CBS}}|$. In our calculations, we consider only a single determinant Slater Jastrow wave function, and we see that a considerable correlation energy can be recovered with this methodology.

Table 3.2 shows the results obtained for the FN-DMC energy for the neutrals, anions and cations as well as the atomization energy for the neutral and charged dimers.

Table 3.2: Total FN-DMC energy, in a.u., for the atom and dimers and the atomization energy E_a, in eV, for the dimers. M represents the spin multiplicity of the system and R_0 is the bond length in Å. The number in parentheses indicates the statistical uncertainty in the last shown digit.

Cluster	M	R_0	Energy	E_a		
				FN-DMC	CCSD(T)	Exp.
B	2		−24.6405(2)			
B^-	3		−24.6521(2)			
B^+	1		−24.3295(1)			
B_2	1	1.641	−49.3611(2)	2.18(1)	2.08[a]	
B_2	3	1.616	−49.3837(3)	2.79(1)	2.79[a]	2.9(6)[c]
B_2^-	4	1.621	−49.4644(3)	4.67(1)	4.74[a]	
B_2^+	2	1.823	−49.0345(3)	1.76(1)	1.68[b]	0.8(6)[d]

Extracted values from [a] Ref.[33], [b]Ref.[95](values obtained from CCSD(T) heats of formation at 0 K), [c]Ref.[101] and [d]Ref.[20]

The obtained atomization energies of the neutral dimer, defined as $\Delta E(B_2 \rightarrow 2B)$, in the singlet and triplet states are 2.18(1) and 2.79(1) eV, respectively. These results are in good agreement with the values of CCSD(T) [33] which are 2.08 and 2.79 eV, respectively, and agree with the experimental value obtained by Chase *et al.* [101] which is provided with a large uncertainty. For the anionic and cationic dimers in the quadruplet and doublet spin states, respectively, the FN-DMC atomization energy defined as, $\Delta E(B_2^- \rightarrow B + B^-)$ for the anion, and $\Delta E(B_2^+ \rightarrow B + B^+)$ for the

cation, agree within about 0.1 eV with the CCSD(T) [33] values. However, the available experimental measurements [20] for the cationic ones provide a value too low, about half the theoretical value. As far as we know, no experimental results are available for the atomization energy of the anionic boron dimer. In general, the FN-DMC method (even with single determinant) is comparable to CCSD(T) in accuracy. Thus, it is expected that the theoretical results in this case should be more reliable than the experimental ones which should have large not reported uncertainty. Later, we will return to the discussion of the atomization energy to analyze the aromaticity in terms of resonance energy.

We conclude that our methodology to obtain the total energy of boron clusters reproduces results that are in agreement with experimental and theoretical available results. This gives us reliability in the results obtained for the total energy and electronic properties of larger clusters, with up to 13 atoms, studied in this work.

Study of the electronic properties of neutral boron clusters B_n ($n = 3$–13), its anions and cations

In this section, the theoretical approach to the electron affinity and the ionization potential is discussed in the context of atomic and molecular systems [102]. We define the electron binding energies such as Adiabatic Detachment Energy (ADE), Vertical Detachment Energy (VDE), Adiabatic Ionization Potential (AIP) and Vertical Ionization Potential (VIP), which are fundamental quantities in this work. We also discuss the decomposition of these electron binding energies in terms of three physical components, which provide informations about the nature of the energy involved in the stabilization of the cluster. Subsequently, we present the results obtained in this work for the electron binding energy and the energy decomposition for each boron cluster, B_n ($n = 3$–13), their anion and cations, and we compare our results with experimental and theoretical results available in literature. As a matter of organization, we separated our results and discussion by cluster size. We start by discussing the neutral, anion and cation boron trimer (B_3, B_3^- e B_3^+) and we conclude with the 13-atomic boron clusters, (B_{13}, B_{13}^- e B_{13}^+).

Electron Affinity and Ionization Potential

The Electron Affinity (EA) and the Ionization Potential (IP) are two fundamental quantities of theoretical, computational and experimental interest in the study of clusters, since these quantities provide us with information about the electronic structures of such systems.

The electron affinity of a neutral cluster is defined as the minimal amount of energy necessary to bind an electron to its structure to form the anionic cluster. This binding energy of the electron to the cluster can be theoretically estimated as the energy

difference between the neutral and the anionic cluster,

$$\Delta E_e \equiv EA = E_n(N) - E_a(N+1), \tag{3.2}$$

where $E_n(N)$ represents the total energy of the neutral cluster and $E_a(N+1)$ the total energy of the anionic cluster. The indexes n and a indicate the electronic state of the neutral and anionic system, respectively. For the electronic ground-state, the equation 3.2 is written as

$$\Delta E_e \equiv EA = E_0(N) - E_0(N+1). \tag{3.3}$$

The equilibrium geometry of each structure can define three types of electron affinity. If both structures in equation (3.2) are calculated at the equilibrium geometry of the neutral system, this energy difference is known as *Vertical Electron Affinity* (VEA) or *Vertical Attachment Energy* (VAE). We can interpret the VEA as the energy necessary to the near-instantaneous addition of an electron to a neutral cluster. During such a process there is no time for the geometry relaxation; thus, both structures are at the optimized equilibrium geometry of the neutral cluster. If the energies in equation (3.2) are calculated considering the equilibrium geometry of the anion, thus, this process is know as *Vertical Detachment Energy* (VDE). Conceptually, the process of VDE is equivalent to the VEA, but in VDE the energy involved is due to the removal of an electron from the anionic cluster, without geometry relaxation. Thus, the resulting neutral clusters are at the equilibrium geometry of the anion. When the total energies of the neutral and anion in equation (3.2) are calculated at their respective equilibrium geometries, this process is known as *Adiabatic Electron Affinity* (AEA) or *Adiabatic Detachment Energy* (ADE). In this process the electron is removed from the anionic cluster and the formed neutral cluster relaxes its structure reaching equilibrium geometry. A qualitative diagram of potential energy is shown in Figure 3.1 where the three types of electron affinity are illustrated. Nowadays, due to the advance in experimental apparatus and techniques, experiments using photoelectron spectroscopy can evaluate the ADE and VDE of clusters with good accuracy. Thus, in this context, the theoretical and computational calculations of VDE and ADE are very important to determine the geometry and electronic properties of these systems.

The Ionization Potential (IP) is the amount of energy necessary to remove an electron, the one that is most weakly bonded to the nucleus (the valence electron), of a neutral cluster, to form a cationic cluster. The IP can be theoretically calculated as,

$$\Delta E_e \equiv IP = \ E_c(N-1) - E_n(N), \tag{3.4}$$

where $E_c(N-1)$ is the energy of the cationic system and the index c indicates the electronic

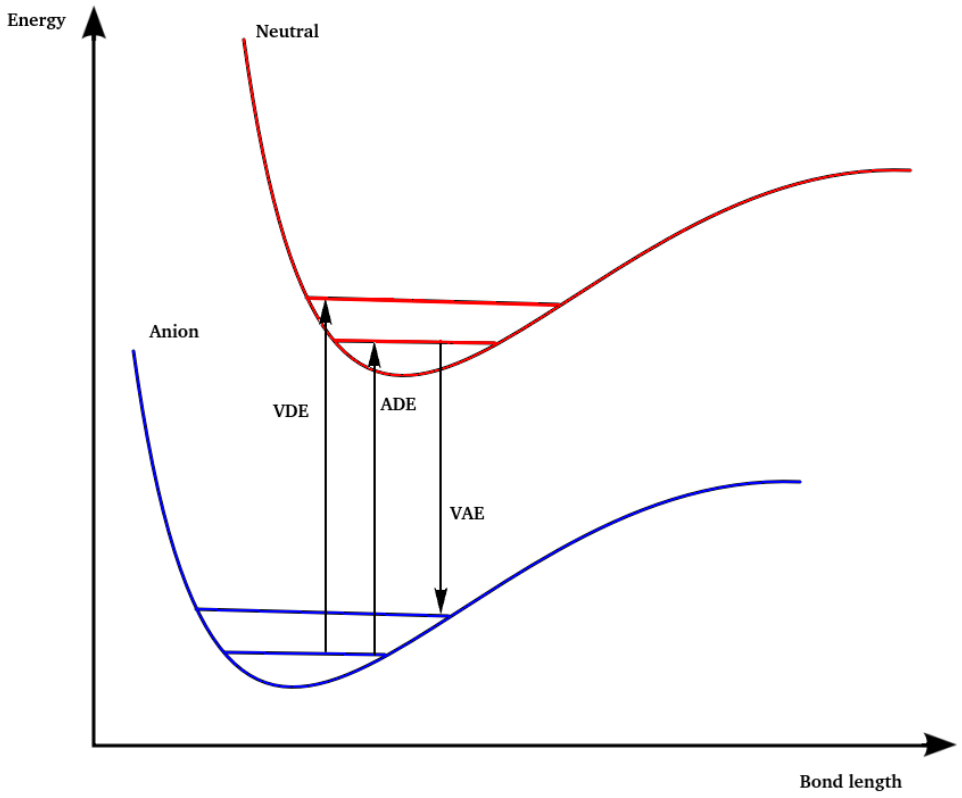

Figure 3.1: Illustrative diagram of potential representing different types of electron affinities.

state of the structure. For the electronic ground-state we have,

$$\Delta E_e \equiv IP = \ E_0(N-1) - E_0(N). \tag{3.5}$$

In relation to the equilibrium geometry of the structures we can define two types of ionization potential of interest. The process of removal of an electron from a neutral cluster without relaxation of the structure is called *Vertical Ionization Potential* (VIP). In this case, both energies in equation (3.4) are calculated at the equilibrium geometry of the neutral cluster. The *Adiabatic Ionization Potential* (AIP) is defined considering equation (3.4) with energies calculated at their respective equilibrium geometries. This means that in this process, when an electron is removed from its valence shell, the neutral cluster relaxes its geometry forming the equilibrium geometry of the cation. The diagram in Figure 3.2 represents such ionization potentials.

These electron binding energies are fundamental quantities in cluster science since they provide us with an insight of the electronic structure of clusters. Furthermore, understanding the nature of these binding energies is of considerable interest for a comprehension of the chemical bonding theory in clusters. In the next section, we discuss an approach that provides a physical insight into the nature of the binding energies of clusters in terms of the electrostatic and exchange energy, the relaxation energy and the electron correlation energy.

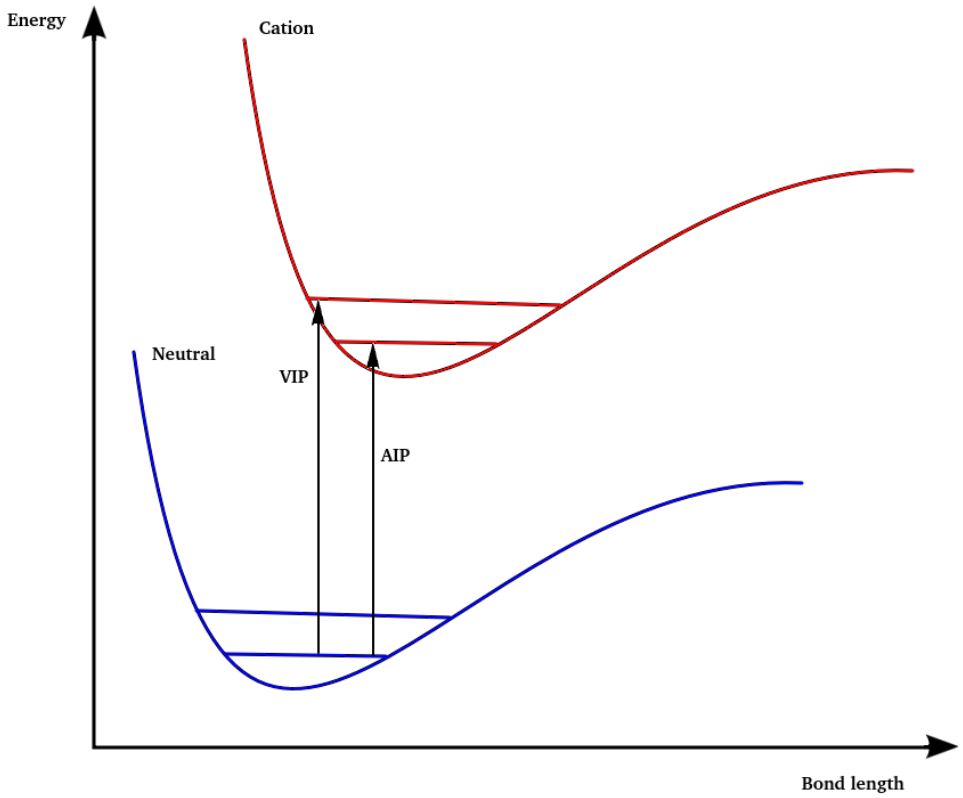

Figure 3.2: Illustrative diagram of potential representing different types of ionization potentials.

Decomposition of the electron binding energies

In order to study the nature of the electron binding energies previously discussed, we decomposed them into three physical components by adopting the Kaplan *et al.* [47] procedure as

$$\Delta E_e = \Delta E_e^{\mathrm{KT}} + \Delta E_{\mathrm{relax}}^{\mathrm{HF}} + \Delta E_e^{\mathrm{corr}}, \tag{3.6}$$

where, ΔE_e is the electron binding energy such as VDE, ADE, VIP and AIP. For the electronic ground-state, the Koopmans term ΔE_e^{KT} is defined as

$$\Delta E_e^{\mathrm{KT}} = E_0^{\mathrm{SCF}}(N-1)_{\mathrm{nonrelax}} - E_0^{\mathrm{SCF}}(N), \tag{3.7}$$

for the ionization potential, and

$$\Delta E_e^{\mathrm{KT}} = E_0^{\mathrm{SCF}}(N) - E_0^{\mathrm{SCF}}(N+1)_{\mathrm{nonrelax}}, \tag{3.8}$$

for the electron affinity. In equations (3.7) and (3.8) the energies are calculated at HF level with the Self Consistent Field (SCF) procedure, and the energies $E_0^{\mathrm{SCF}}(N-1)_{\mathrm{nonrelax}}$ and $E_0^{\mathrm{SCF}}(N+1)_{\mathrm{nonrelax}}$ are calculated with the same SCF orbitals of the neutral structure $E_0^{\mathrm{SCF}}(N)$.

According to Koopmans' theorem [66], we can also calculate the term ΔE_e^{KT} as

$$\Delta E_e^{\mathrm{KT}} = -\epsilon_e, \tag{3.9}$$

where ϵ_e corresponds, for the IP, to the energy of the last occupied orbital of the neutral cluster and, for EA, it corresponds to the first unoccupied (virtual) orbital of the neutral cluster. Koopmans' theorem is discussed in more details in section 2.1.1 of this work. We see that because the term ΔE_e^{KT} is obtained at a SCF method within an approximation of the "frozen" orbitals, i.e., the SCF orbitals of the clusters with $(N+1)$ or $(N-1)$ electrons are considered the same as the neutral cluster, this term takes into account only electrostatic and exchange energy, and the energy due to the relaxation of the structure and the orbitals is not considered. The remaining HF energy is denoted by $\Delta E_{\mathrm{relax}}^{\mathrm{HF}}$, which is the relaxation energy that takes into account the orbital relaxation or the charge redistribution effects and also the geometrical relaxation. This term is calculated as,

$$\Delta E_{\mathrm{relax}}^{\mathrm{HF}} = \Delta E_e^{\mathrm{HF}} - \Delta E_e^{\mathrm{KT}}. \tag{3.10}$$

The last term, $\Delta E_e^{\mathrm{corr}}$, is the correlation energy and is defined, following the general definition of Löwdin [103], by

$$\Delta E_e^{\mathrm{corr}} = \Delta E_e - \Delta E_e^{\mathrm{HF}}. \tag{3.11}$$

This term depends on the method used to treat the electron correlation of the system. In this work, we used the Diffusion Monte Carlo within the fixed node approximation to calculate the exact energy of the system. Thus, in our methodology, the electron correlation energy in the binding energy is defined as the difference between the exact ground-sate (approximately given by the FN-DMC energy) and the HF energy in a complete basis set limit, and is calculated as,

$$\Delta E_e^{\mathrm{corr}} = \Delta E_e^{\mathrm{FN-DMC}} - \Delta E_e^{\mathrm{HF-CBS}}. \tag{3.12}$$

This methodology of energy decomposition is very useful because it gives us an understanding, at the electronic level, of the contribution of different types of interactions in cluster formation.

Now, we discuss our obtained results for the boron clusters, from B_3 up to B_{13}, their anions and cations. First of all, we point out some general considerations about

the studied boron clusters. Then, we present geometric structures[2], obtained at DFT level, and the HF-CBS, DFT and FN-DMC energies obtained for the neutral, anionic and cationic boron clusters studied in this work. From the obtained total energy we calculate the electron binding energies ADE, VDE, AIP and VIP. These electron binding energy are compared with experimental and theoretical data available in literature, and their decomposition is discussed. We end up the presentation of the results discussing the stability of some specific small neutral and charged boron clusters in terms of the aromaticity.

Overall considerations

Concerning the total energy of the neutral, anionic and cationic boron clusters, all structures follow the same trend. When the neutral clusters gain one electron forming the anionic one, they become energetically more stable, whereas when they lose one electron forming the cationic state, their ground-state energies increase. However, the gain or loss of a second electron, respectively, in the anionic and in the cationic states will lead to an increase of their ground-state energies.

Our search for the structure that represents the ground-state of each boron cluster was performed using Gaussian09 program at DFT level with B3LYP/6-311+G*. Several isomers were considered, and a large number of input geometries were optimized with different spin multiplicities. The isomers that presented very close energies were analyzed at FN-DMC level, with zero time step extrapolation. The lowest-lying energy structures at FN-DMC were defined as the ground-state. We determined the ground-state of the boron clusters in full agreement with the best geometries reported in literature. Furthermore, with these obtained geometries, the FN-DMC results showed a very good agreement with the available experimental data, supporting the hypothesis that these structures, chosen as the ground-state of the boron clusters, must be the most populated in the experiments.

We also calculated the electron correlation energy per electron for each of the lowest-energy boron clusters, using the results of the total energy obtained from HF-CBS and FN-DMC calculations. We obtained values for the electron correlation per electron that were a little lower than 1 eV. This is reasonable since for the normal phase of metals, the typical value is 1 eV [104]. Figure 3.3 shows the size-dependence of the electron correlation energy per electron of the boron clusters B_n, from $n = 3$ up to $n = 13$, their anions and cations. From $n = 3$ to $n = 7$, the electron correlation per electron of the neutral, anionic, and cationic clusters varies rapidly, and they show an alternating pattern. The closed-shell systems are relatively more favorable in terms of correlation

2. The cartesian coordinates used in this work are available in Apendix C

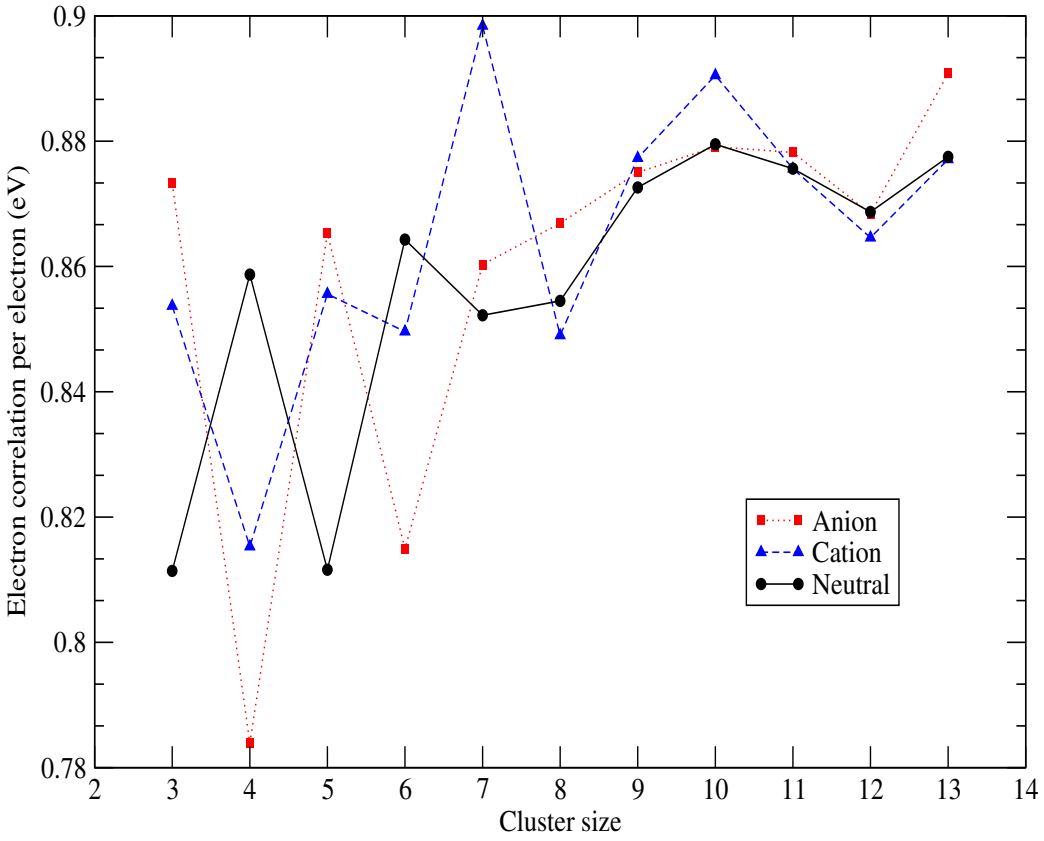

Figure 3.3: Size-dependence of the electron correlation per electron, in eV, for the neutral (black circles), anionic (red square), and cationic (blue up triangle) lowest-energy boron clusters. Values obtained from FN-DMC and HF-CBS calculations.

energy than the neighbors of open-shell systems. From $n = 8$ to $n = 10$, the electron correlation increases and varies more smoothly, for the three states. From $n = 10$ to $n = 12$, the electron correlation decreases and for $n = 13$ it increases again, for all three states, whether for open- or closed-shell systems.

A fundamental quantity to measure the relative stability of a cluster is the atomic binding energy per atom[3](ABE). The atomic binding energy is the amount of energy required to separate the atoms of a cluster, which are bonded to one another, infinitely apart. In other words, the atomic binding energy is the minimum amount of energy necessary to maintain the atoms of a cluster bonded to one another. This quantity can be estimated by the following formulas,

$$\mathrm{ABE}(B_n) = [nE(B) - E(B_n)]/n, \tag{3.13}$$

3. This quantity is also known as "average binding energy", but, because in this work we are treating the binding energy at atomic and electronic level, we distinguish them by atomic and electronic binding energies.

Table 3.3: FN-DMC results for the atomic binding energy per atom, in eV, for the lowest-energy boron clusters, and G3B3 results [34, 95] for comparison. Statistical error in the last decimal place is indicated in the parentheses.

	ABE (eV)			ABE (eV)			ABE (eV)	
	FN-DMC	G3B3		FN-DMC	G3B3		FN-DMC	G3B3
B_3	2.962(6)	2.82	B_7	4.363(6)	4.08	B_{11}	4.813(6)	4.54
B_3^-	3.806(5)	3.80	B_7^-	4.693(5)	4.47	B_{11}^-	5.076(5)	4.86
B_3^+	2.531(5)	2.28	B_7^+	4.660(5)	4.10	B_{11}^+	4.829(5)	4.57
B_4	3.637(7)	3.40	B_8	4.594(6)	4.31	B_{12}	4.867(6)	4.65
B_4^-	3.976(5)	3.82	B_8^-	4.925(5)	4.70	B_{12}^-	5.015(5)	4.85
B_4^+	3.343(5)	2.99	B_8^+	4.558(5)	4.25	B_{12}^+	4.829(5)	4.60
B_5	3.893(6)	3.65	B_9	4.628(6)	4.36	B_{13}	4.916(6)	4.63
B_5^-	4.275(6)	4.14	B_9^-	4.932(5)	4.69	B_{13}^-	5.163(5)	4.91
B_5^+	3.909(5)	3.60	B_9^+	4.662(5)	4.33	B_{13}^+	5.008(5)	4.71
B_6	4.069(6)	3.80	B_{10}	4.769(6)	4.50			
B_6^-	4.423(5)	4.33	B_{10}^-	5.027(5)	4.79			
B_6^+	4.009(5)	3.69	B_{10}^+	4.820(5)	4.47			

$$\mathrm{ABE}(B_n^-) = [(n-1)E(B) + E(B^-) - E(B_n^-)]/n, \tag{3.14}$$

$$\mathrm{ABE}(B_n^+) = [(n-1)E(B) + E(B^+) - E(B_n^+)]/n, \tag{3.15}$$

for the neutral, anionic, and cationic boron clusters with n atoms, respectively. The quantities $E(B)$, $E(B^-)$, $E(B^+)$, $E(B_n)$, $E(B_n^-)$, and $E(B_n^+)$ are the total energy of the B-atom, anion B^-, cation B^+, B_n cluster, B_n^- cluster, and B_n^+ cluster, respectively.

Table 3.3 shows our FN-DMC results for the ABE for the neutral, anionic, and cationic lowest-energy boron clusters. For comparison, we also show the values obtained from the G3B3 heats of formation at 0 K, obtained by Tai *et al.* [34, 95]. Note that, the G3B3 method always underestimates the FN-DMC value about 6% for the neutrals, 4% for the anions, and 8% for the cations, but agree qualitatively following the same trend.

Figure 3.4 shows the size-dependence of the atomic binding energy per atom, obtained from FN-DMC calculations. We see that the atomic binding energy per atom increases as a function of n, for the neutral, anionic, and cationic boron clusters. For the small-size boron clusters (from $n = 3$ up to $n = 8$), the ABE grows rapidly, and from $n = 8$ up to $n = 13$ the ABE varies more smoothly. Among the three states (neutral, anionic, and cationic), the anionic clusters present the highest ABE, i.e., the anionic clusters are the ones which show the highest average energy of stabilization per atom, except for the hepta-atomic boron clusters, where cation B_7^+ shows the highest ABE, but very close to the ABE of the anion. Among the neutral and cationic clusters, for the cases $n = 3, 4, 6, 8, 12$, the neutral clusters have a higher ABE than the cation, and for the cases $n = 5, 7, 9, 10, 11, 13$ the cation clusters show a higher ABE than the neutral.

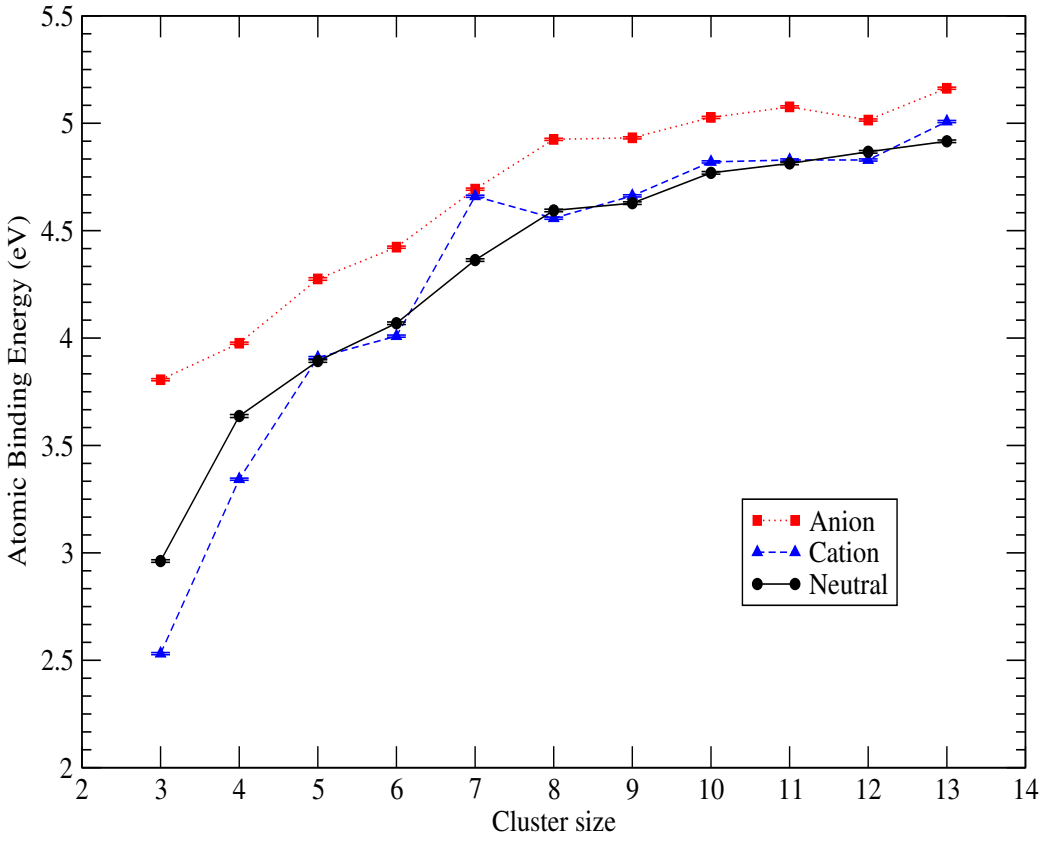

Figure 3.4: Size-dependence of the atomic binding energy per atom, in eV, for the neutral (black circles), anionic (red square), and cationic (blue up triangle) lowest-energy boron clusters. Values obtained from FN-DMC calculations.

B_3, B_3^- and B_3^+

The geometric structures of lowest energy are shown in Figure 3.5, which are in agreement with the ones reported in literature [15, 19, 95]. All three structures, neutral, anion and cation, form an equilateral triangle with bond length of 1.548, 1.542 and 1.564 Å, respectively. The spin multiplicities that configures the ground-state of these clusters are, doublet for the neutral, singlet for the anion and singlet for the cation.

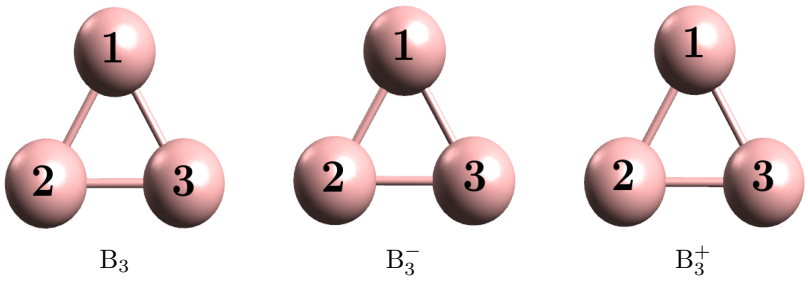

B_3 B_3^- B_3^+

Figure 3.5: Ground-state geometric structures of trimer boron clusters, obtained at B3LYP/6-311+G*

The results obtained for the total energy at HF-CBS, DFT and FN-DMC levels are given in Table 3.4, for the relaxed structures, neutral, anion and cation and the

unrelaxed clusters which are, the neutral with the anion geometry ($B_3^{0,-}$) and the cation with the neutral geometry ($B_3^{+,0}$).

Table 3.4: Total energy, in a.u., at HF-CBS, DFT (B3LYP/6-311+G*) and FN-DMC, and spin multiplicity M for the ground-state trimer boron clusters. Statistical error in the last decimal place is indicated in the parentheses.

Cluster	M	Energy		
		HF-CBS	DFT	FN-DMC
B_3	2	−73.8008	−74.2983	−74.2481(4)
B_3^-	1	−73.8392	−74.3970	−74.3527(4)
B_3^+	1	−73.4504	−73.9361	−73.8896(4)
$B_3^{0,-}$	2	−73.8004	−73.2982	−73.2479(3)
$B_3^{+,0}$	1	−73.4509	−74.9359	−74.8891(5)

In Table 3.5 we present results for the electron binding energy, obtained from the total energy at FN-DMC level, together with experimental results and other theoretical approaches in literature for comparison.

Table 3.5: The ADE, VDE, AIP, and VIP values for the anionic and neutral trimer boron clusters and comparison with the experimental results; the energies are in eV.

		DFT	G3B3	CCST	FN-DMC$_{\text{(This work)}}$	Exp.
ADE	B_3^-	2.688	2.91[c]	2.88[c]	2.85(2)	2.82(2)[a]
VDE	B_3^-	2.691		2.88[a]	2.85(1)	2.82(2)[a]
AIP	B_3	9.813	9.87[d]		9.76(2)	9.7[b], 14.0[b]
VIP	B_3	9.861			9.77(2)	

[a]Ref. [15], [b]Ref. [20] [c]Ref. [34], [d]Ref. [95], and DFT values from Ref. [35]

The values for the ADE and VDE show good agreement with the experimental results of Zhai *et al.* [15] within the statistical error, as well as with the theoretical results of the CCSD(T) obtained by Zhai *et al.* [15] and Tai *et al.* [34], G3B3 by Tai *et al.* [34] and DFT-B3LYP by Akman *et al.* [35], with the deviation being smaller than 0.2 eV. The experimental accuracy of AIP in comparison with ADE and VDE is not good because only the lower and upper boundaries of AIP are determined in the experiments. Our FN-DMC results agree with the lower boundary value of AIP for B_3, and the VIP and AIP DFT results of Akman*et al.* [35] overestimate the FN-DMC values by about 0.1 eV. The G3B3 results of Tai *et al.* [34] are also larger than the FN-DMC values of AIP by about 0.1 eV. The overall agreement between the FN-DMC results and the available experimental data for the electron binding energies VDE, ADE, and AIP is a good indication that our calculations are quite accurate for the boron trimer.

Table 3.6 shows the results obtained for the decomposition of the electron binding energies ADE, VDE, AIP and VIP in the ground-state of the trimer boron cluster.

For the anionic cluster B_3^-, the main factor of stabilization of the attached electron is the correlation energy, which contributes with 64% for the ADE and 63% for the VDE.

Table 3.6: Decomposition of the ADE, VDE, AIP, and VIP of the trimer boron clusters. Statistical error in the last decimal place is indicated in the parentheses. All energies are in eV.

		$\Delta E_e^{\mathtt{KT}}$	$\Delta E_{\mathtt{relax}}^{\mathtt{HF}}$	$\Delta E_e^{\mathtt{corr}}$	ΔE_e
ADE	B_3^-	0.37	0.67	1.81(2)	2.85(2)
VDE	B_3^-	0.37	0.69	1.79(1)	2.85(1)
AIP	B_3	9.94	−0.41	0.23(2)	9.76(2)
VIP	B_3	9.94	−0.42	0.25(2)	9.77(2)

The electrostatic and exchange interactions, described by the Koopmans energy $\Delta E_e^{\mathtt{KT}}$, contribute about 13% for both ADE and VDE, and the relaxation effects are 23% for ADE and 24% for VDE. For the neutral cluster, the Koopmans contribution $\Delta E_e^{\mathtt{KT}}$ is absolute in stabilizing the formation of B_3 with 102%[4] for both AIP and VIP. It means that this cluster is very stable even at HF level. The relaxation energy plays a destabilizing role, but its contribution to both AIP and VIP is small being less than 5%, and the correlation energy of the detached electron represents only 3% for both AIP and VIP. Therefore, in terms of the formation characteristics we can infer that the neutral and the anion trimer boron cluster are quite different. The neutral cluster has well defined features determined by the electrostatic and exchange interactions, while the anionic one is stabilized by the relaxation energy and the correlation effects.

B_4, B_4^- and B_4^+

For the clusters with four boron atoms, the lowest energy structures, shown in Figure 3.6, have planar and rhombic geometries with equal bond lengths (the external bond lengths). The values of the bond lengths are 1.522 Å for the neutral, 1.568 Å for the anion and 1.546 Å for the cation. The spin multiplicities of the ground-state are singlet, doublet, and doublet for the neutral, anion, and cation, respectively. These obtained structures are in agreement with literature [15, 19, 95]. The isomers with square geometry have energy very close to the ground-state, which are the rhombic ones. The energy differences in the square and rhombic structures, according to our FN-DMC calculations, are 0.06(2), 0.22(2) and 0.03(2) eV for B_4, B_4^- and B_4^+, respectively.

4. Note that in the case of negative values of the energy in the decomposition of the electron binding energies, which means that this energy contributes in destabilizing the system, the sum of percentages are not normalized at 100%.

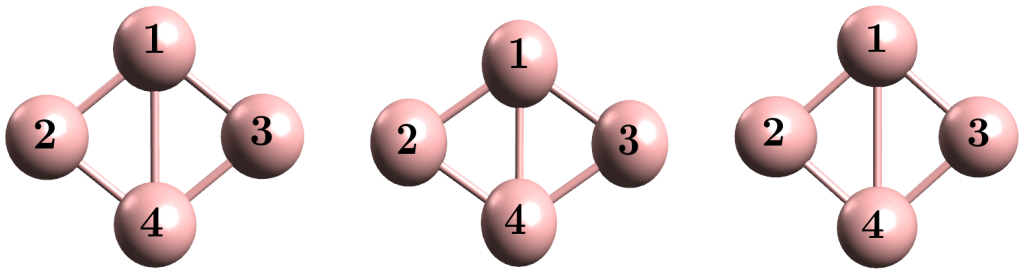

B_4 B_4^- B_4^+

Figure 3.6: Ground-state geometries of the boron clusters with four atoms, obtained at B3LYP/6-311+G*

Table 3.7 shows the total energies obtained for the ground-state tetramer boron clusters, and Table 3.8 displays the values for the FN-DMC electron binding energies with available experimental and theoretical results, for comparison. For ADE and VDE, the

Table 3.7: Total energy, in a.u., at HF-CBS, DFT (B3LYP/6-311+G*) and FN-DMC, and spin multiplicity M for the ground-state four-atomic boron clusters. Statistical error in the last decimal place is indicated in the parentheses.

Cluster	M	Energy		
		HF-CBS	DFT	FN-DMC
B_4	1	−98.4656	−99.1575	−99.0967(6)
B_4^-	2	−98.5531	−99.2269	−99.1581(4)
B_4^+	2	−98.1731	−98.8110	−98.7424(4)
$B_4^{0,-}$	1	−98.4447	−99.1451	−99.0845(5)
$B_4^{+,0}$	2	−98.1701	−98.8089	−98.7381(4)

Table 3.8: The ADE, VDE, AIP, and VIP values for the anionic and neutral tetramer boron clusters and comparison with the experimental results; the energies are in eV.

		DFT	G3B3	CCST	FN-DMC(This work)	Exp.
ADE	B_4^-	1.624	1.67[d]	1.68[d]	1.67(2)	1.6(1)[b]
VDE	B_4^-	1.834		1.85[a]	2.00(2)	1.99(5)[a]
AIP	B_4	9.430	9.86[e]		9.64(2)	9.8[c], 11.8[c]
VIP	B_4	9.486			9.76(2)	

[a]Ref. [15], [b]Ref. [19], [c]Ref. [20] [d]Ref. [34], [e]Ref. [95], and DFT values from Ref. [35]

FN-DMC results agree with the experimental results of Zai *et al.* [15] and Wang *et al.* [19] and theoretical results such as CCST and G3B3 of Tai *et al.* [34] and Zai *et. al* [15] and DFT of Akman *et. al* [35]. For AIP, our FN-DMC result is a little lower than the experimental AIP lower boundary, with a discrepancy of about 0.2 eV. The VIP and AIP DFT results of Akman *et. al* [35] underestimate the FN-DMC by about 0.2 eV and the G3B3 of Tai *et al.* [34] is larger than the FN-DMC value of AIP by about 0.2 eV. Thus, in general, our FN-DMC results are in agreement with theoretical and experimental results in literature.

Table 3.9 shows the decomposition of the electron binding energy ADE, VDE, AIP, and VIP for the tetramer boron clusters.

Table 3.9: Decomposition of the ADE, VDE, AIP, and VIP of the tetramer boron clusters. Statistical error in the last decimal place is indicated in the parentheses. All energies are in eV.

		$\Delta E_e^{\mathtt{KT}}$	$\Delta E_{\mathtt{relax}}^{\mathtt{HF}}$	$\Delta E_e^{\mathtt{corr}}$	ΔE_e
ADE	B_4^-	−0.02	2.40	−0.71(2)	1.67(2)
VDE	B_4^-	0.92	2.03	−0.95(2)	2.00(2)
AIP	B_4	8.91	−0.95	1.68(2)	9.64(2)
VIP	B_4	8.91	−0.87	1.72(2)	9.76(2)

For VDE and ADE the main factor that contributes to the stabilization of the excess electron comes from the relaxation effects, which represent 148% of ADE and 102% of VDE. The electron correlation energy takes part in the destabilization of the cluster in both processes, ADE and VDE. The correlation energy contributes to destabilizing the system with 43% of ADE and 48% of VDE. The Koopmans contribution represents roughly 50% of VDE, while for ADE it is less than 1%, therefore being negligible. For the neutral cluster, the main contribution in the stabilization of the system is the Koopmans contribution $\Delta E_e^{\mathtt{KT}}$, which represents about 92% of the AIP and 91% of the VDE. It means that this cluster is very stable at HF level. The relaxation energy contributes to the destabilization of the system and represents, for the AIP and VIP, about of 10%. The correlation energy of the detached electron in B_4 represents about 17% of the AIP and 18% of the VIP. We conclude that, for the tetramer boron cluster, the anionic cluster has features determined by the structural and orbitals relaxation energy and by the electron correlation effects while for the neutral cluster the stabilization of the system is predominantly due to the electrostatic and exchange energy with small contributions of the relaxation, destabilizing the system, and correlation effects.

B_5, B_5^- and B_5^+

Figure 3.7 shows the geometries obtained for the neutral and charged five-atomic boron clusters. The spin multiplicity obtained is, doublet for the neutral, singlet for the anionic and singlet for the cationic structures. These geometries obtained with the respective spin states agree with the structures for the penta-atomic boron clusters reported in literature [19,27,31,35,95]. We note that, when one electron is attached to the neutral cluster, forming the anionic cluster, the geometric structure changes slightly, i.e., the geometry is preserved but the bond lengths change. When an electron is detached from the neutral structure, forming the cationic cluster, the geometry changes considerably, forming an equilateral pentagon with bond length of 1.551 Å.

Table 3.10 shows the values obtained for the ground-state total energy of the penta-atomic boron clusters, and Table 3.11 shows the electron binding energies obtained

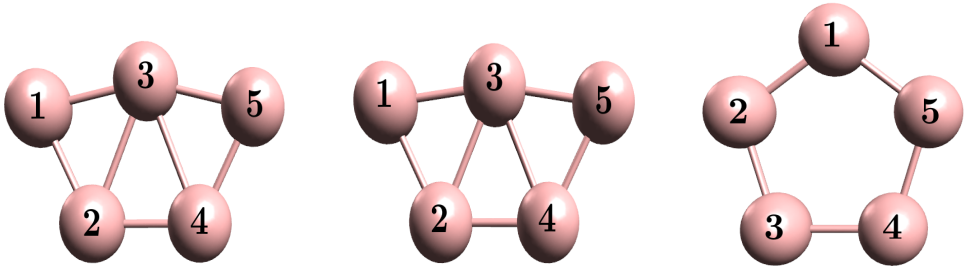

B_5 B_5^- (i) B_5^+

Figure 3.7: Ground-state geometries of the boron clusters with five atoms, obtained at B3LYP/6-311+G*

with FN-DMC calculations. For comparison, the available theoretical and experimental results of the electron binding energies are also shown in Table 3.11.

Table 3.10: Total energy, in a.u., at HF-CBS, DFT (B3LYP/6-311+G*) and FN-DMC, and spin multiplicity M for the ground-state of the penta-atomic boron clusters. Statistical error in the last decimal place is indicated in the parentheses.

Cluster	M	Energy		
		HF-CBS	DFT	FN-DMC
B_5	2	−123.1721	−124.0030	−123.9178(5)
B_5^-	1	−123.1728	−124.0809	−123.9996(7)
B_5^+	1	−122.8551	−123.6929	−123.6097(6)
$B_5^{0,-}$	2	−123.1700	−123.9983	−123.9139(6)
$B_5^{+,0}$	1	−122.8331	−123.6740	−123.5926(6)

Table 3.11: The ADE, VDE, AIP, and VIP values for the anionic and neutral penta-atomic boron clusters and comparison with the experimental results; the energies are in eV.

		DFT	G3B3	CCST	FN-DMC(This work)	Exp.
ADE	B_5^-	2.167	2.48[b]	2.29[b]	2.22(2)	2.33(2)[a]
VDE	B_5^-	2.305	2.64[b]	2.47[b]	2.33(2)	2.40(2)[a]
AIP	B_5	8.439	8.45[d]		8.38(2)	7.8[c], 8.1[c]
VIP	B_5	8.952			8.85(2)	

[a]Ref. [27], [b]Ref. [34], [c]Ref. [20], [d]Ref. [95] and DFT values from Ref. [35]

Our FN-DMC results for the ADE and VDE agree with experimental results of Zhai *et al.* [27], showing a discrepancy of about 5% and 3% eV, respectively. When compared to other theoretical results, our FN-DMC values show a very good agreement with results of the CCSD(T) and G3B3 obtained by Tai *et al.* [34], where the largest deviation is about 0.3 eV. The DFT values obtained by Akman *et al.* [35] show a good agreement with our FN-DMC results. They underestimate the FN-DMC values for the ADE and VDE by about 0.03 eV, respectively, and overestimate the FN-DMC values by 0.06 and 0.1 eV, for AIP and VIP, respectively. The FN-DMC result for AIP agrees with the G3B3 obtained by Tai *et al.* [95], with a deviation of 0.07 eV. In comparison with the experimental data, the AIP is a little higher than the available upper bond

obtained by Hanley *et al.* [20]. We conclude that the overall agreement with theoretical and experimental data is a good indicator that our calculations for the penta-atomic boron cluster is accurate. Now, we turn our discussion to the decomposition of the electron binding energies of the five-atomic boron clusters. Table 3.12 shows the contribution of the electrostatic and exchange energy, the orbital and geometry relaxation energy, and the electron correlation energy for the ADE, VDE, AIP and VIP.

Table 3.12: Decomposition of the ADE, VDE, AIP, and VIP of the penta-atomic boron clusters. Statistical error in the last decimal place is indicated in the parentheses. All energies are in eV.

		$\Delta E_e^{\mathtt{KT}}$	$\Delta E_{\mathtt{relax}}^{\mathtt{HF}}$	$\Delta E_e^{\mathtt{corr}}$	ΔE_e
ADE	B_5^-	0.37	−0.35	2.20(2)	2.22(2)
VDE	B_5^-	0.45	−0.37	2.25(2)	2.33(2)
AIP	B_5	9.89	−1.26	−0.25(2)	8.38(2)
VIP	B_5	9.89	−0.67	−0.37(2)	8.85(2)

We see that the main factor in the stabilization of the attached electron in the cluster B_5^- is the electron correlation energy, which contributes about 99% of ADE and 96% of VDE. The relaxation effects, $\Delta E_{\mathtt{relax}}^{\mathtt{HF}}$, contribute to destabilizing the system with about 16% for both ADE and VDE, and the electrostatic and exchange energy, $\Delta E_e^{\mathtt{KT}}$, contributes in stabilization with 17% for ADE and 19% for VDE. For the neutral cluster, the electrostatic and exchange interactions dominate the stabilization of the B_5, with roughly 112% for both AIP and VIP. Both the relaxation and electron correlation energies play a destabilizing role in neutral system, but its contribution is small being less than 15% for AIP and less than 8% for VIP. Therefore, we conclude that the anionic cluster is very sensitive to the electron correlation effects, which is absolute in stabilizing the system, while the neutral cluster is stabilized by the electrostatic and exchange interactions. In both systems, neutral and anionic, the relaxation effects contribute to destabilizing the system, but their contribution is small, if compared to the total value of the electron binding energy.

B_6, B_6^- and B_6^+

The ground-state structures of the hexa-atomic boron clusters B_6, B_6^-, and B_6^+ are controversial in literature [19,34]. A variety of isomers have been reported for the ground-state of the neutral hexa-tomic boron cluster. We obtained the pentagonal pyramidal structure with singlet spin multiplicity as the ground-state of the neutral system B_6(i), which is in agreement with the references [28,31,34]. We also consider the second lowest energy neutral structure B_6(ii), which has a triplet spin multiplicity, for reasons that will be further discussed. The geometries of the neutral boron clusters discussed here are shown in Figure 3.8. Our obtained structure that represents the ground-state of the anionic hexa-atomic boron cluster, B_6^-(i), has a quadruplet spin multiplicity. The second

lowest energy structure is a doublet, B_6^-(ii). The doublet is 0.42 eV higher in energy than the quadruplet, at FN-DMC calculation. Both structures are planar and their geometries are shown in Figure 3.8. The quadruplet structure, as far as we know, is not reported in the literature and the doublet is reported as the ground-state of the anionic boron cluster with six atoms [19, 28, 34]. However, our DFT B3LYP/6-311+G* and FN-DMC calculations indicated the quadruplet as the structure with the lowest energy. The shape of the cationic ground-state B_6^+ is reported as a planar hexagon, by Akman *et al.* [35] and Tai *et al.* [95]. Our results indicated that the ground-state of the cationic cluster is a pentagonal pyramid, which is a distorted case of the singlet neutral B_6, see Figure 3.8. This pentagonal pyramid is also reported by Tai *et al.* [95] as an almost degenerated case in energy of the planar hexagon cationic cluster. In our FN-DMC calculations, the planar hexagon is 0.75 eV higher in energy than the pentagonal pyramid.

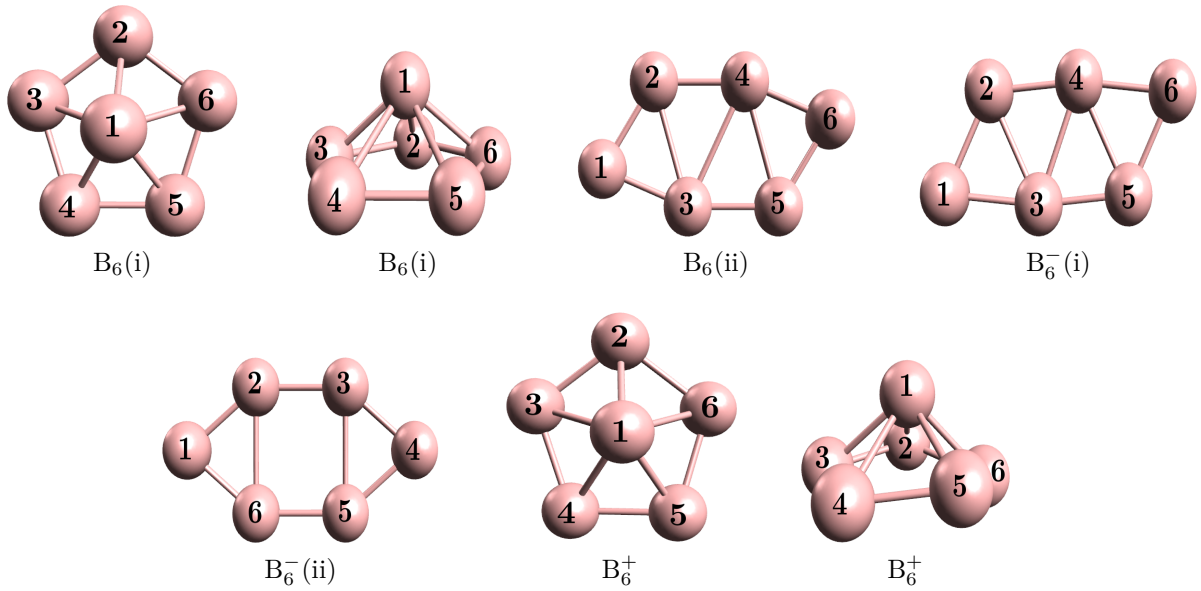

Figure 3.8: Ground-state geometries of the hexaatomic boron clusters, obtained at B3LYP/6-311+G*

The total energies, obtained with HF-CBS, DFT and FN-DMC methods, of the hexaatomic boron clusters are shown in Table 3.13.

Table 3.14 shows the FN-DMC values obtained for the electron binding energies. Other theoretical results are also shown for comparison. Although we have obtained a singlet as the ground-state of the neutral cluster, in the calculation of ADE we consider that the final state can also be triplet neutral clusters. The reason is because, as reported by Alexandrova *et al.* [28], there are features in the PES experiment that indicate that the process of photodetachment of the anion will yield a triplet as the final state [28] i.e., the neutral cluster in the ADE and VDE processes is a triplet.

In order to illustrate the complexity in the estimation of the electron binding energies of the hexaatomic boron clusters, we consider three ADEs processes and two VDEs which are possible in the PES experiment, and we compare our FN-DMC results

Table 3.13: Total energy, in a.u., at HF-CBS, DFT (B3LYP/6-311+G*) and FN-DMC, and spin multiplicity M for the ground-state of the hexaatomic boron clusters. Statistical error in the last decimal place is indicated in the parentheses.

Cluster	M	Energy		
		HF-CBS	DFT	FN-DMC
B_6	1	−147.7873	−148.8275	−148.7402(5)
B_6	3	−147.8259	−148.8295	−148.7306(5)
B_6^-	2	−147.8613	−148.9100	−148.8145(6)
B_6^-	4	−147.9016	−148.9217	−148.8299(5)
B_6^+	2	−147.5106	−148.5077	−148.4161(5)
$B_6^{0,-}$ *	3	−147.8184	−148.8195	−148.7205(6)
$B_6^{0,-}$ **	3	−147.8223	−148.8241	−148.7202(6)
$B_6^{+,0}$ ***	2	−147.4994	−148.5004	−148.4121(6)

*The energy of $B_6^{0,-}$ is calculated with the geometry of the quadruplet anionic cluster.**The energy of $B_6^{0,-}$ is calculated with the geometry of the doublet anionic cluster.***The energy of $B_6^{+,0}$ is calculated with the geometry of the triplet neutral cluster.

Table 3.14: The ADE, VDE, AIP, and VIP values for the anionic and neutral hexaatomic boron clusters and comparison with the experimental results; the energies are in eV.

		DFT	G3B3	CCST	FN-DMC(This work)	Exp.[a]
ADE	B_6^-	2.658	3.23[b]	2.59[b]	2.02(2)[1]	3.01(4)
ADE	B_6^-		3.50[b]	2.93[b]	2.28(2)[2]	3.01(4)
ADE	B_6^-				2.70(2)[3]	3.01(4)
VDE	B_6^-		3.74[b]	3.12[b]	2.57(2)[4]	3.01(4)
VDE	B_6^-				2.98(2)[5]	3.01(4)
AIP	B_6	8.410	8.59[c]	8.82[c]	8.82(2)	
VIP	B_6	9.116			8.93(2)	

[a]Ref. [28], [b]Ref. [34], [c]Ref. [95] and DFT values from Ref. [35]
[1]Considering the doublet anion and the singlet neutral.[2] Considering the doublet anion and the triplet neutral.[3] Considering the quadruplet anion and the triplet neutral.[4] Considering the doublet anion and the triplet neutral with the geometry of the doublet anion.[5] Considering the quadruplet anion and the triplet neutral with the geometry of the quadruplet anion.

with other available theoretical approaches and with the experimental data. These three considered ADE processes are the ones in which: the initial state is the doublet anionic cluster and the final state is the singlet neutral cluster; the initial state is the doublet anionic cluster and the final state is the triplet neutral cluster; and the initial state is the quadruplet anion and final is the triplet neutral, denoted here by ADE^1, ADE^2, and ADE^3, respectively. The two transitions considered for the VDE are the ones in which, the initial state is the doublet anionic cluster and the final state is the triplet neutral cluster with the geometry of the doublet anionic cluster, and, the initial state is the quadruplet anionic cluster and the final state is the triplet with the geometry of the quadruplet anionic cluster, denoted by VDE^4, and VDE^5, respectively. For the considered ADEs and VDEs we do not see a good agreement between our FN-DMC results and the G3B3 and CCSD(T) theoretical results of Tai *et al.* [34]. In all available cases for VDE and ADE, our FN-DMC underestimated the results of G3B3 and CCSD(T), with deviations from 0.7

to 1.2 eV. Our FN-DMC results that agree with the experiment are obtained considering the quadruplet anionic cluster. For the ADE[3], where we considered the triplet neutral cluster as the final state, as suggested by Alexandrova *et al.* [28] (see discussion above), we obtained a value of 2.70 eV, which is the best obtained in our work for the hexaatomic boron clusters, showing a discrepancy of 10%. For the VDE[5] an excellent agreement with the experimental data is obtained, within the statistical errors. Thus, based on our FN-DMC calculations, we may infer that the obtained geometry of the quadruplet anionic cluster can possibly represent the ground-state of the hexa-atomic anionic boron cluster. Furthermore, although the obtained ground-state of the neutral boron cluster with six atoms is a singlet, the triplet neutral cluster provides a better result for the ADE process, which is in agreement with Alexandrova's *et al.* [28] interpretation of the PES experiment. Therefore, in the decomposition of the electron binding energies we will only consider the ADE[3] and VDE[5] processes to evaluate the contribution of the electrostatic and exchange energies, the orbital and geometrical relaxation, and the electron correlation effects. For the AIP, our FN-DMC result is in a good agreement with the available theoretical results obtained by Tai *et al.* [95], within the statistical error of the FN-DMC calculation, for the CCSD(T) value, and with a deviation of 0.26 eV for the G3B3 value. The DFT values of Akman *et al.* [35] underestimate the FN-DMC value by about 0.4 eV, for the AIP, and overestimate the FN-DMC value by about 0.2 eV, for the VIP. As far as we know, there are no available experimental results for the AIP of the boron clusters greater than B_5.

Table 3.15 shows the results for the decomposition of the electron binding energies ADE, VDE, AIP, and VIP.

Table 3.15: Decomposition of the ADE, VDE, AIP, and VIP of the hexa-atomic boron clusters. Statistical error in the last decimal place is indicated in the parentheses. All energies are in eV.

		$\Delta E_e^{\mathtt{KT}}$	$\Delta E_{\mathtt{relax}}^{\mathtt{HF}}$	$\Delta E_e^{\mathtt{corr}}$	ΔE_e
ADE	B_6^-	0.92	1.14	0.64(2)	2.70(2)
VDE	B_6^-	1.43	0.83	0.72(2)	2.98(2)
AIP	B_6	9.03	−0.45	0.24(2)	8.82(2)
VIP	B_6	9.03	−0.15	0.05(2)	8.93(2)

In the total value of ADE, there is a significant contribution of the three terms which represent, the electrostatic and exchange $\Delta E_e^{\mathtt{KT}}$, relaxation of the orbitals and geometry $\Delta E_{\mathtt{relax}}^{\mathtt{HF}}$, and the electron correlation $\Delta E_e^{\mathtt{corr}}$. The term $\Delta E_e^{\mathtt{KT}}$ contributes roughly 34% to the stabilization of the attached electron in B_6^-; the term $\Delta E_{\mathtt{relax}}^{\mathtt{HF}}$ contributes 42%; and the $\Delta E_{\mathtt{relax}}^{\mathtt{HF}}$ 24%. For VDE, the main factors in the stabilization of the anion are the electrostatic and exchange interactions, which contribute 48%, and the relaxation of orbitals and the electron correlation contribute 28% and 24%, respectively. For the neutral cluster, the Koopmans contribution is absolute in stabilizing the formation of B_6 with roughly 102% for both the AIP and VIP. The relaxation effects $\Delta E_{\mathtt{relax}}^{\mathtt{HF}}$ play a destabilizing role, but its contribution is smaller than 5% for AIP and VIP. The electron

correlation effects on the stabilization of the neutral cluster are negligible, being smaller than 3%, which means that the neutral cluster is very stable at HF level. Therefore, we conclude that the stabilization of the anion B_6^- is characterized by the three physical terms discussed above, where the major contribution comes from the electrostatic and exchange interactions and the relaxation energy, while the neutral system has features well defined by the electrostatic and exchange energies.

B_7, B_7^- and B_7^+

The obtained structures that represent the ground-state of the hepta-atomic boron clusters are shown in Figure 3.9. The geometry of the neutral cluster is a hexagonal pyramid slightly distorted with a doublet spin multiplicity. For the anionic state we obtained two structures very close in energy, with spin multiplicities that were triplet B_7^-(i) and singlet B_7^-(ii). As mentioned by Tai *et al.* [34], the lowest-lying structure of B_7^- is not as well established. Our FN-DMC calculation indicated the triplet as the structure with the lowest energy, with a small separation gap of 0.13(2) eV. The anionic structures have a geometry that is a nearly planar hexagon capped by one electron at the center. The structure of the cationic cluster is similar to the anionic cluster and has a singlet spin multiplicity. All these obtained structures are in agreement with theoretical studies in literature [19, 29, 31, 34, 35, 95].

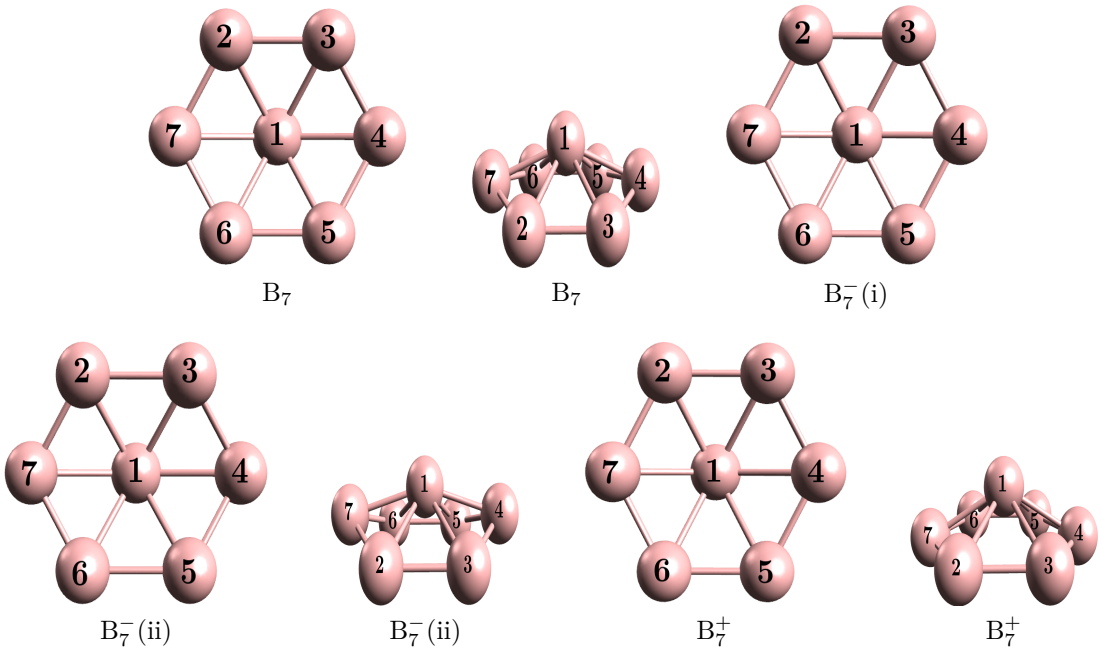

Figure 3.9: Ground-state geometries of the hepta-atomic boron clusters, obtained at B3LYP/6-311+G*

Table 3.16 shows the obtained total energies at HF-CBS, DFT and FN-DMC levels. Table 3.17 shows the FN-DMC results for the electron binding energies, the available experimental data and other theoretical results.

Table 3.16: Total energy, in a.u., at HF-CBS, DFT (B3LYP/6-311+G*) and FN-DMC, and spin multiplicity M for the ground-state of the hepta-atomic boron clusters. Statistical error in the last decimal place is indicated in the parentheses.

Cluster	M	Energy		
		HF-CBS	DFT	FN-DMC
B_7	2	−172.5096	−173.7102	−173.6058(5)
B_7^-	1	−172.5442	−173.7975	−173.6977(7)
B_7^-	3	−172.5642	−173.8038	−173.7024(5)
B_7^+	1	−172.2488	−173.4179	−173.3713(6)
$B_7^{0,-}$ *	2	−172.5030	−173.7044	−173.5997(8)
$B_7^{0,-}$ **	2	−172.4911	−173.7002	−173.5945(5)
$B_7^{+,0}$	1	−172.2365	−173.4074	−173.3018(6)

*The energy of $B_7^{0,-}$ is calculated with the geometry of the singlet anionic cluster. **The energy of $B_7^{0,-}$ is calculated with the geometry of the triplet anionic cluster.

For the case of the hepta-atomic boron cluster, we consider the triplet and singlet anionic cluster for the estimation of the electron binding energies ADE and VDE, because, as reported by Alexandrova *et al.* [19], there exist experimental evidences of the coexistence of isomers in the B_7^- cluster beam of the PES experiment. Also, their ab initio calculations suggest that at least two isomers (the triplet and singlet) coexist in the beam of the B_7^- cluster and both contribute to the photoelectron spectra of B_7^-.

Table 3.17: The ADE, VDE, AIP, and VIP values for the anionic and neutral hepta-atomic boron clusters and comparison with the experimental results; the energies are in eV.

		DFT	G3B3	CCST	FN-DMC(This work)	Exp.[a]
ADE	B_7^-		2.72[b]	2.62[b]	2.50(2)[1]	2.55(2)
ADE	B_7^-	2.545	2.67[b]	2.56[b]	2.63(2)[2]	2.55(2)
VDE	B_7^-		2.93[b]	2.87[b]	2.67(2)[3]	2.85(2)
VDE	B_7^-	2.819	2.86[b]	2.92[b]	2.94(2)[4]	2.85(2)
AIP	B_7	7.955	8.13[c]	8.36[c]	7.93(2)	
VIP	B_7	8.240			8.27(2)	

[a]Ref. [29], [b]Ref. [34], [c]Ref. [95], and DFT values from Ref. [35].
[1]Considering the singlet anionic cluster;[2]Considering the triplet anionic cluster;[3]Considering the singlet anionic cluster and the neutral with the geometry of the singlet anionic cluster;[4]Considering the triplet anionic cluster and the neutral with the geometry of the triplet anionic cluster.

Our FN-DMC results for the ADEs and VDEs are in a good agreement with other theoretical results such as the G3B3 and CCSD(T) of Tai *et al.* [34]. For the case of the ADE with the singlet anionic cluster our FN-DMC presents a deviation of 0.22 and 0.12 eV in comparison with G3B3 and CCSD(T) methods, respectively. For the case of the ADE with the triplet anionic cluster our FN-DMC result showed a deviation smaller than 0.07 eV in comparison with G3B3 and CCSD(T). For the VDE considering the singlet anionic cluster and the neutral cluster with the geometry of the singlet anionic cluster, our FN-DMC result are 0.3 and 0.2 eV lower than the CCSD(T) and G3B3 values, respectively. The FN-DMC value for the VDE in which we consider the triplet anionic

cluster and the neutral with the geometry of the triplet anionic cluster is 0.02 and 0.08 eV higher than the CCSD(T) and G3B3 values, respectively. Note, however the good agreement between our FN-DMC values and the DFT results of Akman *et al.* [35], where the DFT values underestimate the FN-DMC results for the ADE and VDE by 0.08 and 0.12 eV, respectively. In comparison to the experimental data, our FN-DMC results show a very good agreement. For the two considered ADEs we obtained a discrepancies, between our FN-DMC results and the experimental data, smaller than 3%. For the VDEs, our FN-DMC results show discrepancies of 6% for the case of the singlet anionic cluster, and 3% for the case of the triplet anionic cluster. These results for the considered ADEs and VDEs at FN-DMC level are in complete agreement with the observation of Alexandrova *et al.* [19] about the coexistence of the singlet and triplet clusters in the PES experiment, as discussed above. Our FN-DMC result for AIP is in agreement with the CCSD(T) and G3B3 of Tai *et al.* [95], with a deviation smaller than 0.4 eV. The DFT results of Akman *et al.* [35] show a good agreement with our FN-DMC results, for both AIP and VIP.

Table 3.18 shows the decomposition of the considered ADEs, VDEs, AIP and VIP.

Table 3.18: Decomposition of the ADE, VDE, AIP, and VIP of the hepta-atomic boron clusters. Statistical error in the last decimal place is indicated in the parentheses. All energies are in eV.

		$\Delta E_e^{\mathtt{KT}}$	$\Delta E_{\mathtt{relax}}^{\mathtt{HF}}$	$\Delta E_e^{\mathtt{corr}}$	ΔE_e
ADE[1]	B_7^-	0.36	0.58	1.56(2)	2.50(2)
ADE[2]	B_7^-	0.36	1.13	1.14(2)	2.63(2)
VDE[3]	B_7^-	0.83	0.29	1.55(2)	2.67(2)
VDE[4]	B_7^-	1.23	0.76	0.95(2)	2.94(2)
AIP	B_7	9.41	−2.31	0.83(2)	7.93(2)
VIP	B_7	9.41	−1.98	0.84(2)	8.27(2)

[1]Considering the singlet anionic cluster;[2]Considering the triplet anionic cluster;[3]Considering the singlet anionic cluster and the neutral with the geometry of the singlet anionic cluster;[4]Considering the triplet anionic cluster and the neutral with the geometry of the triplet anionic cluster.

The main factor in the stabilization of the attached electron in B_7^- for the ADE[1], which consider the singlet anionic cluster, is the electron correlation energy, which contributes with roughly 62%. The contribution of the Koopmans energy and the relaxation energy are about 14% and 23%, respectively. For the ADE[2], the main factors in the stabilization are the relaxation and electron correlation effects. These both factors contribute with about 43%, and the electrostatic and exchange energy contributes with 14%. For the VDE[3], which consider the singlet anionic cluster and the neutral with the geometry of the singlet anionic cluster, the main factor in the stabilization is the electron correlation energy, which contributes with 58%. The Koopmans energy contributes with 31% and the relaxation energy contributes with 11%. For the VDE[4], the main factors in the stabilization of the attached electron are the electrostatic and exchange energy and the electron correlation energy, with contributions of 42% and 32%. The orbitals

relaxation energy contributes with roughly 26% for the VDE[4]. For the neutral cluster, the factors that stabilize the system are similar for both process, AIP and VIP. The major contribution in the stabilization of the neutral cluster is the Koopmans energy, $\Delta E_e^{\mathtt{KT}}$, which contributes with 119% for the AIP, and 114% for the VIP. The relaxation energy, $\Delta E_{\mathtt{relax}}^{\mathtt{HF}}$, contributes in destabilizing the system with, 30% for the AIP, and 24% for the VIP. The contribution of the electron correlation energy is small for both AIP and VIP, and represents about 10% for both process.

B_8, B_8^- and B_8^+

The octa-atomic neutral, anionic, and cationic boron clusters have an unusual characteristics, not commonly observed for clusters of this size, which is the non-predominance of three-dimensional structures i.e., the predominance of the planarity in these clusters [30]. The geometric shapes of the obtained octa-atomic clusters are shown in Figure 3.10. The spin multiplicity of the neutral, anionic and cationic boron clusters with eight atoms are triplet, doublet, and doublet, respectively. The geometric structure of the neutral cluster is a planar heptagon with a central atom, where the bond lengths between the central atom and the others are 1.791 Å. The anionic and cationic clusters also present a heptagonal geometry with a central atom but, the bond lengths between the central atom and the other varies a little. For the anion, these distances vary between 1.766 and 1.803 Å, while, for the cation, vary between 1.790 e 1.828 Å. We see that the neutral cluster, when an electron is attached to its structure, rearrange its structure in such a way to diminish the average bond length between the central atom and the others, while, when an electron is detached from the neutral cluster, this average bond length increase. These obtained structures with its respective spin multiplicity are in agreement with the ground-state structures reported in literature [19, 30, 34, 35, 95].

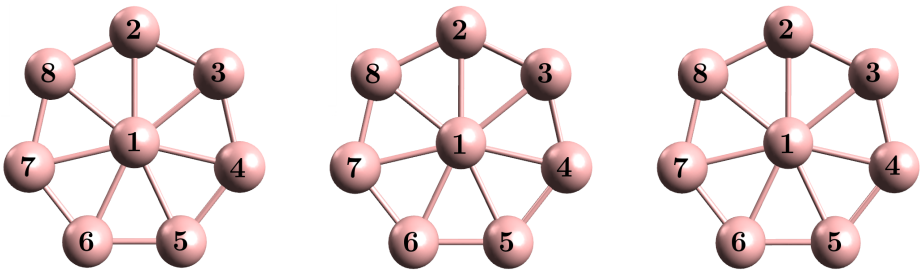

Figure 3.10: Ground-state geometries of the octa-atomic boron clusters, obtained at B3LYP/6-311+G*.

Table 3.19 shows the obtained total energy for the octa-atomic boron clusters at HF-CBS, DFT and FN-DMC levels. From now on, we consider the extrapolation of the HF-CBS energies only up to the basis aug-cc-PVQZ. The reason is that the full-electron calculations with this basis demands a considerable computational effort and, for

the most of cases that we have tried, the SCF procedure does not converge for the basis aug-cc-PV5Z. Table 3.20 shows the FN-DMC results for the electron binding energies. For the octa-atomic anionic boron cluster, two experimental VDEs are available in literature, which represent two peaks in the PES spectra [19,30]. Zhai *et al.* [30] consider that these two VDEs represents different final states of the neutral cluster. In one, the final state is a triplet neutral cluster, which represents the first peak in the PES spectra, and in the other the final state is a singlet neutral cluster, which represents the second peak. In this work we consider both transitions to estimate the VDEs of the octa-atomic anionic boron cluster.

Table 3.19: Total energy, in a.u., at HF-CBS, DFT (B3LYP/6-311+G*) and FN-DMC, and spin multiplicity M for the ground-state of the octa-atomic boron clusters. Statistical error in the last decimal place is indicated in the parentheses.

Cluster	M	Energy		
		HF-CBS	DFT	FN-DMC
B_8	3	−197.2186	−198.5962	−198.4747(7)
B_8^-	2	−197.2772	−198.6994	−198.5835(5)
B_8^+	2	−196.9363	−198.2792	−198.1531(6)
$B_8^{0,-}$	1	−197.1780	−198.5730	−198.4560(6)
$B_8^{0,-}$	3	−197.2166	−198.5944	−198.4733(5)
$B_8^{+,0}$	2	−196.9322	−198.2761	−198.1486(6)

Table 3.20: The ADE, VDE, AIP, and VIP values for the anionic and neutral octa-atomic boron clusters and comparison with the experimental results; the energies are in eV.

		DFT	G3B3	CCST	FN-DMC(This work)	Exp.[a]
ADE	B_8^-	2.789	3.11[b]	3.02[b]	2.96(2)	3.02(2)
VDE	B_8^-		3.12[b]	2.99[b]	3.00(2)[1]	3.02(2)
VDE	B_8^-	2.841	3.56[b]	3.44[b]	3.47(2)[2]	3.35(2)
AIP	B_8	8.625	8.72[c]	8.97[c]	8.75(2)	
VIP	B_8	8.710			8.87(2)	

[a]Ref. [30], [b]Ref. [34], [c]Ref. [95], and DFT values from Ref. [35].
[1]Considering the triplet neutral cluster with the geometry of the doublet anionic cluster;[2]Considering the singlet neutral cluster with the geometry of the doublet anionic cluster.

Our FN-DMC results are in a very good agreement with available theoretical results in literature. Comparing with the CCSD(T) results of Tai *et al.* [34], for the ADE and VDEs, our results show a deviation of 0.06 eV for the ADE, 0.01 eV for the VDE[1], and 0.03 eV for the VDE[2]. In comparison with the G3B3 results of Tai *et al.* [34], we obtained a deviation of 0.15, 0.12, and 0.09 eV, for the ADE, VDE[1], and VDE[2], respectively. The available DFT results of Akman *et al.* [35], for the ADE and VDE[2], underestimate the FN-DMC results by 0.17 and 0.63 eV, respectively. The FN-DMC results show a very good agreement with the experimental data of Zhai *et al.* [30]. For the ADE, VDE[1], and VDE[2], we obtained very accurate results, showing a discrepancies

of 2%, 0.7%, and 3%, respectively. The FN-DMC result for the AIP shows a deviation of 0.22 and 0.03 eV, in relation to CCSD(T) and G3B3 obtained by Tai *et al.* [95]. The DFT results of Akman *et al.* [35] underestimate our FN-DMC results by roughly 0.16 eV, for both AIP and VIP. These overall agreement between our results and available theoretical and experimental results is a good indicator of the accuracy in our calculations. It also indicates that the obtained ground-state geometric structures correspond to those with the major contribution in the spectra of the PES experiment.

Table 3.21 shows the values obtained for the decomposition of the electron binding energies ADE, VDE, AIP, and VIP.

Table 3.21: Decomposition of the ADE, VDE, AIP, and VIP of the octa-atomic boron clusters. Statistical error in the last decimal place is indicated in the parentheses. All energies are in eV.

		$\Delta E_e^{\mathtt{KT}}$	$\Delta E_{\mathtt{relax}}^{\mathtt{HF}}$	$\Delta E_e^{\mathtt{corr}}$	ΔE_e
ADE	B_8^-	0.69	0.90	1.37(2)	2.96(2)
VDE[1]	B_8^-	0.78	0.87	1.35(2)	3.00(2)
VDE[2]	B_8^-	1.85	0.85	0.77(2)	3.47(2)
AIP	B_8	9.77	−2.09	1.07(2)	8.75(2)
VIP	B_8	9.77	−1.98	1.08(2)	8.87(2)

[1]Considering the triplet neutral cluster with the geometry of the doublet anionic cluster;[2]Considering the singlet neutral cluster with the geometry of the doublet anionic cluster.

For the ADE and VDE[1], the main factor of stabilization of the attached electron in B_8^- is the electron correlation energy, which contributes with roughly 46%. The contribution of the electrostatic and exchange energy is about 23% for the ADE and 26% for the VDE[1], and the relaxation effects contribute with about 30% for both ADE and VDE[1]. For the VDE[2] we see a different scenario, where the main factor in the stabilization is the electrostatic and exchange energy, described by the Koopmans $\Delta E_e^{\mathtt{KT}}$ energy, which contributes with about 53%. The relaxation energy, $\Delta E_{\mathtt{relax}}^{\mathtt{HF}}$, and the correlation energy, $\Delta E_e^{\mathtt{corr}}$, contributes to the stabilization with roughly 24% and 22%, respectively. For the neutral cluster, the Koopmans contribution is the main factor in stabilizing the B_8 cluster with 112% and 110% for the AIP and VIP, respectively. The relaxation energy plays a destabilizing role and its contribution is about 24% for the AIP, and 22% for the VIP. The contribution of the electron correlation energy is about 12% for both AIP and VIP. Therefore, we conclude that the stabilization of the anionic octa-atomic boron cluster is mainly due to the electron correlation effects, with a small contribution of the relaxation energy and electrostatic and exchange energy, while the neutral cluster is absolutely stabilized by the electrostatic and exchange energy, with small contribution of the electron correlation energy and the relaxation effects, where the latter contributes to the destabilization of the system.

B_9, B_9^- and B_9^+

The ground-state structure of the neutral nine-atomic boron cluster is not well established yet [30,34]. Zhai *et al.*[30] reported a doublet wheel-structure, which is a planar octagon with a central atom, as the global minimum of the B_9 cluster, while Tai *et al.* [34] reported a heptagonal bipyramid with spin multiplicity doublet as the ground-state. Our FN-DMC results indicated the doublet heptagonal bipyramid as the lowest-energy structure with a difference in energy of 0.54(3) eV from the planar structure, which is in agreement with Tai *et al.* [34]. For the anionic cluster we obtained as the ground-state a singlet which is a planar octagon with a central atom, where the bond lengths between the central atom and the peripheral ones alternate between 1.975 and 1.977 Å. This obtained anionic structure is in agreement with those reported in the literature [19, 30, 31, 34]. The ground-state of the cationic nona-atomic boron cluster $B9^+$ is a singlet heptagonal distorted bipyramid, which agrees with Tai *et al.* [95], but disagrees with the ground-state reported by Akman *et al.* [35], which is a octagon with a central atom.

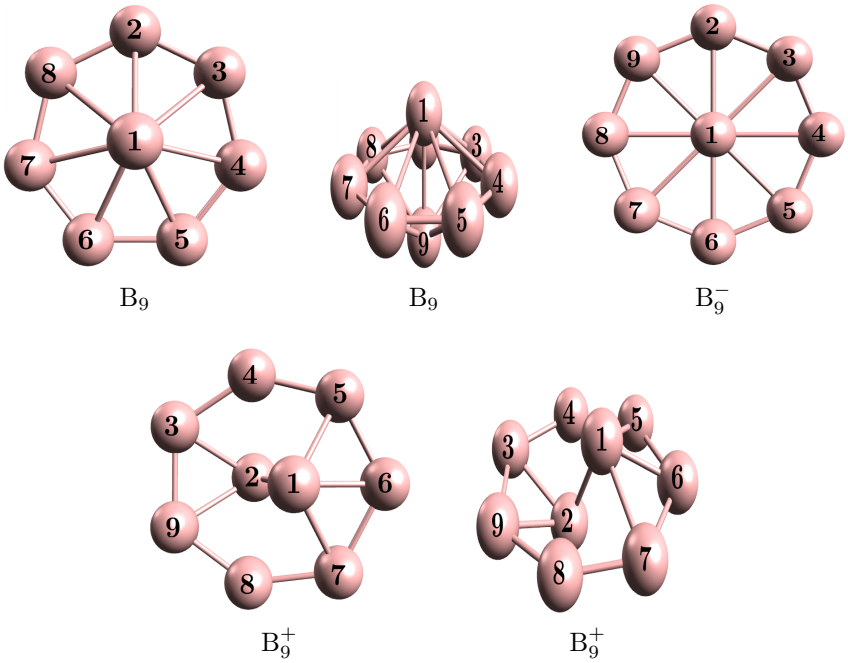

Figure 3.11: Ground-state geometries of the nona-atomic boron clusters, obtained at B3LYP/6-311+G*.

Table 3.22 shows the obtained total energies for the considered nona-atomic boron clusters at HF-CSB, DFT, and FN-DMC calculations, and Table 3.23 shows the FN-DMC results for the ADE, VDE, AIP, and VIP. For comparison, we also show experimental data and other theoretical approaches results in Table 3.23.

For the ADE, the FN-DMC value is 0.02 eV higher than the G3B3 result of Tai *et al.* [34] and, as far as we know, there is no available value at CCSD(T) level for the ADE of the B_9^- cluster. For the VDE, we see an agreement between our result and other

Table 3.22: Total energy, in a.u., at HF-CBS, DFT (B3LYP/6-311+G*) and FN-DMC, and spin multiplicity M for the ground-state of the nona-atomic boron clusters. Statistical error in the last decimal place is indicated in the parentheses.

Cluster	M	Energy		
		HF-CBS	DFT	FN-DMC
B_9	2	−221.8520	−223.4100	−223.2951(6)
B_9^-	1	−221.9281	−223.5358	−223.4073(6)
B_9^+	1	−221.5769	−223.1114	−223.9954(7)
$B_9^{0,-}$	2	−221.8498	−223.4129	−223.2730(6)
$B_9^{+,0}$	1	−221.5571	−223.0858	−223.9685(6)

Table 3.23: The ADE, VDE, AIP, and VIP values for the anionic and neutral nona-atomic boron clusters and comparison with the experimental results; the energies are in eV.

		DFT	G3B3	CCST	FN-DMC(This work)	Exp.[a]
ADE	B_9^-	3.282	3.03[b]		3.05(2)	3.39(6)
VDE	B_9^-	3.342	3.63[b]	3.45[b]	3.68(2)	3.46(6)
AIP	B_9	8.112	8.46[c]		8.16(2)	
VIP	B_9	8.191			8.89(2)	

[a]Ref. [30], [b]Ref. [34], [c]Ref. [95], and DFT values from Ref. [35]

available theoretical approaches. Our FN-DMC result is 0.23 and 0.05 eV higher than the CCSD(T) and G3B3 of Tai *et al.* [34], respectively, and the DFT value of Akman *et al.* underestimate the FN-DMC by 0.33 eV. In comparison to the experimental data of Zhai *et al.* [30], our FN-DMC values shows a discrepancies of 10% and 6% for the ADE and VDE, respectively. The DFT results underestimate both FN-DMC values for the AIP and VIP by 0.05 and 0.70 eV, respectively. Our FN-DMC result for the AIP is 0.3 eV lower than the G3B3 of Tai *et al.*[95].

Table 3.24 shows the decomposition of the ADE, VDE, AIP, and VIP for the nona-atomic boron clusters.

Table 3.24: Decomposition of the ADE, VDE, AIP, and VIP of the nona-atomic boron clusters. Statistical error in the last decimal place is indicated in the parentheses. All energies are in eV.

		ΔE_e^{KT}	$\Delta E_{\mathrm{relax}}^{\mathrm{HF}}$	$\Delta E_e^{\mathrm{corr}}$	ΔE_e
ADE	B_9^-	−0.40	2.47	0.98(2)	3.05(2)
VDE	B_9^-	1.31	0.82	1.55(2)	3.68(2)
AIP	B_9	9.48	−1.99	0.67(2)	8.16(2)
VIP	B_9	9.48	−1.46	0.87(2)	8.89(2)

We see that for the ADE, the main contribution in the stabilization of the attached electron in B_9^- is the orbital and geometry relaxation energy, $\Delta E_{\mathrm{relax}}^{\mathrm{HF}}$, which contributes with 81%. This large contribution of the relaxation effects in the ADE is in agreement with the significant change in the geometry of the anion, when one electron is detached from it, forming the neutral cluster. The electron correlation effects and the electrostatic

and exchange energy contributes with 32% and 13%, where the electrostatic and exchange energy contributes in destabilizing the system. For the VDE process, the main factors in the stabilization of the system are the electrostatic and exchange energy, describe by the Koopmans term $\Delta E_e^{\mathtt{KT}}$, and the electron correlation effects, $\Delta E_e^{\mathtt{corr}}$, which contributes with roughly 36% and 42%, respectively. The contribution of the orbitals relaxation is small but significant to the VDE value. Its contribution represents about 22% of the VDE. For the neutral cluster, the main factor in the stabilization of the system is the Koopmans energy, which contributes with 116% and 107% for the AIP and VIP, respectively. For both process, AIP and VIP, the relaxation energy plays a destabilizing role, with contribution of 24% for the AIP and 16% for the VIP. The electron correlation effects has a small impact in the stabilization of the neutral cluster, being less than 10% for both AIP and VIP. Thus, we conclude that the neutral cluster is well characterized by the electrostatic and exchange energy, while the anionic ones are stabilized by the relaxation energy and correlation effects in the ADE, and by the electrostatic and exchange energy and the electron correlation effects in the VDE.

B_{10}, B_{10}^- and B_{10}^+

In literature, there is a consensus about the structures that represent the ground-state of the neutral, anionic, and cationic 10-atomic boron clusters. The ground-state geometry of the clusters B_{10}, B_{10}^-, and B_{10}^+, obtained in this work, are shown in Figure 3.12. These geometries are in agreement with those reported in literature [14,19,34,35,95]. The geometry of the B_{10}, B_{10}^-, and B_{10}^+ are very similar, i.e., the addition/remotion of one electron from the neutral structure slightly changes the geometry of the cluster. They are quasi planar structures which are formed by two hexagon with a central atom as subunits. In these three structures one central atom is above the plane formed by the eight peripheral atoms and another one is below the plane. The spin multiplicity of the neutral, anion, and cation are singlet, doublet and doublet, respectively.

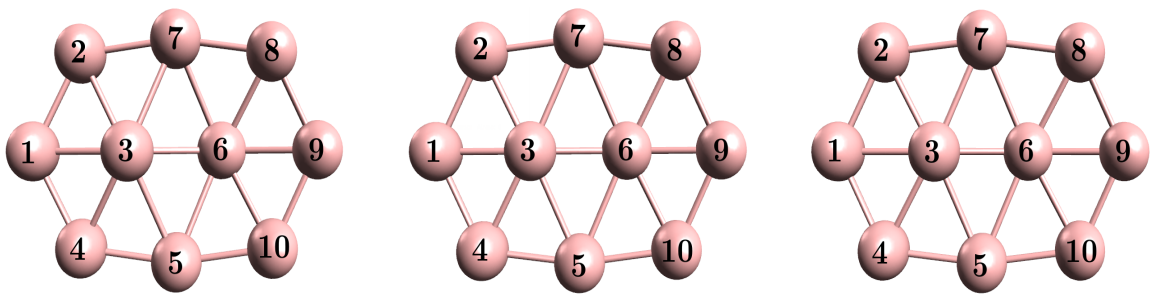

B_{10} B_{10}^- B_{10}^+

Figure 3.12: Ground-state geometries of the 10-atomic boron clusters, obtained at B3LYP/6-311+G*.

Table 3.25 shows the total energy of the 10-atomic boron clusters obtained in this

work at different levels, and Table 3.26 shows the obtained electron binding energies at FN-DMC level and other theoretical and experimental results for comparison.

Table 3.25: Total energy, in a.u., at HF-CBS, DFT (B3LYP/6-311+G*) and FN-DMC, and spin multiplicity M for the ground-state of the 10-atomic boron clusters. Statistical error in the last decimal place is indicated in the parentheses.

Cluster	M	Energy		
		HF-CBS	DFT	FN-DMC
B_{10}	1	−246.5416	−248.3011	−248.1576(7)
B_{10}^{-}	2	−246.6165	−248.4004	−248.2641(6)
B_{10}^{+}	2	−246.2619	−247.9860	−247.8655(4)
$B_{10}^{0,-}$	1	−246.5182	−248.2894	−248.1505(6)
$B_{10}^{+,0}$	2	−246.2561	−247.9763	−247.8318(5)

Table 3.26: The ADE, VDE, AIP, and VIP values for the anionic and neutral 10-atomic boron clusters and comparison with the experimental results; the energies are in eV.

		DFT	G3B3	FN-DMC(This work)	Exp.[a]
ADE	B_{10}^{-}	2.714	2.85[b]	2.90(3)	2.88(9)
VDE	B_{10}^{-}	3.091	3.22[b]	3.09(2)	3.06(3)
AIP	B_{10}	8.685	8.61[c]	7.95(2)	
VIP	B_{10}	8.844		8.87(2)	

[a]Ref. [14], [b]Ref. [34], [c]Ref. [95], and DFT values from Ref. [35]

Our FN-DMC results for ADE and VDE are in agreement with G3B3 results obtained by Tai *et al.* [34], with a deviation of 0.05 eV for ADE, and 0.13 eV for VDE. The DFT result of Akman *et al.* [35] for the VDE underestimate the FN-DMC result by 0.19 eV, and, for the ADE, the DFT result is within the statistical error of the FN-DMC result. In comparison with the experimental data of Zhai *et al.* [14], our FN-DMC results showed a very good agreement, with a discrepancies of 0.7% for the ADE and 1% for the VDE, and both results are within the statistical error of the experimental data. The FN-DMC value for the AIP is lower than the G3B3 result of Tai *et al.* [95], with a deviation of 0.7 eV. The DFT result of Akman *et al.* [35], for the AIP, agrees with the G3B3 obtained by Tai *et al.* [95] and overestimate the FN-DMC value by 0.7 eV. For the VIP, the DFT result is in agreement with the FN-DMC, with a small deviation of 0.03 eV. For the boron clusters with 10, 11, 12, and 13 atoms, we do not found any Coupled Cluster results for the ADE, VDE, AIP, and VIP, for comparison. The overall agreement between our FN-DMC results and the theoretical and experimental available values is a good indicator of the correctness of the structures obtained by our methodology and the accuracy of our FN-DMC calculations.

Table 3.27 shows the decomposition of the electron binding energies for the 10-atomic boron clusters.

Table 3.27: Decomposition of the ADE, VDE, AIP, and VIP of the 10-atomic boron clusters. Statistical error in the last decimal place is indicated in the parentheses. All energies are in eV.

		$\Delta E_e^{\mathtt{KT}}$	$\Delta E_{\mathtt{relax}}^{\mathtt{HF}}$	$\Delta E_e^{\mathtt{corr}}$	ΔE_e
ADE	B_{10}^-	0.88	1.16	0.86(3)	2.90(3)
VDE	B_{10}^-	1.60	1.07	0.42(2)	3.09(2)
AIP	B_{10}	8.77	−1.00	0.18(2)	7.95(2)
VIP	B_{10}	8.77	−1.16	1.26(2)	8.87(2)

For ADE, the main factor in the stabilization of the attached electron in the B_{10}^- cluster is the relaxation energy, which contributes with 40%, while the Koopmans energy and the electron correlation effects contribute with 30% each. For VDE, the major contributions in the stabilization of the anionic boron cluster is the electrostatic and exchange energy and the relaxation energy, which contribute with 52% and 35%, respectively, and the electron correlation energy contributes with 13%. For the AIP and VIP, the Koopmans energy is the main factor in the stabilization of the neutral 10-atomic boron cluster, which contribute with 110% for the AIP and 99% for the VIP. The contribution of the electron correlation effects are small for both electron binding energies AIP and VIP, they represent about 2% and 14%, respectively, while the relaxation energy plays a destabilizing role, which contributes with 12% for the AIP and 13% for the VIP. We conclude that the neutral cluster is characterized by the electrostatic and exchange energy, described by the Koopmans factor $\Delta E_e^{\mathtt{KT}}$, while the anionic cluster is stabilized mainly by the relaxation energy and the Koopmans energy, with small sensitivity to electron correlation effects.

B_{11}, B_{11}^- and B_{11}^+

The geometry of the 11-atomic neutral and charged boron clusters obtained in this work are shown in Figure 3.13. The obtained ground-state geometry of the neutral cluster is not in agreement with the ground-state reported by Tai *et al.* [34] and Zhai *et al.* [14]. Our ground-state geometry corresponds to the second lowest energy structure reported by Tai *et al.* [34], which is planar with 9 atoms forming a distorted ring around two atoms at the center. The geometry obtained for the anionic cluster B_{11}^- is in agreement with Zhai *et al.* [14], Tai *et al.* [34], and Czekner *et al.* [37]. For the cationic cluster, our geometry is not in agreement with Tai *et al.* [95] and Akman *et al.* [35], and also we do not find in literature any reported structure that is similar to our cationic 11-atomic boron cluster. The spin multiplicity of the neutral, anionic, and cationic 11-atomic boron clusters are doublet, singlet, and singlet, respectively.

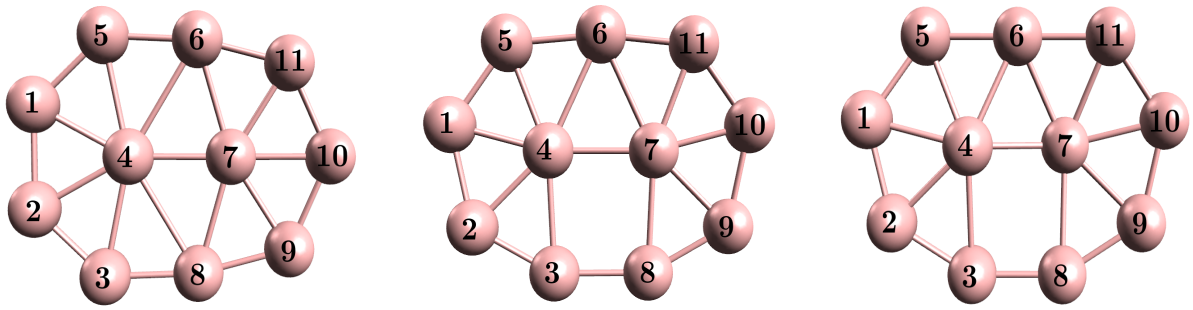

B_{11} B_{11}^- B_{11}^+

Figure 3.13: Ground-state geometries of the 11-atomic boron clusters, obtained at B3LYP/6-311+G*.

The total energy of the 11-atomic boron clusters are shown in Table 3.28, at different levels of calculation. The electron binding energies ADE, VDE, AIP, and VIP, at FN-DMC level, are shown in Table 3.29, and available theoretical and experimental data are also shown for comparison.

Table 3.28: Total energy, in a.u., at HF-CBS, DFT (B3LYP/6-311+G*) and FN-DMC, and spin multiplicity M for the ground-state of the 11-atomic boron clusters. Statistical error in the last decimal place is indicated in the parentheses.

Cluster	M	Energy		
		HF-CBS	DFT	FN-DMC
B_{11}	2	−271.2213	−273.1546	−272.9910(8)
B_{11}^-	1	−271.3140	−273.2773	−273.1215(6)
B_{11}^+	1	−270.9618	−272.8625	−272.6993(6)
$B_{11}^{0,-}$	2	−271.2165	−273.1522	−272.9966(5)
$B_{11}^{+,0}$	1	−270.9301	−272.8525	−272.6884(6)

Table 3.29: The ADE, VDE, AIP, and VIP values for the anionic and neutral 11-atomic boron clusters and comparison with the experimental results; the energies are in eV.

		DFT	G3B3	FN-DMC(This work)	Exp.
ADE	B_{11}^-	3.282	3.48[c]	3.55(3)	3.43(2)[a]
VDE	B_{11}^-	3.404	3.63[c]	3.40(2)	3.426(10)[a]; 3.401(2)[b]
AIP	B_{11}	7.993	8.01[d]	7.94(3)	
VIP	B_{11}	8.231		8.23(3)	

[a]Ref. [14], [b]Ref. [37], [c]Ref. [34] [d]Ref. [95], and DFT values from Ref. [35]

Our FN-DMC results for ADE and VDE are in a good agreement with the G3B3 results obtained by Tai *et al.* [34], with a deviation of 0.07 and 0.23 eV, respectively. The DFT results of Akman *et al.* [35] underestimate the FN-DMC value by 0.27 eV, for the ADE. For the VDE, the DFT value is within the statistical error of the FN-DMC result. The FN-DMC values for the ADE and VDE show a very good agreement with the experimental data of Zhai *et al.* [14] and Czekner *et al.* [37]. For the ADE, we obtained a discrepancy of 3%, and, for the VDE, the FN-DMC value is within the statistical error

of both experimental results. Our FN-DMC result for the AIP is in agreement with the G3B3 result obtained by Tai *et al.* [95], and the DFT result of Akman, with a deviation of 0.07 eV and 0.05 eV, respectively. The DFT result of Akman, for the VIP, is within the error of the FN-DMC value. In general, we see a very good agreement between our quantum Monte Carlo calculations, the experiment data, and other available theoretical results.

Table 3.30 shows the decomposition of the ADE, VDE, AIP, and VIP for the 11-atomic boron cluster.

Table 3.30: Decomposition of the ADE, VDE, AIP, and VIP of the 11-atomic boron clusters. Statistical error in the last decimal place is indicated in the parentheses. All energies are in eV.

		$\Delta E_e^{\mathtt{KT}}$	$\Delta E_{\mathtt{relax}}^{\mathtt{HF}}$	$\Delta E_e^{\mathtt{corr}}$	ΔE_e
ADE	B_{11}^-	1.49	1.03	1.03(3)	3.55(3)
VDE	B_{11}^-	1.82	0.83	0.75(2)	3.40(2)
AIP	B_{11}	7.89	−0.83	0.88(3)	7.94(3)
VIP	B_{11}	7.89	0.03	0.31(3)	8.23(3)

For ADE and VDE, the main factor in the stabilization of the anionic cluster B_{11}^- is the electrostatic and exchange energy, which contributes with about 42% for the ADE, and 54% for the VDE. For the ADE, the contribution of the relaxation energy and the correlation effects are about 30%, for both energies, and for the VDE, 24% and 22%, respectively. For the AIP and VIP, the Koopmans energy is absolute in stabilize the neutral cluster. It means that the electron binding energy of the valence electron in the neutral cluster is well described by the electrostatic and exchange energy. The contribution of the Koopmans energy is about 99% for the AIP, and 96% for the VIP. For the AIP, the relaxation energy, which plays a destabilizing role, and the electron correlation energy contribute with 10% and 11%, respectively. For the VIP, the relaxation energy is negligible being smaller than 0.4% and the the electron correlation effects contributes with only 4%.

B_{12}, B_{12}^- and B_{12}^+

The ground-state geometry of the neutral, anionic, and cationic 12-atomic boron clusters are very similar. Figure 3.14 shows the obtained geometry in this work, which are clusters formed by three hexagonal pyramid as subunits. All three clusters, neutral, anion, and cation, are slightly distorted out of the plane, which make them convex structures. The spin multiplicity of the neutral, anionic, and cationic clusters are singlet, doublet, and doublet. These ground-state configurations are in agreement with those reported in literature [14, 34, 37, 95].

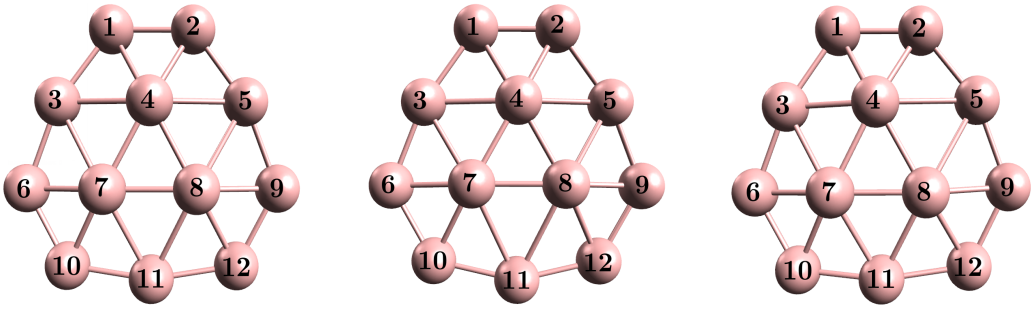

B_{12} B_{12}^- B_{12}^+

Figure 3.14: Ground-state geometries of the 12-atomic boron clusters, obtained at B3LYP/6-311+G*.

Table 3.31 shows the total energy of the 12-atomic boron clusters, obtained at different levels, and Table 3.32 shows our FN-DMC results for the ADE, VDE, AIP, and VIP, with theoretical and experimental results for comparison.

Table 3.31: Total energy, in a.u., at HF-CBS, DFT (B3LYP/6-311+G*) and FN-DMC, and spin multiplicity M for the ground-state of the 12-atomic boron clusters. Statistical error in the last decimal place is indicated in the parentheses.

Cluster	M	Energy		
		HF-CBS	DFT	FN-DMC
B_{12}	1	−295.9169	−298.0269	−297.8323(9)
B_{12}^-	2	−295.9623	−298.1020	−297.909(1)
B_{12}^+	2	−295.6298	−297.7078	−297.5044(9)
$B_{12}^{0,-}$	1	−295.9084	−298.0198	−297.825(1)
$B_{12}^{+,0}$	2	−295.6186	−297.7033	−297.5006(8)

Table 3.32: The ADE, VDE, AIP, and VIP values for the anionic and neutral 12-atomic boron clusters and comparison with the experimental results; the energies are in eV.

		DFT	G3B3	FN-DMC(This work)	Exp.
ADE	B_{12}^-	2.044	2.33[c]	2.09(4)	2.21(4)[a]
VDE	B_{12}^-	2.237	2.41[c]	2.28(4)	2.26(4)[a]; 2.221(2)[b]
AIP	B_{12}	8.684	8.91[d]	8.92(3)	
VIP	B_{12}	8.803		9.03(3)	

[a]Ref. [14], [b]Ref. [37], [c]Ref. [34] [d]Ref. [95], and DFT values from Ref. [35]

Our FN-DMC results for ADE and VDE are in agreement with the G3B3 of Tai *et al.*[34], with a deviation of 0.24 and 0.13 eV, respectively. The DFT results of Akman *et al.* [35] is in agreement with our FN-DMC values, within the statistical error of the FN-DMC. In comparison to the experimental data of Zhai *et al.* [14] and Czekner *et al.* [37], our FN-DMC results showed a good agreement, with a discrepancies of 5% for ADE, 3% for VDE obtained by Czekner *et al.*, and within the statistical error of the VDE value obtained by Zhai *et al.*. The FN-DMC value for the AIP is in agreement with the G3B3

result obtained by Tai *et al.* [95]. The DFT values of Akman *et al.* underestimate the FN-DMC values by about 0.23 eV for the AIP and VIP.

Table 3.33: Decomposition of the ADE, VDE, AIP, and VIP of the 12-atomic boron clusters. Statistical error in the last decimal place is indicated in the parentheses. All energies are in eV.

		$\Delta E_e^{\mathtt{KT}}$	$\Delta E_{\mathtt{relax}}^{\mathtt{HF}}$	$\Delta E_e^{\mathtt{corr}}$	ΔE_e
ADE	B_{12}^-	0.31	0.92	0.86(4)	2.09(4)
VDE	B_{12}^-	0.64	0.83	0.81(4)	2.28(4)
AIP	B_{12}	9.07	−1.26	1.11(3)	8.92(3)
VIP	B_{12}	9.07	−0.95	0.91(3)	9.03(3)

The major contributions in the stabilization of the attached electron in the anion B_{12}^- are the relaxation energy and the electron correlation energy, which contribute with 44% and 41% for the ADE, respectively. For the VDE, the contribution of the relaxation and electron correlation energies are about 36%, for each term. The contribution of the electrostatic and exchange interactions are roughly 15% and 28% for the ADE and VDE, respectively. The AIP and VIP process are well described by the electrostatic and exchange energy, at HF level. The contribution of the Koopmans energy, in the AIP and VIP process, represent about 102% and 100%, respectively. The relaxation energy plays a destabilizing role and represents about 14% and 10% for the AIP and VIP, respectively. The electron correlation energy contributes with about 12% and 10% for the AIP and VIP, respectively. For the AIP and VIP, because the relaxation energy plays a destabilizing role, the magnitude of the relaxation energy and electron correlation energy practically cancel each other. Therefore, we conclude that the stabilization of the attached electron in the anion cluster is characterized mainly by the relaxation and electron correlation energies, while the neutral cluster is very well characterized by electrostatic and exchange energy.

B_{13}, B_{13}^- and B_{13}^+

The obtained ground-state of the anionic 13-atomic boron cluster has a singlet spin state and its geometry is shown in Figure 3.15. This anionic cluster B_{13}^- is in agreement with the one reported by Tai *et al.* [34] and Sergeeva *et al.* [32]. For the ground-state of the neutral 13-atomic boron cluster, we have obtained two doublet isomers, that are very close in energy at FN-DMC level, the B_{13}(i) and the B_{13}(ii). Our FN-DMC calculations indicated that the cluster B_{13}(i) is the structure with the lowest energy, and the cluster B_{13}(ii) is 0.05(3) eV higher in energy than the B_{13}(i) cluster. These results are in agreement with Tai *et al.* [34], which report that these two structures are degenerate in energy and are the most stable isomers. A third isomer B_{13}(iii), which is a doublet and higher in energy than B_{13}(i) and B_{13}(ii), is also considered in the study of the 13-atomic boron clusters because of the similarity of its geometry with the geometry of the anionic cluster. The geometry of these three considered neutral structures are shown in Figure 3.15. The

ground-state of the cationic 13-atomic boron cluster is a singlet with a geometry similar to the neutral B_{13}(i), see Figure 3.15. This cationic structure is in agreement with the one reported by Tai *et al.* [95].

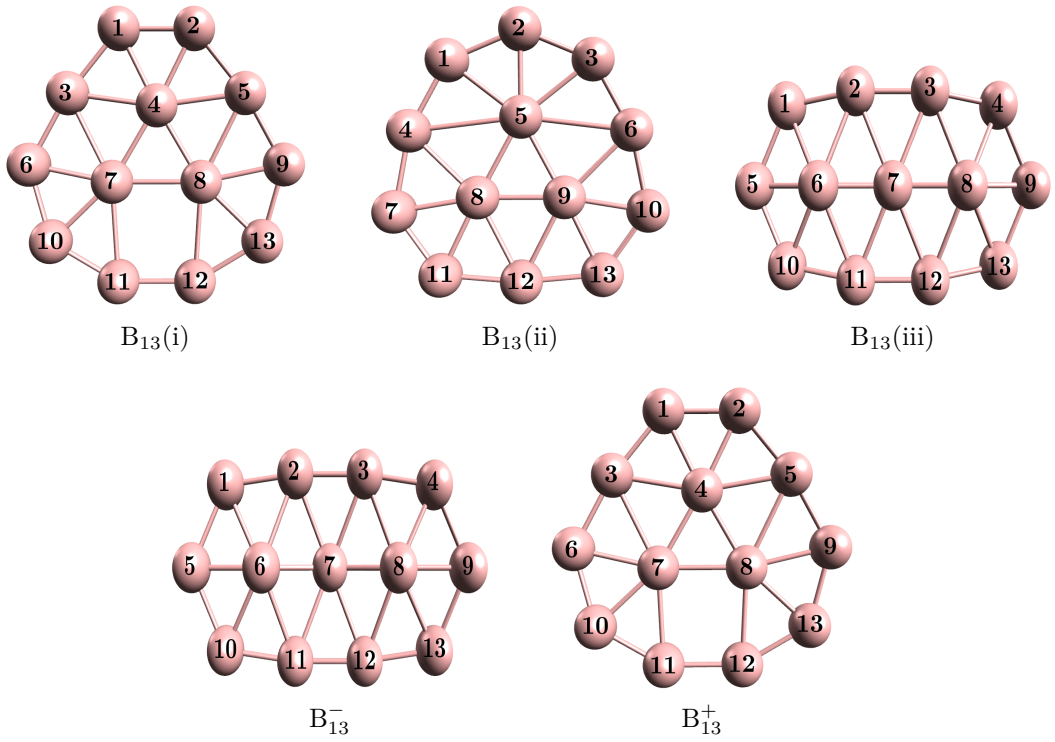

Figure 3.15: Ground-state geometries of the 13-atomic boron clusters, obtained at B3LYP/6-311+G*.

The total energy, obtained in this work, of the neutral, anionic, and cationic 13-atomic boron clusters are shown in Table 3.34, for different levels of calculations. In Table 3.35 we present our FN-DMC results for the electron binding energies ADE, VDE, AIP and VIP. Because we are considering two neutral clusters, denoted by B_{13}(i) and B_{13}(ii), which are degenerate in energy, we calculated two ADEs and two AIPs. Our interpretation is that each of these two neutral isomers can possibly be that one formed as the final state for the ADE process in the PES experiment. We also consider the ADE between the anionic B_{13}^{-} and the neutral B_{13}(iii), because of their similar structure. This consideration is also made by Tai *et al.* [34] and a better agreement between the theoretical and experimental ADE is obtained.

Our FN-DMC results for ADE and VDE are in agreement with G3B3 results of Tai *et al.* [34], with a deviation smaller than 0.1 eV. The DFT results of Akman *et al.* underestimate the FN-DMC values by about 0.03 and 0.2 eV for the ADE and VDE, respectively. We see a good agreement between our FN-DMC results and the experimental data. Because we are considering three isomer for the neutral cluster, we calculated three adiabatic detachment energies. The obtained values for the ADEs in which we consider the neutral clusters B_{13}(i) and B_{13}(i) (which are clusters degenerated in energy) as the

Table 3.34: Total energy, in a.u., at HF-CBS, DFT (B3LYP/6-311+G*) and FN-DMC, and spin multiplicity M for the ground-state 13-atomic boron clusters. Statistical error in the last decimal place is indicated in the parentheses.

Cluster	M	Energy		
		HF-CBS	DFT	FN-DMC
B_{13}(i)	2	−320.5788	−322.8560	−322.675(1)
B_{13}(ii)	2	−320.5767	−322.8543	−322.6730(7)
B_{13}(iii)	2	−320.5511	−322.8560	−322.6660(7)
B_{13}^{-}	1	−320.6441	−322.9725	−322.8048(7)
B_{13}^{+}	1	−320.3451	−322.5951	−322.4080(5)
$B_{13}^{0,-}$	2	−320.5497	−322.8383	−322.6623(7)
$B_{13}^{+,0}$	1	−320.3396	−322.5911	−322.4068(9)

Table 3.35: The ADE, VDE, AIP, and VIP values for the anionic and neutral 13-atomic boron clusters and comparison with the experimental results; the energies are in eV.

		DFT	G3B3	FN-DMC$_{\text{(This work)}}$	Exp.[a]
ADE	B_{13}^{-}	3.502	3.62[b]	3.53(3)[1]	3.78(2)
ADE	B_{13}^{-}			3.59(3)[2]	3.78(2)
ADE	B_{13}^{-}		3.81[b]	3.78(3)[3]	3.78(2)
VDE	B_{13}^{-}	3.649	3.98[b]	3.88(3)	3.78(2)
AIP	B_{13}	7.941	7.24[c]	7.27(3)[1]	
AIP	B_{13}			7.21(3)[2]	
VIP	B_{13}	8.144		7.30(3)	

[a]Ref. [14], [b]Ref. [34], [c]Ref. [95], and DFT values from Ref. [35]
[1]Considering the neutral cluster B_{13}(i);[2]Considering the neutral cluster B_{13}(ii); [3]Considering the neutral cluster B_{13}(iii).

final states are, 3.53(3) eV and 3.59 eV, respectively. Both results are in a good agreement with the experimental results, showing a discrepancies of 7% and 5%, respectively. The FN-DMC value for the ADE in which the shape of the anionic structure is preserved, i.e., the final state is the neutral cluster B_{13}(iii), is 3.78(3) eV, which is within the statistical error of the experimental result. Our FN-DMC value obtained for the VDE is in a good agreement with the experimental data, showing a discrepancy of 3%. The FN-DMC result for the AIP shows a good agreement with the available G3B3 result of Tai *et al.* [95], with a deviation of 0.03 eV. The DFT values of Akman *et al.* [35], for the AIP and VIP, overestimate the FN-DMC results by 0.67 and 0.84 eV, respectively.

The decomposition of the electron binding energies ADE^1 and ADE^2 are very similar. The main factor in the stabilization of the electron attached in the anionic cluster is the electron correlation energy, which contributes with roughly 50%, for both ADE^1 and ADE^2. The contribution of the Koopmans energy $\Delta E_e^{\mathtt{KT}}$ and the relaxation energy $\Delta E_{\mathtt{relax}}^{\mathtt{HF}}$ are about 24% and 27%, respectively, for both ADE^1 and ADE^2. The ADE^3 process is quite different from the ADE^1 and ADE^2. The contribution of the electrostatic and exchange energy $\Delta E_e^{\mathtt{KT}}$, the relaxation energy $\Delta E_{\mathtt{relax}}^{\mathtt{HF}}$, and the electron correlation energy $\Delta E_e^{\mathtt{corr}}$, are very close, representing 38%, 29%, and 33%, respectively. For the VDE

Table 3.36: Decomposition of the ADE, VDE, AIP, and VIP of the 13-atomic boron clusters. Statistical error in the last decimal place is indicated in the parentheses. All energies are in eV.

		$\Delta E_e^{\mathtt{KT}}$	$\Delta E_{\mathtt{relax}}^{\mathtt{HF}}$	$\Delta E_e^{\mathtt{corr}}$	ΔE_e
ADE^1	B_{13}^-	0.84	0.94	1.75(3)	3.53(3)
ADE^2	B_{13}^-	0.88	0.95	1.76(3)	3.59(3)
ADE^3	B_{13}^-	1.43	1.10	1.25(3)	3.78(3)
VDE	B_{13}^-	1.74	0.83	1.31(3)	3.88(3)
AIP^1	B_{13}	7.27	−0.91	0.91(3)	7.27(3)
AIP^2	B_{13}	7.20	−0.90	0.91(3)	7.21(3)
VIP	B_{13}	7.27	−0.76	0.79(3)	7.30(3)

the main factors in the stabilization are the Koopmans energy and the electron correlation energy, which contribute with 45% and 34%, respectively, and the contribution of the orbitals relaxation represents 21%. For the neutral cluster, the Koopmans contribution is absolute in stabilizing the formation of the neutral cluster, with roughly 100% for the AIP^1, AIP^2, and VIP. The relaxation energy plays a destabilizing role, with contribution about 13% for the AIP^1 and AIP^2, and 10% for the VIP. The electron correlation energy contribute in the stabilization of the neutral cluster with about 13% for the AIP^1 and AIP^2, and 11% for the VIP.

Figures 3.16, 3.17, 3.18 and 3.19, summarize our quantum Monte Carlo results for the Adiabatic Detachment Energy, the Vertical Detachment Energy, the Adiabatic Ionization Potential, and the Vertical Ionization Potential of the boron clusters studied in this work as a function of the number of atoms of the cluster (cluster size). For the ADE and VDE, Figures 3.16 and 3.17, we compare our FN-DMC results with the available experimental results from references [14,15,19,27–30,37]. In subsequent Figures, 3.18 and 3.19, we compare the AIP and VIP FN-DMC results to those theoretical of Tai *et al.* [95] from the literature, such as CCSD(T) and G3B3, when available.

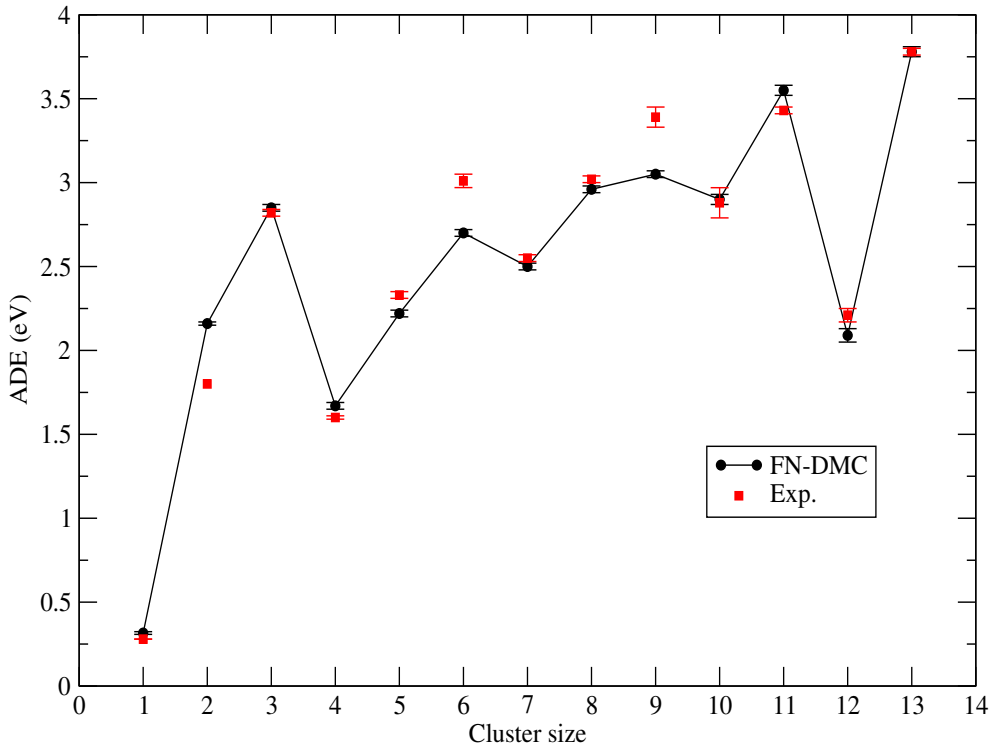

Figure 3.16: Size-dependence of the Adiabatic Detachment Energy (ADE in eV). Values obtained from FN-DMC calculations (black circles), and experimental results (red square) for comparison from Refs. [14, 15, 19, 27–30, 37].

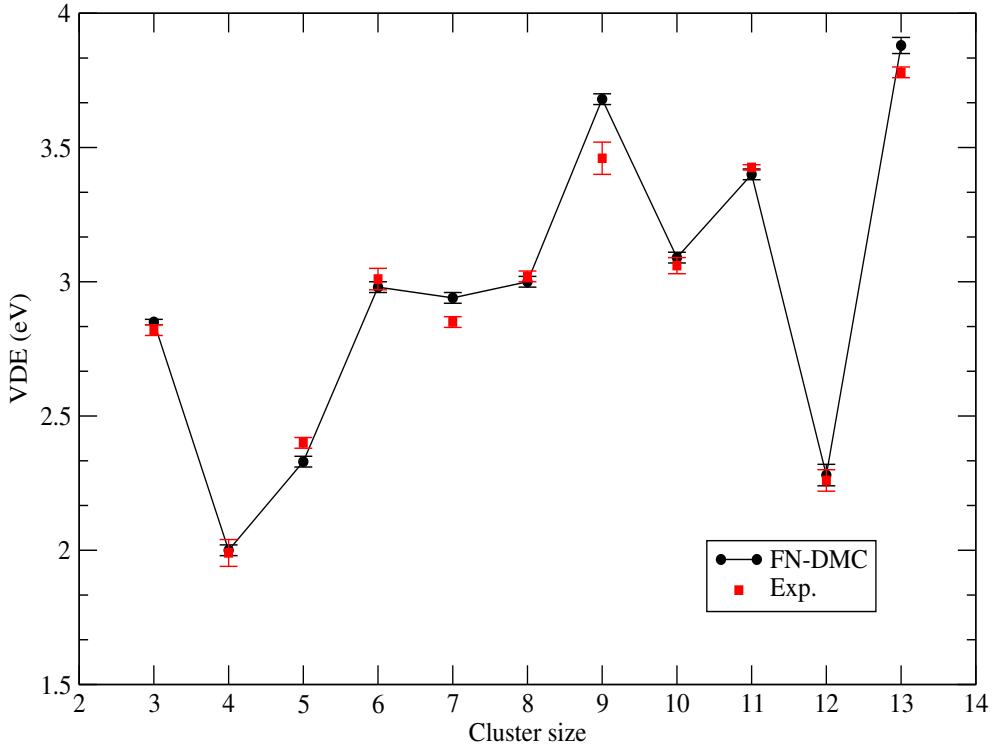

Figure 3.17: Size-dependence of the Vertical Detachment Energy (VDE in eV). Values obtained from FN-DMC calculations (black circles), and experimental results (red square) for comparison from Refs. [14, 15, 19, 27–30, 37].

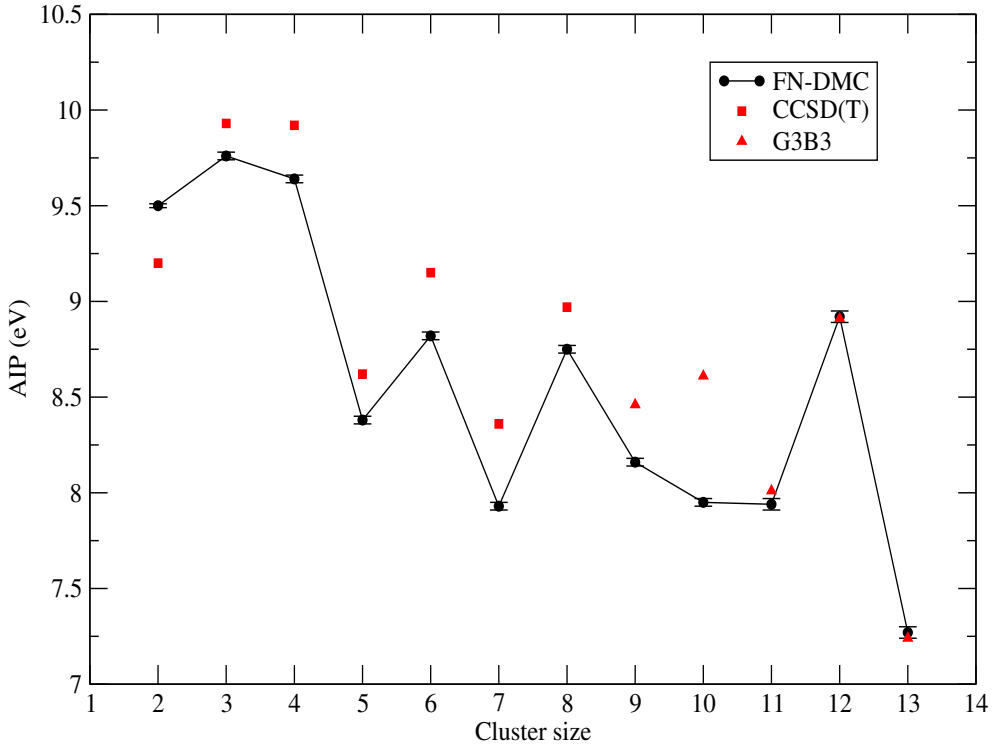

Figure 3.18: Size-dependence of the Adiabatic Ionization Potential (AIP in eV). Values obtained from FN-DMC calculations (black circles), and theoretical results (red square for CCSD(T) and up triangle for G3B3) for comparison from Ref. [95].

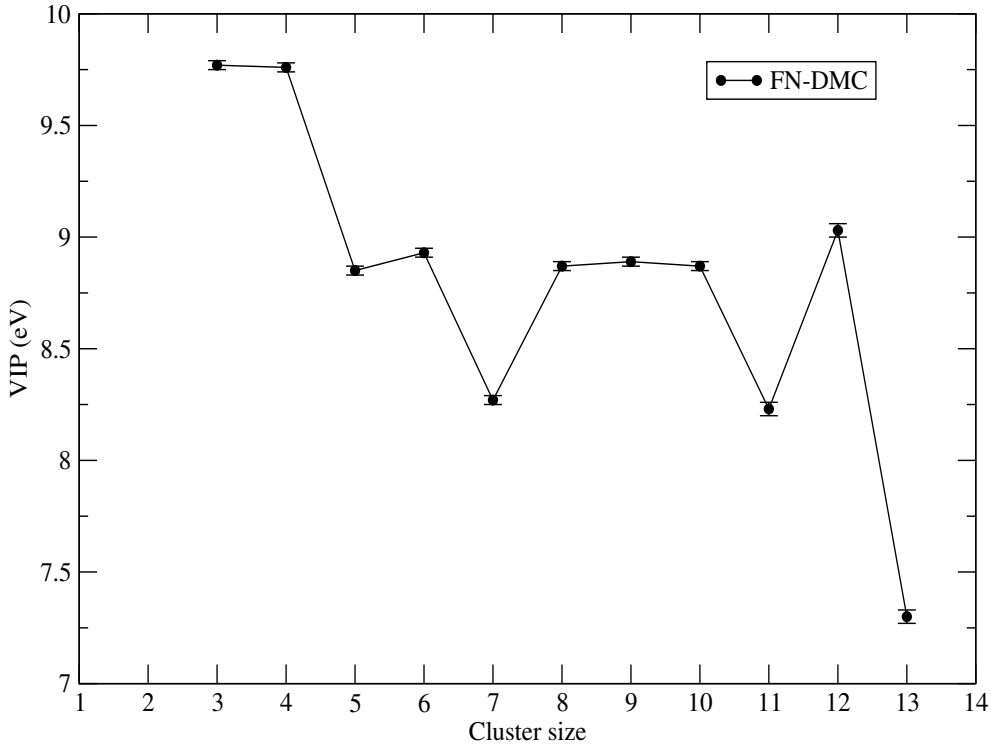

Figure 3.19: Size-dependence of the Vertical Ionization Potential (VIP in eV). Values obtained from FN-DMC calculations (black circles).

Aromaticity of B_3 and B_4, its anions and cations

In this section, we discuss the aromaticity of six small boron clusters, B_3, B_3^-, B_3^+, B_4, B_4^- and B_4^+. Because aromaticity is not a property directly observable and it still lacks a well-founded physical basis for its definition, quantification of the aromaticity remain elusive. There are several available methods to quantify the aromaticity, and most of them require a reference system which in general is some aromatic organic molecule. For example, there are the structural-based harmonic oscillator model of aromaticity (HOMA) [105, 106], the electronic-based descriptors such as the aromatic fluctuation (FLU) index[107], the bond order index of aromaticity (BOIA) [108], and the aromatic descriptor θ [109]. Other approaches, such as the resonance energies (REs) or aromatic stabilization energies (ASE) [110], suffer from the lack of appropriate reference systems [111,112]. Meanwhile, the most common methods used to discuss aromaticity in inorganic clusters are the basic electron counting based on the $4n + 2$ Hückel's rule [113], the magnetic-based indicators of aromaticity known as the nucleus-independent chemical shifts (NICS) [114], and the electronic multicenter indices (MCI) for multifold aromaticity in inorganic species [108,115–117]. In this work, we quantify the aromaticity of this small boron clusters using two criteria based on the electronic structure principles descriptor and the resonance energy. To quantify the aromaticity from the electronic structure principles, we follow the procedure by Chattaraj *et al.* [53], in which we apply a method based on the energy difference between two isomer systems [118,119], a linear and a cyclic one. In the linear isomer, the electrons are localized, while in the cyclic one, they can perform a cyclic delocalization. We also quantify the aromaticity based on the resonance energy in terms of Dewar's approach [120]. In this approach, we evaluate the resonance energy (RE) through the difference between the dissociation energy of the cluster and the dissociation energy of a classical structure with localized bonds. Before we discuss these two approaches used in this work to quantify the aromaticity of the trimer and tetramer boron clusters, we present the geometries obtained for the cyclic and linear clusters, at DFT level, and the total energies obtained at HF-CBS, DFT, and FN-DMC levels. To favor the read we may repeat some results already shown in previous sections.

The obtained ground-state geometries for the cyclic and linear trimer and tetramer boron clusters are shown in Figures 3.20 (neutrals), 3.21 (anions) and 3.22 (cations).

Table 3.37 shows the obtained values for the ground-state energies at HF-CBS, DFT and FN-DMC levels, for the cyclic and linear structures.

Here, the unrelaxed structures $B_n^{+,0}$, $B_n^{0,-}$ and $B_n^{2+,+}$ are used to calculate the vertical ionization potential of the relaxed neutral, anion and cation clusters, respectively, and the unrelaxed structures $B_n^{-,0}$, $B_n^{2-,-}$ and $B_n^{0,+}$ are used to calculate the vertical electron affinity of the relaxed neutral, anion and cation clusters, respectively. We see

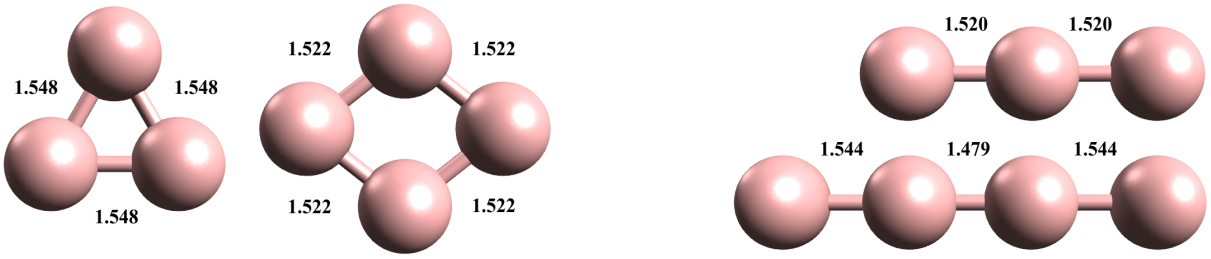

Figure 3.20: Cyclic (left) and linear (right) lowest energy structures of the neutral with three and four atoms boron clusters. The indicated bond lengths are in ångstrom (Å).

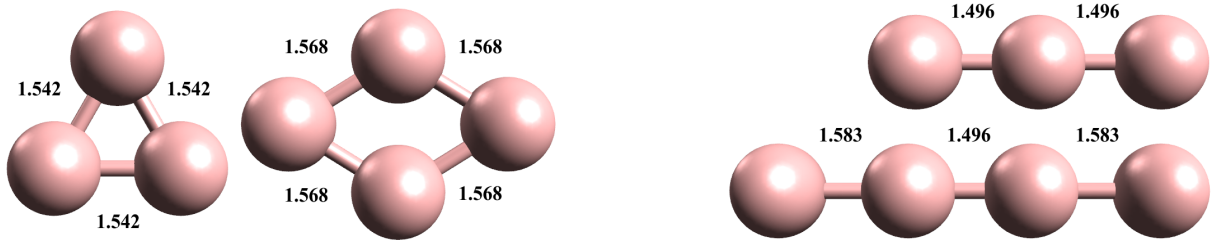

Figure 3.21: Cyclic (left) and linear (right) lowest energy structures of the anionic with three and four atoms boron clusters. The indicated bond lengths are in ångstrom (Å).

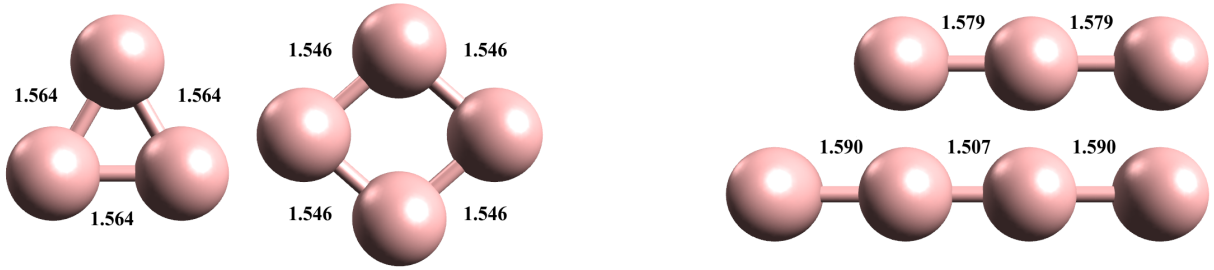

Figure 3.22: Cyclic (left) and linear (right) lowest energy structures of the cationic with three and four atoms boron clusters. The indicated bond lengths are in ångstrom (Å).

that, in all methods, the vertical gain or loss of a second electron, respectively, in the anionic and the cationic states will lead to an increase of their ground-state energies.

Aromaticity from the electronic structure principles

In general, three quantities are defined as an aromatic descriptor connected with the electronic structure principles, namely, the minimum energy, the maximum hardness, and the minimum electrophilicity [53]. The quantities, hardness (η) and electrophilicity (ω) can be theoretically defined in the context of the Density Functional Theory and can be estimated based on the total energies of the systems involved in the reaction.

In equation 2.72 the Lagrange multiplier μ is interpreted as the chemical potential of the studied system [67], which is quantitatively defined as the partial derivative of the total energy of the system with respect to the total number of electrons for a fixed external

Table 3.37: The ground-state energies (in a.u.) from HF-CBS, DFT and FN-DMC calculations for the boron clusters with three an four atoms ($n = 3$ and 4). The digits in parentheses are estimated standard errors in the last decimal places.

Cluster	Cyclic			Linear		
$n = 3$	HF-CBS	DFT	FN-DMC	HF-CBS	DFT	FN-DMC
B_n	−73.8008	−74.2983	−74.2481(4)	−73.7806	−74.2384	−74.1792(4)
B_n^-	−73.8392	−74.3970	−74.3527(4)	−73.8047	−74.3191	−74.2623(5)
B_n^+	−73.4504	−73.9361	−73.8896(4)	−73.5375	−73.9299	−73.8709(4)
$B_n^{+,0}$	−73.4509	−73.9359	−73.8891(5)	−73.5346	−73.9262	−73.8663(4)
$B_n^{-,0}$	−73.7126	−74.3970	−74.3519(5)	−73.8391	−74.3184	−74.2622(5)
$B_n^{0,-}$	−73.8004	−74.2982	−74.2479(3)	−73.7803	−74.2377	−74.1785(4)
$B_n^{2-,-}$	−73.7747	−74.2488	−74.2496(8)	−73.7069	−74.2161	−74.1629(5)
$B_n^{0,+}$	−73.8013	−74.2980	−74.2481(4)	−73.7754	−74.2347	−74.1750(4)
$B_n^{2+,+}$	−72.8709	−73.2951	−73.2537(4)	−72.8751	−73.3169	−73.2617(3)
$n = 4$	HF-CBS	DFT	FN-DMC	HF-CBS	DFT	FN-DMC
B_n	−98.4656	−99.1575	−99.0967(6)	−98.3847	−99.0525	−98.9730(5)
B_n^-	−98.5531	−99.2269	−99.1581(4)	−98.3959	−99.1393	−99.0277(5)
B_n^+	−98.1731	−98.8110	−98.7424(4)	−98.1463	−98.7442	−98.6608(5)
$B_n^{+,0}$	−98.1701	−98.8089	−98.7381(4)	−98.1434	−98.7415	−98.6564(5)
$B_n^{-,0}$	−98.5258	−99.2015	−99.1313(6)	−98.3937	−99.1377	−99.0559(6)
$B_n^{0,-}$	−98.4447	−99.1451	−99.0845(5)	−98.3833	−99.0508	−98.9652(6)
$B_n^{2-,-}$	−98.3898	−99.1002	−99.0415(6)	−98.3450	−99.0760	−98.9981(5)
$B_n^{0,+}$	−98.4637	−99.1555	−99.0955(4)	−98.3821	−99.0499	−98.9724(6)
$B_n^{2+,+}$	−97.6184	−98.2068	−98.1402(4)	−97.6924	−98.2126	−98.1308(4)

potential, and the electronegativity (χ) is the negative of the chemical potential [121],

$$\mu = \left(\frac{\partial E}{\partial N}\right)_{v(\mathbf{r})}, \tag{3.16}$$

and

$$\chi = -\mu = -\left(\frac{\partial E}{\partial N}\right)_{v(\mathbf{r})}. \tag{3.17}$$

The chemical hardness [122] (η) is defined as the second partial derivative of the total energy with respect to the number of electrons for a fixed external potential,

$$\eta = \frac{1}{2}\left(\frac{\partial^2 E}{\partial N^2}\right)_{v(\mathbf{r})} = \frac{1}{2}\left(\frac{\partial \mu}{\partial N}\right)_{v(\mathbf{r})}, \tag{3.18}$$

and the electrophilicity (ω) is defined, by Parr *et al.* [123], as,

$$\omega \equiv \frac{\mu^2}{2\eta} = \frac{\chi^2}{2\eta}. \tag{3.19}$$

To obtain approximative expressions for the chemical hardness and the electrophilicity we use the finite difference method. We write the total energy for a system

with $(N+1)$ electrons and for a system with $(N-1)$ electrons as,

$$E(N+1) = E(N) + \left(\frac{\partial E(N)}{\partial N}\right)_{v(\mathbf{r})} + \frac{1}{2}\left(\frac{\partial^2 E(N)}{\partial N^2}\right)_{v(\mathbf{r})} + (o^3), \tag{3.20}$$

$$E(N-1) = E(N) - \left(\frac{\partial E(N)}{\partial N}\right)_{v(\mathbf{r})} + \frac{1}{2}\left(\frac{\partial^2 E(N)}{\partial N^2}\right)_{v(\mathbf{r})} - (o^3), \tag{3.21}$$

where we consider the expansion till the third order term and the partial derivatives are taken for a fixed external potential. Subtracting 3.21 from 3.20 and using 3.17, we can write,

$$\chi \approx \frac{\text{VIP} + \text{VEA}}{2}, \tag{3.22}$$

where VEA and VIP are defined from equations 3.3 and 3.5, respectively, for a vertical process. Adding 3.20 to 3.21 and using 3.18, we obtain,

$$\eta \approx \frac{\text{VIP} - \text{VEA}}{2}. \tag{3.23}$$

Thus, we can calculate ω as,

$$\omega = \frac{(\text{VIP} + \text{VEA})^2}{4(\text{VIP} - \text{VEA})}. \tag{3.24}$$

We see that to estimate the electronegativity (and the chemical potential), the chemical hardness and the electrophilicity by equations 3.22, 3.23 and 3.24, respectively, is very convenient because they only depend on the total energy of the system with N, $(N+1)$ and $(N-1)$ electrons.

To quantify the aromaticity of the studied system, we follow a procedure of Chattaraj *et al.* [53], which is based on the energy difference between two isomer systems. In one isomer the electrons can perform a cyclic delocalization, and the aromatic descriptors of this system will be denoted by A_{cyclic}, where A corresponds to the total energy E, the hardness (η) or the electrophilicity (ω), $(A \equiv E, \eta, \omega)$. In the other isomer, a linear system, the electrons are localized, and the aromatic descriptor of this system will be denoted by A_{linear}. The difference, $A_{\text{aro}} = A_{\text{cyclic}} - A_{\text{linear}}$, is an indicator of the aromaticity of the system. It is expected for the aromatic (antiaromatic) system to have $E_{\text{aro}} < 0$, $\omega_{\text{aro}} < 0$, and $\eta_{\text{aro}} > 0$ ($E_{\text{aro}} > 0$, $\omega_{\text{aro}} > 0$, and $\eta_{\text{aro}} < 0$) [53, 118, 119].

The results for the aromatic descriptors, the total energy, the hardness and the electrophilicity for the cyclic and linear structures are shown in Table 3.38.

For all studied systems, the cyclic system has lower energy than the linear one. For the hardness, the cyclic system has a higher value than the linear one except for B_3^+. Now, for the electrophilicity, the cyclic system has lower electrophilicity than the linear one for B_3^-, B_4^-, and B_4. But for the other, B_3, B_3^+, and B_4^+, it is the opposite, the linear system has lower electrophilicity. Thus, the DMC results for the three descriptors support

Table 3.38: The total energy (E), hardness (η), electrophilicity (ω), and $A_{\rm aro}(A \equiv E, \eta, \omega)$ of the cyclic and linear isomers B_3^-, B_4^-, B_3, B_4, B_3^+, and B_4^+ clusters. The energy is in a.u., whereas the hardness and electrophilicity are given in eV.

	$A(E,\eta,\omega)$	Cyclic (A_c)	Linear (A_l)	$A_{aro} = A_c - A_l$
B_3^-	E	−74.3527(4)	−74.2623(5)	−0.0904(6)
	η	2.83(1)	2.49(1)	0.34(2)
	ω	0.0001(1)	0.009(1)	−0.009(1)
B_4^-	E	−99.1581(4)	−99.0277(5)	−0.1304(6)
	η	2.59(1)	1.25(1)	1.34(2)
	ω	0.066(3)	0.080(5)	−0.014(6)
B_3	E	−74.2481(4)	−74.1792(4)	−0.0689(6)
	η	3.47(1)	3.13(1)	0.34(2)
	ω	5.71(3)	4.64(3)	1.07(4)
B_4	E	−99.0967(6)	−98.9730(5)	−0.1237(8)
	η	4.41(2)	3.18(1)	1.23(2)
	ω	3.25(2)	4.65(3)	−1.40(4)
B_3^+	E	−73.8896(4)	−73.8709(4)	−0.0187(6)
	η	3.93(1)	4.15(1)	0.22(1)
	ω	23.82(8)	18.60(6)	5.22(9)
B_4^+	E	−98.7424(4)	−98.6608(5)	−0.0816(6)
	η	3.39(1)	2.97(1)	0.42(2)
	ω	24.92(9)	22.1(1)	2.9(1)

the aromaticity of the B_3^-, B_4^-, and B_4 planar clusters, in agreement with other theoretical approaches [15,19]. For the other clusters, our results for B_3, B_3^+, and B_4^+ partially satisfy the aromatic principles. In particular, B_3^+ does not satisfy the maximum principle of hardness, while the others do not satisfy the principle of minimum electrophilicity as they have positive values for $\omega_{\rm aro}$ which mean that their linear structures are less susceptible than the cyclic ones to donate or accept electrons. The electrophilicity is very sensitive to the electron correlation and, because our calculations consider single determinant orbital only, the lack of static correlation may be a possible reason for the failure of the aromatic principle discussed above.

Aromaticity based on the resonance energy

We now discuss the criterion for the aromaticity based on the resonance energy in terms of Dewar's approach [120]. One of the most remarkable properties of aromatic compounds is its resonance structure, which is due to the delocalized electrons that can perform cyclic motion in the structure thus enhancing their stability. Here, we evaluate the resonance energy (RE) through the difference between the dissociation of the cluster and the dissociation energy of a classical structure with localized bonds. The RE of the neutral, anionic, and cationic boron clusters can be calculated by using the following

expressions [34]:

$$E_r(B_n) = E_a(B_n) - n_b E_a(B_2), \tag{3.25}$$

$$E_r(B_n^-) = E_a(B_n^-) - (n_b - 1)E_a(B_2) - E_a(B_2^-), \tag{3.26}$$

and

$$E_r(B_n^+) = E_a(B_n^+) - (n_b - 1)E_a(B_2) - E_a(B_2^+). \tag{3.27}$$

Here, E_a is the atomization energy of the clusters, defined as,

$$E_a(B_n) = B_n \rightarrow nB, \tag{3.28}$$

$$E_a(B_n^-) = B_n^- \rightarrow (n-1)B + B^-, \tag{3.29}$$

$$E_a(B_n^+) = B_n^+ \rightarrow (n-1)B + B^+, \tag{3.30}$$

and n_b is the number of boron-boron (BB) bonds in the boron cluster with n atoms. It is expected a positive value of the resonance energy for aromatic systems and a negative value of RE for antiaromatic systems.

Table 3.39 shows the total energy and the atomization energy E_a values of the boron atom, dimers, trimers, and tetramers used in the dissociation process for the RE expressed in equations 3.25 – 3.27. For the sake of comparison, we also include in Table 3.39 the most recent available theoretical and experimental results.

Table 3.39: Total energy in a.u. and E_a in eV for the boron atom, dimer, trimer, and tetramer. The total energies of the trimers and tetramers (presented in Table3.2) are shown again here to facilitate the readability of this table. The number in parentheses indicates the statistical uncertainty in the last shown digit.

Cluster	M	Energy	E_a		
			FN-DMC	CCSD(T)	Exp.
B	2	−24.6405(2)			
B^-	3	−24.6521(2)			
B^+	1	−24.3295(1)			
B_2	1	−49.3611(2)	2.18(1)	2.08[a]	
B_2	3	−49.3837(3)	2.79(1)	2.79[a]	2.9(6)[c]
B_2^-	4	−49.4644(3)	4.67(1)	4.74[a]	
B_2^+	2	−49.0345(3)	1.76(1)	1.68[b]	0.8(6)[d]
B_3	2	−74.2481(4)	8.89(1)	8.47[a]	
B_3^-	1	−74.3527(4)	11.42(1)	11.34[a]	
B_3^+	1	−73.8896(4)	7.59(1)	6.84[b]	
B_4	1	−99.0967(6)	14.55(2)	13.70[a]	
B_4^-	2	−99.1581(4)	15.91(2)	15.38[a]	
B_4^+	2	−98.7424(4)	13.37(1)	11.96[b]	

[a]Take from Ref. [33], [b]Take from Ref. [95](values obtained from CCSD(T) heats of formation at 0 K.), [c]Take from Ref. [101], e [d]Take from Ref. [124]

We see that for the neutral and charged trimers and tetramers, the FN-DMC

E_a values follow the same trend as the CCSD(T), but they are consistently higher with disagreement as large as up to 1.4 eV. Such discrepancies may result from different sources, such as zero point-energies (ZPE) (which is absent in our calculations), the structural bond-lengths (which should differ to some extent from those in literature), and the fixed-node approximation. However, in general, our FN-DMC (even with single determinant) obtained values are comparable to the CCSD(T) in the accuracy. Once we have got the atomization energies, we can turn to the discussion of the aromaticity of the studied boron clusters through the calculations of resonance energies. Unfortunately, to the best of our knowledge, there is no available experimental data for the RE of those systems. In table 3.40, we show the RE results for the neutral and charged boron trimers and tetramers obtained from the evaluation of equations 3.28–3.30 and 3.25–3.27. The resonance energy values are in terms of the atomization energy of the neutral dimer in the singlet state, which yields the most significant resonance energies in comparison with the other neutral dimer spin state. To highlight the differences between them, we list the results in kcal/mol instead of eV. We are considering here that the boron trimer is composed of three boron-boron bonds and the tetramer by five.

Table 3.40: The resonance energies (REs) fo the trimer and tetramer neutral, anionic, and cationic boron clusters. All energies are in kcal/mol.

Cluster	BB bonds	FN-DMC	CCSD(T)[a]
B_3	3	54.2(8)	51.4
B_3^-	3	55.1(7)	56.3
B_3^+	3	33.9(7)	23.1
B_4	5	84(1)	76.1
B_4^-	5	58(1)	53.5
B_4^+	5	67(1)	45.2

[a]Values obtained from CCSD(T) heats of formation at 0 K from Refs.[33,95]

The FN-DMC values of the clusters with the largest resonance energies are 55.1(7) for B_3^- and 84(1) for B_4, in kcal/mol. They agree with those of Nguyen *et al.* [33] which are 56.3 and 76.1 kcal/mol, respectively. However, we notice some disagreement of those with the smallest resonance energies that we obtain for B_3^+ and B_4^- with 33.9(7) and 58(1) kcal/mol, respectively, while they have got B_3^+ with 23.1 and B_4^+ with 45.2 kcal/mol. Thus, we found for FN-DMC that the order of decreasing RE of the trimer is $B_3^- > B_3 > B_3^+$ whereas for the tetramer, it is $B_4 > B_4^+ > B_4^-$. The Molecular orbital (MO) analysis of Alexandrova *et al.* [15] pointed out that the B_3^- cluster is double (σ- and π-) aromatic, B_3 is π-aromatic and partially σ-aromatic, and B_3^+ is just π-aromatic. For the tetramer, they pointed out that the B_4 cluster is double (σ- and π-) aromatic, B_4^+ is π-aromatic and partially σ-aromatic, and B_4^- is π-aromatic and σ-antiaromatic. That agrees with our results, i.e., the more delocalized (aromatic) bonding characteristics a system has, the more resonant it will be. Furthermore, we noticed some qualitative trends

between our results from RE and the NICS results by Jin and Li [125], i.e., they show the following order for the degree of aromaticity: $B_4^- > B_4 > B_4^+$, which disagrees, with our FN-DMC results, only for the degree of aromaticity of the B_4^-. These obtained results for the aromaticity of the trimers and tetramers boron clusters are published in [126].

CHAPTER 4

Conclusions and Future Perspectives

In this work, we performed fixed-node diffusion quantum Monte Carlo simulations, using the single-particle orbital from density functional theory, to study the electron binding energy of the neutral clusters B_n ($n = 3 - 13$), their anions B_n^- and cations B_n^+, and the aromaticity of small neutral and charged boron clusters with three and four atoms. The Hartree-Fock calculations in the limit of complete basis set (CBS) have been performed to extract the correlation effect from the FN-DMC results.

The atomic binding energy per atom, obtained from FN-DMC calculations, increases as a function of n for the neutral, anionic, and cationic boron clusters. In general, among the three states, the anionic clusters showed the highest atomic binding energy, which indicates relative stability of the anionic clusters. To study the binding energy of the valence electron in the anionic and neutral clusters, we have calculated the electron binding energies ADE, VDE, AIP, and VIP, for different isomers of the boron clusters. The obtained results are in excellent agreement with the available experimental data, showing that the cluster structures chosen for the calculations must be the most populated in the experiments. We noted that for some adiabatic detachment process, in which we consider the neural cluster with a similar geometry of the anionic cluster, the theoretical results show a better agreement with the experimental data. It may indicate that when one electron is detached from the anionic cluster, the cluster tends to maintain its geometric structure, avoiding significantly structural changes, even though the predicted lowest-energy geometry of the neutral cluster is not similar to the anionic cluster.

We decompose the binding energies into three physical components: the electrostatic potential and exchange interaction, the relaxation energy, including both the orbital and the geometrical relaxation, and the electronic correlation energy. We have found that the leading contribution that characterizes the cluster's stability is the electrostatic and exchange interactions for the neutral clusters, while for the anionic the three physical

terms in the decomposition of the electron binding energies contribute to the stabilization of the attached electron.

We have also studied the aromaticity of the neutral and charged three- and four-atom boron clusters based on the electronic structure principles descriptor and the resonance energy. The FN-DMC results for the three aromatic descriptors, namely, the energy, hardness, and electrophilicity, support the aromaticity of B_3^-, B_4^-, and B_4, whereas for B_3, B_4^+, and B_4+, they are partially satisfied probably due to the lack of static correlation not considered in our calculations. The resonance energy has been obtained from the atomization energy. In comparison to the resonance energy of an organic aromatic system like benzene C_6H_6, of about 20 kcal/mol, they are found to be considerably high, being 55.1(7) for B_3^-, 54.2(8) for B_3, 33.9(7) for B_3^+, 84(1) for B_4, 67(1) for B_4^+, and 58(1) for B_4-, in kcal/mol. Therefore, the order of decreasing the stability of the trimer is $B_3^- > B_3 > B_3^+$, while for the tetramer it is $B_4 > B_4^+ > B_4^-$, in agreement with the results from the molecular orbital analysis. Based on the excellent agreement between the obtained QMC results, accurate quantum chemistry methods, and the experiments, we believe indeed that QMC is becoming a new alternative and a powerful research tool for ab initio electronic structure calculations.

In future work, we are going to extend the boron clusters up to the bulk limit to understand how the properties of the clusters evolve as a function of size, shape, and when doped, as a function of composition.

APPENDICES

APPENDIX A

The Quantum Variational Principle

We present a straightforward proof of the variational principle[61] in quantum mechanics, which is very useful to estimate the ground state energy E_0 of a system when the exact solution for the Schrödinger equation is not viable.

The variational theorem ensures that given a trial wave function Ψ, which tries to imitate the true ground state Φ, the expected value of the Hamiltonian of the system with respect to Ψ is an upper bound to the ground state energy of the system E_0, which is characterized by the exact wave function Φ, i.e.,

$$\frac{\langle\Psi|\hat{H}|\Psi\rangle}{\langle\Psi|\Psi\rangle} \geq \frac{\langle\Phi|\hat{H}|\Phi\rangle}{\langle\Phi|\Phi\rangle} = E_0. \tag{A.1}$$

To proof this theorem, consider the trial wave function $|\Psi\rangle$, which we can expand as,

$$|\Psi\rangle = \sum_{k}^{\infty} |k\rangle\langle k|\Psi\rangle, \tag{A.2}$$

where $|k\rangle$ is an eigenket of $\hat{H}$,

$$\hat{H}|k\rangle = E_k|k\rangle. \tag{A.3}$$

Replacing A.2 in A.1 and using $E_k = E_k + E_0 - E_0$, we obtain,

$$\begin{aligned}\frac{\langle\Psi|\hat{H}|\Psi\rangle}{\langle\Psi|\Psi\rangle} &= \frac{\sum_{k=0}^{\infty}|\langle k|\Psi\rangle|^2 E_k}{\sum_{k=0}^{\infty}|\langle k|\Psi\rangle|^2} \\ &= \frac{\sum_{k=1}^{\infty}|\langle k|\Psi\rangle|^2 (E_k - E_0)}{\sum_{k=0}^{\infty}|\langle k|\Psi\rangle|^2} + E_0 \\ &\geq E_0 \end{aligned} \tag{A.4}$$

where we use the fact that $(E_k - E_0)$ is necessarily positive.

APPENDIX B

The Koopmans' Theorem

In this appendix we present a discussion for the Koopmans' theorem[60], which arises in the context of the Hartree-Fock approximation and proposes a physical interpretation for the orbitals energies in the process of adding or removing an electron of a system. In general, the equation 2.36 has an infinity number of eigenfunctions, i.e.,

$$f|\chi_j\rangle = \epsilon_j|\chi_j\rangle \qquad\qquad j = 1, 2, \ldots, \infty, \tag{B.1}$$

where each solution $|\chi_j\rangle$ of this equation has a spin orbital energy ϵ_j. The N spin orbitals with the lowest orbital energies correspond to the occupied orbitals in a N-electron system described by the wave function $|\Psi\rangle$, and the remaining infinity spin orbitals are the virtual, or unoccupied, orbitals. In our notation, the occupied orbitals are represented by the indexes $a, b, \ldots$ and the virtual by $r, s, \ldots$.

We can obtain an expression for the energy by multiplying B.1 from the left by $\langle\chi_i|$,

$$\langle\chi_i|f|\chi_j\rangle = \epsilon_j\langle\chi_i|\chi_j\rangle = \epsilon_j\delta_{ij}. \tag{B.2}$$

Using 2.37 for the Fock operator, we obtain an equation for the orbital energy,

$$\begin{aligned}\epsilon_i = \langle\chi_i|f|\chi_i\rangle &= \langle\chi_i|h + \sum_b(\mathcal{J}_b - \mathcal{K}_b)|\chi_j\rangle \\ &= \langle\chi_i|h|\chi_i\rangle + \sum_b\langle\chi_i\chi_b|\chi_i\chi_b\rangle - \langle\chi_i\chi_b|\chi_b\chi_i\rangle.\end{aligned} \tag{B.3}$$

Therefore, we can write the energy for an occupied and a virtual orbitals, respectively, as,

$$\epsilon_a = \langle a|h|a\rangle + \sum_{b=1}^{N}\langle ab|ab\rangle - \langle ab|ba\rangle \tag{B.4}$$

and

$$\epsilon_r = \langle r|h|r\rangle + \sum_{b=1}^{N}\langle rb|rb\rangle - \langle rb|br\rangle. \tag{B.5}$$

The energy of a N-electrons neutral system is given (see equation 2.32)

$$E_0(N) = \sum_a \langle a|h|a\rangle + \frac{1}{2}\sum_a\sum_b \langle ab|ab\rangle - \langle ab|ba\rangle, \tag{B.6}$$

where the sum is over all occupied orbitals.

Lets consider the case of removing an electron from an occupied orbital of a neutral system, e.g. from the orbital χ_c, and that all the other orbitals are maintained the same. Thus, the energy of the system with $N-1$ electrons will be given by,

$$E_c(N-1) = \sum_{a\neq c} \langle a|h|a\rangle + \frac{1}{2}\sum_{a\neq c}\sum_{b\neq c} \langle ab|ab\rangle - \langle ab|ba\rangle. \tag{B.7}$$

With this results we can calculate the ionization potential (IP), at HF level, as,

$$\begin{aligned} IP &= E_c(N-1) - E_0(N) \\ &= -\langle c|h|c\rangle - \frac{1}{2}\sum_a \langle ac|ac\rangle - \langle ac|ca\rangle - \frac{1}{2}\sum_b \langle cb|cb\rangle - \langle cb|bc\rangle \\ &= -\langle c|h|c\rangle - \sum_b \langle cb|cb\rangle - \langle cb|bc\rangle = -\epsilon_c. \end{aligned} \tag{B.8}$$

With the same considerations, one can calculate the electron affinity (EA), the amount energy required to add an electron in a neutral system. The result is,

$$EA = E_0(N) - E_r(N+1) = -\epsilon_r, \tag{B.9}$$

where $E_r(N+1)$ represents the energy of the system when added an electron to the unoccupied orbital χ_r, and ϵ_r is the energy of this orbital.

APPENDIX C

Cartesian Coordinates of Atoms in the Clusters B_n $(n = 3 - 13)$

		x	y	z
B_3				
	B1	-0.774095	-0.001756	0.000000
	B2	0.774095	-0.001756	0.000000
	B3	0.000000	1.339019	0.000000
B_3^-				
	B1	-0.771056	0.000000	0.000000
	B2	0.771056	0.000000	0.000000
	B3	0.000000	1.335507	0.000000
B_3^+				
	B1	-0.78177	-0.006192	0.000000
	B2	0.781776	-0.006192	0.000000
	B3	0.000000	1.347891	0.000000
B_4				
	B1	1.219567	-0.049867	0.000000
	B2	-1.169568	-0.050133	0.000000
	B3	0.024895	0.893703	0.000000
	B4	0.025105	-0.993703	0.000000

B_4^-

B1	1.358482	-0.049851	0.000000
B2	-1.308490	-0.050149	0.000000
B3	0.024912	0.774642	0.000000
B4	0.025096	-0.874642	0.000000

B_4^+

B1	0.000000	0.000000	0.000000
B2	1.162344	1.019348	0.000000
B3	1.162344	-1.019348	0.000000
B4	2.324688	0.000000	0.000000

B_5

B1	-4.573899	2.846036	-0.002372
B2	-3.033086	3.203480	-0.000211
B3	-1.472142	2.948356	0.001618
B4	-3.753304	1.516266	-0.002770
B5	-2.201239	1.566331	-0.000945

B_5^-

B1	-4.624404	2.864418	-0.002404
B2	-3.029820	3.114052	-0.000250
B3	-1.422218	2.970351	0.001637
B4	-3.766440	1.539763	-0.002838
B5	-2.190787	1.591884	-0.000825

B_5^+

B1	-4.270204	2.781220	-0.002098
B2	-3.050251	3.738293	0.000437
B3	-1.769096	2.864759	0.001122
B4	-3.746908	1.321680	-0.003022
B5	-2.197211	1.374517	-0.001119

B_6(i)

B1	1.767923	-0.458974	-0.168076
B2	0.240514	1.648573	-0.131750
B3	1.771295	2.144010	-0.162579
B4	0.238017	0.039553	-0.134992
B5	2.716109	0.841322	-0.182371
B6	1.365743	0.841495	0.779769

B_6(ii)

B1	-4.617675	2.880833	-0.003064
B2	-3.065757	3.197189	-0.006509
B3	-1.502594	2.977103	-0.006744
B4	-3.692420	1.284583	0.004121
B5	-2.140506	1.600998	0.001317
B6	-5.255567	1.504715	0.004539

B_6^-(i)

B1	-4.637233	2.856491	-0.002824
B2	-3.066170	3.062604	-0.005636
B3	-1.413767	3.013967	-0.007280
B4	-3.692002	1.419205	0.003581
B5	-2.120940	1.625318	0.001263
B6	-5.344407	1.467837	0.004557

B_6^-(ii)

B1	-4.637233	2.856491	-0.002824
B2	-3.066170	3.062604	-0.005636
B3	-1.413767	3.013967	-0.007280
B4	-3.692002	1.419205	0.003581
B5	-2.120940	1.625318	0.001263
B6	-5.344407	1.467837	0.004557

B_6^+

B1	1.758586	-0.410283	-0.317819
B2	0.230185	1.611462	-0.202767
B3	1.794347	2.124311	-0.214266
B4	0.214804	0.050526	-0.039804
B5	2.733094	0.876165	-0.057396
B6	1.368586	0.803796	0.832054

B_7

B1	0.011186	0.013098	-0.657147
B2	1.668815	0.010789	-0.152696
B3	0.818696	1.310422	0.069308
B4	-0.802278	1.309371	0.062367
B5	-1.650840	0.010048	-0.166807
B6	-0.801824	-1.291526	0.048805
B7	0.819215	-1.291262	0.055581

B_7^-(i)

B1	0.010457	0.011958	-0.452639
B2	1.614159	0.010201	-0.041283
B3	0.811084	1.400299	-0.037283
B4	-0.794283	1.399923	-0.044040
B5	-1.596659	0.009459	-0.054815
B6	-0.793577	-1.380633	-0.058643
B7	0.811788	-1.380266	-0.051885

B_7^-(ii)

B1	0.011229	0.012937	-0.638753
B2	1.707793	0.011365	-0.258149
B3	0.838187	1.247929	0.117199
B4	-0.822612	1.247548	0.110199
B5	-1.688456	0.010579	-0.272460
B6	-0.821985	-1.229904	0.097189
B7	0.838813	-1.229513	0.104186

B_7^+

B1	0.011588	0.013369	-0.721266
B2	1.591941	0.009964	0.003193
B3	0.800037	1.381279	0.007447
B4	-0.783605	1.380911	0.000774
B5	-1.574813	0.009231	-0.010145
B6	-0.782910	-1.362089	-0.013635
B7	0.800730	-1.361723	-0.006957

B_8

B1	0.000216	-0.000053	0.000000
B2	1.790837	-0.000230	0.000001
B3	1.116455	1.399947	0.000001
B4	-0.398251	1.745673	-0.000001
B5	-1.613102	0.777172	0.000000
B6	-1.613244	-0.777080	0.000001
B7	-0.398479	-1.745759	0.000000
B8	1.116279	-1.400230	0.000000

B_8^-

B1	0.000130	-0.000053	0.000000
B2	1.766187	-0.002610	0.000001
B3	1.094917	1.411738	0.000000
B4	-0.392792	1.759181	0.000000
B5	-1.588973	0.788675	0.000000
B6	-1.587978	-0.784859	0.000000
B7	-0.388641	-1.758529	0.000000
B8	1.097860	-1.414104	0.000001

B_8^+

B1	0.000099	-0.000056	0.000000
B2	1.790276	-0.002948	0.000001
B3	1.107500	1.433577	0.000000
B4	-0.397137	1.784331	0.000000
B5	-1.609608	0.802032	0.000000
B6	-1.608715	-0.797752	0.000000
B7	-0.392333	-1.783776	0.000000
B8	1.110628	-1.435968	0.000001

B_9

B1	1.758925	-0.006585	-0.011055
B2	1.096470	1.368471	-0.018387
B3	-0.391442	1.708061	-0.017047
B4	-1.585024	0.757346	-0.008323
B5	-1.584373	-0.769247	0.000955
B6	-0.391418	-1.720401	0.004883
B7	1.096663	-1.381562	-0.000655
B8	0.000082	-0.006999	-0.869754
B9	0.001197	-0.003175	0.843664

B_9^-

B1	0.000000	0.000000	0.000000
B2	1.974961	-0.000120	0.000000
B3	1.397626	1.397642	0.000000
B4	-0.000121	1.975014	0.000000
B5	-1.397729	1.397750	0.000000
B6	-1.974961	0.000120	0.000000
B7	-1.397626	-1.397642	0.000000
B8	0.000121	-1.975014	0.000000
B9	1.397729	-1.397750	0.000000

B_9^+

B1	1.711153	0.017080	-0.050012
B2	1.179405	1.500707	-0.104265
B3	-0.388959	1.825657	-0.102707
B4	-1.503348	0.725233	-0.019758
B5	-1.634745	-0.830061	0.080100
B6	-0.436950	-1.884748	0.092402
B7	1.072702	-1.403148	0.056460
B8	0.121712	0.323764	-0.754077
B9	-0.119889	-0.328575	0.726138

B_{10}

B1	-0.176565	0.309350	-0.388888
B2	1.444187	0.303946	-0.023773
B3	0.771862	1.771037	-0.074924
B4	-0.961372	1.588482	0.237131
B5	-1.909534	0.127144	-0.076098
B6	-0.907336	-1.137810	-0.025716
B7	0.669971	-1.071693	-0.118483
B8	-2.582203	1.594261	-0.127180
B9	-1.807774	2.969785	-0.031832
B10	-0.230467	3.035917	-0.124617

B_{10}^{-}

B1	-0.157257	0.277747	-0.204822
B2	1.480572	0.315396	-0.080312
B3	0.791786	1.783252	-0.074568
B4	-0.980551	1.620304	0.053255
B5	-1.929654	0.114830	-0.076476
B6	-0.933988	-1.164875	-0.082216
B7	0.668062	-1.068644	-0.106977
B8	-2.618427	1.582690	-0.070351
B9	-1.805917	2.966730	-0.043463
B10	-0.203858	3.062990	-0.068451

B_{10}^{+}

B1	-0.165067	0.290476	-0.220815
B2	1.483873	0.271838	-0.071579
B3	0.772005	1.771128	-0.074729
B4	-0.972682	1.607449	0.067365
B5	-1.909855	0.126968	-0.076713
B6	-0.896675	-1.187593	-0.073397
B7	0.685348	-1.096825	-0.112990
B8	-2.621813	1.626287	-0.078445
B9	-1.823200	2.994917	-0.036451
B10	-0.241165	3.085775	-0.076629

B_{11}

B1	-4.314343	3.078397	0.042283
B2	-2.768629	3.235141	-0.004782
B3	-1.205481	3.100592	-0.059655
B4	-3.675933	1.366271	-0.034644
B5	-1.987670	1.590064	-0.089530
B6	-5.316172	1.917018	0.039699
B7	-0.331250	1.818394	-0.131985
B8	-2.293129	-0.211539	-0.137269
B9	-3.826917	-0.457770	-0.091141
B10	-0.828128	0.347290	-0.163956
B11	-5.104148	0.387533	-0.018001

B_{11}^{-}

B1	-4.588063	2.846622	0.036919
B2	-3.058621	3.178288	-0.010752
B3	-1.495253	3.241062	-0.065507
B4	-3.720749	1.351631	-0.028889
B5	-1.964630	1.577092	-0.087337
B6	-5.376551	1.527392	0.035028
B7	-0.404447	2.159880	-0.130084
B8	-1.830702	-0.262796	-0.135349
B9	-3.394951	-0.462901	-0.083286
B10	-0.568458	0.598591	-0.160632
B11	-4.830946	0.055897	-0.019070

B_{11}^{+}

B1	-4.608203	2.843901	-0.049275
B2	-3.041527	3.038619	-0.014371
B3	-1.475336	3.237529	0.020659
B4	-3.665275	1.376172	0.159381
B5	-2.025596	1.595429	-0.274471
B6	-5.416829	1.527415	0.061683
B7	-0.365914	2.171184	-0.156730
B8	-1.840278	-0.268536	-0.114585
B9	-3.383399	-0.463825	-0.104127
B10	-0.575691	0.646535	-0.131876
B11	-4.835324	0.106334	-0.045247

B_{12}

B1	-0.047676	-0.136640	0.285850
B2	1.709626	-0.147956	-0.155339
B3	0.762470	1.335743	0.280204
B4	-0.917251	1.300926	0.283819
B5	-1.806126	-0.217853	-0.149880
B6	-0.799285	-1.477689	-0.277759
B7	0.753732	-1.447160	-0.279952
B8	2.297442	1.353281	-0.289380
B9	-2.452468	1.259525	-0.282448
B10	1.494823	2.683168	-0.291886
B11	-0.107696	2.861984	-0.160439
B12	-1.702192	2.619500	-0.286790

B_{12}^{-}

B1	-0.078839	-0.119561	0.276395
B2	1.822320	-0.209844	-0.152078
B3	0.732248	1.351395	0.270960
B4	-0.932586	1.309931	0.190796
B5	-1.789388	-0.207572	-0.152303
B6	-0.786332	-1.466685	-0.256758
B7	0.788810	-1.419328	-0.276314
B8	2.292964	1.309169	-0.285515
B9	-2.496208	1.289908	-0.250231
B10	1.491973	2.666244	-0.270841
B11	-0.107910	2.842784	-0.163174
B12	-1.751653	2.640386	-0.254937

B_{12}^{+}

B1	-0.084868	-0.139677	0.307817
B2	1.755054	-0.172999	-0.211314
B3	0.746115	1.367627	0.302406
B4	-0.924202	1.305755	0.342624
B5	-1.777674	-0.182318	-0.122759
B6	-0.792330	-1.485193	-0.278849
B7	0.757704	-1.429478	-0.284547
B8	2.284934	1.340744	-0.293862
B9	-2.459609	1.253064	-0.327090
B10	1.504418	2.681068	-0.293122
B11	-0.122914	2.819589	-0.133380
B12	-1.701230	2.628644	-0.331926

$B_{13}(i)$

B1	-0.070977	0.060071	-0.106027
B2	1.642714	0.104586	-0.113159
B3	0.624701	1.724877	-0.116636
B4	-0.956861	1.453156	-0.109114
B5	-1.720297	0.137203	-0.100598
B6	-1.170328	-1.370622	-0.095241
B7	0.739141	-1.450091	-0.102616
B8	2.447427	-2.293801	-0.105676
B9	3.222073	-0.958059	-0.113774
B10	2.196099	1.714717	-0.120581
B11	-0.382659	-2.730342	-0.092628
B12	3.243771	0.600412	-0.120123
B13	1.105039	-3.085837	-0.096897

B_{13}(ii)

B1	-0.021155	-0.395748	-0.086616
B2	2.160032	-0.083440	-0.091845
B3	0.794264	1.173661	-0.113431
B4	-0.901752	1.133977	-0.110613
B5	-2.186719	-0.190549	-0.085558
B6	-1.405651	-1.529881	-0.068528
B7	1.439485	-1.453046	-0.072512
B8	2.419752	1.481260	-0.115627
B9	-2.538473	1.358398	-0.109316
B10	1.493396	2.691797	-0.136223
B11	-0.093111	2.786330	-0.138998
B12	-1.676631	2.613676	-0.132465
B13	0.031014	-2.077526	-0.062278

B_{13}(iii)

B1	0.008638	0.025391	0.240509
B2	1.588487	0.042191	0.334870
B3	0.804803	1.620738	0.085255
B4	-0.822078	1.604679	0.085754
B5	-1.571002	0.008210	0.338067
B6	-0.787822	-1.570248	0.082657
B7	0.838773	-1.553317	0.081262
B8	-2.383679	1.386949	-0.193350
B9	2.370297	1.437869	-0.198903
B10	2.399851	-1.335173	-0.201534
B11	-2.354092	-1.386328	-0.196233
B12	-3.118994	-0.007841	-0.252789
B13	3.135709	0.059412	-0.259574

B_{13}^{-}

B1	0.008139	0.025827	-0.244109
B2	1.561473	0.041935	0.222637
B3	0.799828	1.592341	-0.051693
B4	-0.816566	1.574932	-0.049870
B5	-1.544179	0.008732	0.225970
B6	-0.783211	-1.541100	-0.053277
B7	0.833204	-1.523735	-0.054888
B8	-2.437206	1.376093	-0.046176
B9	2.424304	1.428163	-0.051545
B10	2.453880	-1.324831	-0.054316
B11	-2.407691	-1.376860	-0.049236
B12	-3.167683	-0.008512	0.079678
B13	3.184600	0.059548	0.072816

B_{13}^{+}

B1	-0.040725	0.042369	-0.106103
B2	1.666290	0.080420	-0.112473
B3	0.615828	1.749102	-0.115824
B4	-0.943949	1.454777	-0.108918
B5	-1.715307	0.125166	-0.100446
B6	-1.196439	-1.375017	-0.095915
B7	0.772480	-1.458740	-0.102623
B8	2.404986	-2.293308	-0.104935
B9	3.201453	-0.921576	-0.113831
B10	2.202047	1.736096	-0.121738
B11	-0.398200	-2.745875	-0.092840
B12	3.258668	0.622980	-0.120781
B13	1.092710	-3.110122	-0.096641

Bibliography

[1] R. Johnston, *Atomic and Molecular cluster*. New York, 2002. Cited 2 times in pages 18 and 19.

[2] P. Jena and A. W. Castleman Jr, "Clusters: A bridge acroos the disciplines of physics and chemistry," *Proceedings of the National Academy of Sciences*, vol. 103, p. 10560, 2006. Cited in page 18.

[3] F. Liu, S. N. Khanna, and P. Jena, "Magnetism in small vanadium clusters," *Physical Review B*, vol. 43, no. 10, p. 43, 1991. Cited in page 18.

[4] B. V. Reddy, S. N. Khanna, and B. I. Dunlap, "Giant magnetic moments in 4d clusters," *Physical Review Letters*, vol. 70, no. 21, 1993. Cited in page 18.

[5] A. J. Cox, J. G. Louderback, and L. A. Bloomfield, "Experimental observation of magnetism in rhodium clusters," *Physical Review Letters*, vol. 71, no. 6, 1993. Cited in page 18.

[6] K. Rademann, B. Kaiser, U. Even, and F. Hensel, "Size dependence of the gradual transition to metallic properties in isolated mercury clusters," *Physical Review Letters*, vol. 59, p. 2319, 1987. Cited in page 18.

[7] M. A. Duncan, *Advances in metal and semiconductor clusters*. JAI PRESS INC, 1998. Cited 4 times in pages 10, 19, 24, and 25.

[8] C. R. Hsing, P. L. Ríos, R. J. Needs, and C. M. Wei, "Quantum monte carlo studies of 13-atom simple metallic clusters," *Physical Review B*, vol. 88, p. 165412, 2013. Cited in page 19.

[9] A. J. Williamson, R. Q. Hood, and J. C. Grossman, "Linear-scaling quantum monte carlo calculations," *Physical Review Letters*, vol. 87, no. 24, 2001. Cited in page 19.

[10] M. D. Brown, J. R. Trail, P. L. Ríos, and R. J. Needs, "Energies of the first row atoms from quantum monte carlo," *The Journal of Chemical Physics*, vol. 126, no. 224110, 2007. Cited 2 times in pages 20 and 70.

[11] M. A. Morales, J. McMinis, B. K. Clark, J. Kim, and G. E. Scuseria, "Multideterminant wave functions in quantum monte carlo," *Journal of Chemical Theory and Computation*, vol. 8, pp. 2181–2188, 2012. Cited 2 times in pages 20 and 70.

[12] R. N. Grimes, "Boron clusters come of age," *Journal of Chemical Education*, vol. 81, p. 657, 2004. Cited in page 20.

[13] A. Quandt and I. Boustani, "Boron nanotubes," *ChemPhysChem*, vol. 6, p. 2001, 2005. Cited 2 times in pages 20 and 21.

[14] H.-J. Zhai, B. Kiran, J. Li, and L.-S. Wang, "Hydrocarbon analogues of boron clusters-planarity, aromaticity and antiaromaticity," *Nature Publishing Group*, vol. 2, pp. 827–833, 2003. Cited 13 times in pages 11, 20, 21, 23, 97, 98, 99, 100, 101, 102, 105, 106, and 107.

[15] H.-J. Zhai, L.-S. Wang, A. N. Alexandrova, A. I. Boldyrev, and V. G. Zakrzewski, "Photoelectron spectroscopy and ab initio study of B_3^- and B_4^- anions and their neutrals," *The Journal of Physical Chemistry*, vol. 107, pp. 9319–9328, 2003. Cited 13 times in pages 11, 20, 21, 23, 68, 79, 80, 81, 82, 106, 107, 113, and 115.

[16] C. H. Lee, S. Bhandari, B. Tiwari, N. Yapici, D. Zhang, and Y. K. Yap, "Boron nitride nanotubes: Recent advances in their synthesis, functionalization, and applications," *Molecules*, vol. 21, no. 922, 2016. Cited in page 20.

[17] A. J. Mannix, X.-F. Zhou, B. Kiraly, J. D. Wood, D. Alducin, B. D. Myers, X. Liu, B. L. Fisher, U. Santiago, J. R. Guest, M. J. Yacaman, A. Ponce, A. R. Oganov, M. C. Hersam, and N. P. Guisinger, "Synthesis of borophenes: Anisotropic, two-dimensional boron polymorphs," *Science*, vol. 350, p. 1513, 2015. Cited in page 20.

[18] O. Cretu, H. P. Komsa, O. Lehtinen, G. Algara-Siller, U. Kaiser, K. Suenaga, and A. V. Krasheninnikov, "Experimental observation of boron nitride chains," *ACS Nano*, vol. 8, p. 11950, 2014. Cited in page 20.

[19] A. N. Alexandrova, A. I. Boldyrev, H.-J. Zhai, and L.-S. Wang, "All-boron aromatic clusters as potential new inorganic ligands and building blocks in chemistry," *Coordination Chemistry Reviews*, vol. 250, pp. 2811–2866, 2006. Cited 21 times in pages 11, 21, 23, 24, 67, 68, 79, 81, 82, 85, 86, 89, 90, 91, 92, 93, 95, 97, 106, 107, and 113.

[20] L. Hanley, J. L. Whitten, and S. L. Anderson, "Collisio-induced dissociation and ab initio studies of boron cluster ions: Determination of structures and stabilities," *The Journal of Physical Chemistry*, vol. 92, pp. 5803–5812, 1988. Cited 7 times in pages 21, 70, 71, 80, 82, 84, and 85.

[21] L. Hanley and S. L. Anderson, "Oxidation of small boron cluster ions (B_{1-13}^+) by oxygen," *The Journal of Chemical Physics*, vol. 89, p. 2848, 1988. Cited in page 21.

[22] L. Hanley and S. L. Anderson, "Production and collision-induced dissociation of small boron cluster ions," *The Journal of Physical Chemistry*, vol. 91, p. 5161, 1987. Cited in page 21.

[23] I. Boustani, "Systematic lsd investigation on cationic boron clusters: B_n^+(n= 2–14)," *International Journal of Quantum Chemistry*, vol. 52, p. 1081, 1994. Cited in page 21.

[24] I. Boustani, "A comparative study of ab initio scf-ci and dft. example of small boron clusters," *Chemical Physics Letters*, vol. 233, p. 273, 1995. Cited in page 21.

[25] I. Boustani, "Structure and stability of small boron clusters. a density functional theoretical study," *Chemical Physics Letters*, vol. 240, p. 135, 1995. Cited in page 21.

[26] I. Boustani, "Systematic ab initio investigation of bare boron clusters:mdetermination of the geometryand electronic structures of $B_n(n = 2 - 14)$," *Physical Review B*, vol. 55, p. 16426, 1997. Cited in page 21.

[27] H.-J. Zhai, L.-S. Wang, A. N. Alexandrova, and A. I. Boldyrev, "Electronic structure and chemical bonding of B_5^- and B_5 by photoelectron spectroscopy and ab initio calculations," *Journal of Chemical Physics*, vol. 117, no. 17, 2002. Cited 8 times in pages 11, 21, 23, 68, 83, 84, 106, and 107.

[28] A. N. Alexandrova, A. I. Boldyrev, H.-J. Zhai, L.-S. Wang, E. Steiner, and P. W. Fowler, "Structure and bonding in B_6^- and B_6 : Planarity and antiaromaticity," *The Journal of Physical Chemistry A*, vol. 107, p. 1359, 2003. Cited 10 times in pages 11, 21, 23, 68, 85, 86, 87, 88, 106, and 107.

[29] A. N. Alexandrova, A. I. Boldyrev, H.-J. Zhai, and L.-S. Wang, "Electronic structure, isomerism, and chemical bonding in B_7^- and B_7," *The Journal of Physical Chemistry A*, vol. 108, p. 3509, 2004. Cited 8 times in pages 11, 21, 23, 68, 89, 90, 106, and 107.

[30] H.-J. Zhai, A. N. Alexandrova, K. A. Birch, A. I. Boldyrev, and L.-S. Wang, "Hepta- and octacoordinate boron in molecular wheels of eight- and nine-atom boron clusters: Observation and confirmation," *Angewandte Chemie, International Edition*, vol. 42, p. 6004, 2003. Cited 10 times in pages 11, 21, 23, 68, 92, 93, 95, 96, 106, and 107.

[31] D. Y. Zubarev and A. I. Boldyrev, "Comprehensive analysis of chemical bonding in boron clusters," *Journal of Computational Chemistry*, vol. 28, pp. 251–268, 2007. Cited 8 times in pages 21, 23, 67, 68, 83, 85, 89, and 95.

[32] A. P. Sergeeva, I. A. Popov, Z. A. Piazza, W. L. Li, C. Romanescu, L.-S. Wang, and A. I. Boldyrev., "Understanding boron through size-selected clusters: Structure, chemical bonding, and fluxionality.," *Accounts of Chemical Research*, vol. 47, pp. 1349–1358, 2014. Cited 5 times in pages 21, 23, 67, 68, and 103.

[33] M. T. Nguyen, M. H. Matus, V. T. Ngan, D. J. Grant, and D. A. Dixon, "Thermochemistry and electronic structure of small boron and boron oxide clusters and their anions," *Journal of Physical Chemistry A*, vol. 113, p. 4895–4909, 2009. Cited 5 times in pages 21, 70, 71, 114, and 115.

[34] T. B. Tai, D. J. Grant, M. T. Nguyen, and D. A. Dixon, "Thermochemistry and electronic structure of small boron clusters (B_n, $n = 5 - 13$) and their anions.," *The Journal of Physical Chemistry A*, vol. 114, pp. 994–1007, 2010. Cited 28 times in pages 12, 21, 23, 67, 68, 78, 80, 82, 84, 85, 86, 87, 89, 90, 92, 93, 95, 96, 97, 98, 99, 100, 101, 102, 103, 104, 105, and 114.

[35] N. Akman, M. Tas, C. Özdogan, and I. Boustani, "Ionization energies, coulomb explosion, fragmentation, geometric, and electronic structures of multicharged boron clusters $B_n(n = 2 - 13)$," *Physical Review B*, vol. 84, no. 075463, 2011. Cited 23 times in pages 21, 68, 80, 82, 83, 84, 86, 87, 88, 89, 90, 91, 92, 93, 94, 95, 96, 97, 98, 99, 100, 102, and 105.

[36] J.-I. Aihara, H. Kanno, and T. Ishida, "Aromaticity of planar boron clusters confirmed," *Journal of the American Chemical Society*, vol. 127, p. 13324, 2005. Cited in page 21.

[37] J. Czekner, L. F. Cheung, and L.-S. Wang, "Probing the structures of neutral B_{11} and B_{12} using high-resolution photoelectron imaging of B_{11}^- and B_{12}^-," *The Journal of Physical Chemistry C*, vol. 121, p. 10752, 2016. Cited 8 times in pages 11, 21, 99, 100, 101, 102, 106, and 107.

[38] X.-M. Luo, T. Jian, L.-J. Cheng, W.-L. Li, Q. Chen, R. Li, H.-J. Zhai, S.-D. Li, A. I. Boldyrev, J. Li, and L.-S. Wang, "B_{26}^- : The smallest planar boron cluster with a hexagonal vacancy and a complicated potential landscape," *Chemical Physics Letters*, vol. 683, p. 336, 2017. Cited in page 21.

[39] H.-R. Li, T. Jian, W.-L. Li, C.-Q. Miao, Y.-J. Wang, Q. Chen, X.-M. Luo, K. Wang, H.-J. Zhai, S.-D. Li, and L.-S. Wang, "Competition between quasi-planar and cage-like structures in the B_{29}^- cluster: photoelectron spectroscopy and ab initio calculations," *Physical Chemistry Chemical Physics*, vol. 18, p. 29147, 2016. Cited in page 21.

[40] Q. Chen, W.-J. Tian, L.-Y. Feng, H.-G. Lu, Y.-W. Mu, H.-J. Zhai, S.-D. Li, and L.-S. Wang, "Planar B_{38}^- and B_{37}^- clusters with a double-hexagonal vacancy: molecular motifs for borophenes," *Nanoscale*, vol. 9, p. 4550, 2017. Cited in page 21.

[41] L.-S. Wang, "From planar boron clusters to borophenes and borospherenes," *Proceedings of Spie*, vol. 10174, p. 1017402, 2016. Cited in page 21.

[42] B. G. A. Brito, G.-Q. Hai, and L. Cândido, "A quantum monte carlo study of the structural and electronic properties of small cationic and neutral lithium clusters," *The Journal of Chemical Physics*, vol. 146, p. 174306, 2017. Cited in page 22.

[43] N. L. Moreira, B. G. A. Brito, J. N. T. Rabelo, and L. Cândido, "Quantum monte carlo study of the energetics of small hydrogenated and fluoride lithium clusters," *Journal of Computational Chemistry*, vol. 37, p. 1531, 2016. Cited in page 22.

[44] J. H. Damasceno Jr., J. N. T. Rabelo, and L. Cândido, "A quantum monte carlo study on electron correlation effects in small aluminum hydride clusters," *New Journal of Chemistry*, vol. 39, p. 2195, 2015. Cited in page 22.

[45] B. G. A. Brito, L. Cândido, J. N. T. Rabelo, and G.-Q. Hai, "Binding energies of small lithium clusters: A comparison of different theoretical calculations," *Chemical Physics Letters*, vol. 616, p. 212, 2014. Cited in page 22.

[46] I. G. Kaplan and C. C. Díaz, "Comparative study of the electron affinities of beryllium and magnesium dimers and trimers," *International Journal of Quantum Chemistry*, vol. 104, pp. 468–474, 2005. Cited in page 22.

[47] I. G. Kaplan, O. Dolgounitcheva, J. D. Watts, and J. V. Ortiz, "Nondipole bound anions Be_2^- and Be_3^-," *Journal of Chemical Physics*, vol. 117, pp. 3687–3693, no. 8, 2002. Cited 2 times in pages 22 and 74.

[48] C. C. Díaz-Torrejón, F. Espinosa-Magana, and I. G. Kaplan, "Comparative theoretical study of the electron affinities of the alkaline-earth cluster: Be_n, Mg_n and Ca_n $(n = 2, 3)$," *International Journal of Quantum Chemistry*, vol. 111, pp. 103–110, 2011. Cited in page 22.

[49] A. Kekulé, "Sur la constitution des substances aromatiques," *Bulletin Mensuel de la Société Chimique de Paris*, vol. 3, p. 98, 1865. Cited in page 22.

[50] Z. Chen, C. S. Wannere, C. Corminboeuf, R. Puchta, and P. R. Schleyer, "Nucleus-independent chemical shifts (NICS) as an aromaticity criterion," *Chemical Reviews*, vol. 105, p. 3842, 2005. Cited 2 times in pages 22 and 23.

[51] A. I. Boldyrev and L.-S. Wang, "Beyond organic chemistry: aromaticity in atomic clusters," *Physical Chemistry Chemical Physics*, vol. 18, p. 11589, 2016. Cited in page 23.

[52] F. Feixas, E. Matito, J. Poater, and M. Solà, "Quantifying aromaticity with electron delocalisation measures," *Chemical Society Reviews*, vol. 44, p. 6434, 2015. Cited in page 23.

[53] P. Chattaraj, D. Roy, M. Elango, and U. Subramanian, "Stability and reactivity of all-metal aromatic and antiaromatic systems in light of the principles of maximum hardness and minimum polarizability," *The Journal of Physical chemistry A*, vol. 109, p. 9590, 2005. Cited 4 times in pages 23, 109, 110, and 112.

[54] X. Li, A. E. Kuznetsov, H.-F. Zhang, A. I. Boldyrev, and L.-S. Wang, "Observation of all-metal aromatic molecules," *Science*, vol. 291, p. 859, 2001. Cited in page 23.

[55] A. E. Kuznetsov and A. I. Boldyrev, "Theoretical evidence of aromaticity in X_3^-(X=B,Al,Ga) species," *Structural Chemistry*, vol. 13, pp. 141–148, 2002. Cited in page 23.

[56] C. Romanescu, T. R. Galeev, A. I. B. W-L Li, and L.-S. Wang, "Transition-metal-centered monocyclic boron wheel clusters: A new class of aromatic borometallic compounds," *Accounts of Chemical Research*, vol. 46, pp. 350–359, 2012. Cited in page 23.

[57] L. S. Wang, H. S. Cheng, and J. Fan, "Photoelectron spectroscopy of size-selected transition metal clusters: Fe_n^-, $n = 3 - 24$," *The Journal of Chemical Physics*, vol. 102, no. 24, p. 9480, 1995. Cited 4 times in pages 10, 24, 25, and 26.

[58] J. D. M. Vianna, A. Fazzio, and S. Canuto, *Teoria Quântica de Moléculas e Sólidos*. Livraria da Física, 2004. Cited 8 times in pages 10, 28, 29, 30, 31, 32, 36, and 42.

[59] F. Jensen, *Introduction to computational chemistry*. John Wiley and Sons, 2007. Cited in page 31.

[60] A. Szabo and N. S. Ostlund, *Modern Quantum Chemistry, Introduction to advanced Electronic Structure Theory*. Dover Publications, 1989. Cited 9 times in pages 28, 29, 31, 32, 33, 34, 35, 36, and 122.

[61] J. Sakurai, *Modern Quantum Mechanics*. Addison-Wesley, 1994. Cited 3 times in pages 28, 32, and 120.

[62] M. Born and R. Oppenheimer, "Zur quantentheorie de molekeln," *Annalen der Physik*, vol. 84, p. 457, 1927. Cited 2 times in pages 29 and 31.

[63] J. C. Slater, "The theory of complex spectra," *The Physical Review*, vol. 34, p. 1293, 1929. Cited in page 33.

[64] N. H. Morgon and K. Coutinho, *Métodos de Química Teórica e Modelagem Molecular*. Editora Livraria da Física, 2007. Cited 6 times in pages 33, 41, 42, 43, 50, and 64.

[65] C. C. J. Roothaan, "New development in molecular orbital theory," *Reviews of Modern Physics*, vol. 23, 1951. Cited 2 times in pages 34 and 35.

[66] T. Koopmans, "Über die zuordnung von wellenfunktionen und eigenwerten zu den einzelnen elektronen eines atoms," *Physica*, vol. 1, pp. 104–113, 1993. Cited 2 times in pages 36 and 75.

[67] R. G. Parr and W. Yang, *Density Functional Theory of Atoms and Molecules*. Oxford University Press, 1989. Cited 2 times in pages 36 and 110.

[68] W. Koch and M. C. Holthausen, *A Chemist's Guide to Density Functional Theory*. WILEY-VCH, 2001. Cited 3 times in pages 36, 41, and 43.

[69] P. Hohenberm and W. Kohn, "Inhomogeneous electron gas," *Physical Review*, vol. 136, no. B864, 1964. Cited in page 37.

[70] W. Kohn and L. J. Sham, "Self-consistent equations including exchange and correlation effects," *Physical Review*, vol. 140, no. 4A, 1965. Cited 2 times in pages 40 and 41.

[71] K. Capelle, "A bird's-eye view of density-functional theory," *Brazilian Journal of Physics*, vol. 36, p. 1318, 2006. Cited 3 times in pages 41, 42, and 43.

[72] D. M. Ceperley and B. J. Alder, "Ground state of the electron gas by a stochastic method," *Physical Review Letters*, vol. 45, p. 566, 1980. Cited 2 times in pages 42 and 62.

[73] S. H. Vosko, L. Wilk, and M. Nusair, "Accurate spin-dependent electron liquid correlation energies for local spin density calculations: a critical analysis," *Canadian Journal of Physics*, vol. 58, p. 1200, 1980. Cited in page 42.

[74] J. P. Perdew and Y. Wang, "Accurate and simple analytic representation of the electron-gas correlation energy," *Physical Review B*, vol. 45, p. 13244, 1992. Cited in page 42.

[75] A. D. Becke, "Density-functional exchange-energy approximation with correct asymptotic behavior," *Physical Review A*, vol. 38, p. 3098, 1988. Cited in page 43.

[76] C. Lee, W. Yang, and R. G. Parr, "Development of the colle-salvetti correlation-energy formula into of the electron density," *Physical Review B*, vol. 37, p. 785, 1988. Cited in page 43.

[77] J. P. Perdew, K. Burke, and M. Ernzerhof, "Generalized gradient approximation made simple," *Physical Review Letters*, vol. 77, p. 3865, 1996. Cited in page 43.

[78] A. D. Becke, "Density-functional thermochemistry. iii. the role of exact exchange," *The Journal of Chemical Physics*, vol. 98, p. 5648, 1993. Cited in page 43.

[79] B. Hammond, W. Lester, and P. J. Reynolds, *Monte Carlo Methods in Ab Initio Quantum Chemistry*. World Scientific, 1994. Cited 16 times in pages 10, 43, 44, 45, 46, 47, 48, 49, 53, 56, 57, 59, 60, 61, 62, and 63.

[80] M. P. Allen and D. J. Tildesley, *Computer Simulation of Liquids*. Oxford University Press, New York, 1987. Cited in page 45.

[81] N. Metropolis, A. W. Rosenbluth, M. N. Rosenbluth, A. H. Teller, and E. Teller, "Equation of state calculations by fast computing machines," *The Journal of Chemical Physics*, vol. 21, pp. 1087–1092, 1953. Cited 2 times in pages 47 and 50.

[82] W. M. C. Foulkes, L. Mitas, R. J. Needs, and G. Rajagopal, "Quantum monte carlo simulation of solids," *Reviews of Modern Physics*, vol. 73, p. 33, 2001. Cited 10 times in pages 10, 49, 51, 53, 55, 56, 59, 61, 62, and 69.

[83] C. Umrigar, K. Wilson, and J. Wilkins, "Optimized trial wave functions for quantum monte carlo calculations," *Physical Review Letters*, vol. 60, p. 1719, 1988. Cited 2 times in pages 50 and 68.

[84] P. R. C. Kent, *Techniques and Applications of Quantum Monte Carlo*. PhD thesis, Robinson College Cambridge, 1999. Cited in page 50.

[85] N. D. Drummond, M. D. Towler, and R. J. Needs., "Jastrow correlation factor for atoms, molecules, and solids," *Physical Review B*, vol. 70, p. 235119, 2004. Cited 3 times in pages 51, 52, and 68.

[86] R. Needs, M. Towler, N. Drummond, and P. L. Ríos, *CASINO User's Guide Version 2.13 (2014)*. 2014. Cited 3 times in pages 51, 52, and 68.

[87] T. Kato, "On the eigenfunctions of manyparticle systems in quantum mechanics," *Communications on Pure and Applied Mathematics*, vol. 10, p. 151, 1957. Cited in page 52.

[88] B. M. Austin, D. Y. Zubarev, and W. A. Lester Jr., "Quantum monte carlo and related approaches," *Chemical Reviews*, vol. 112, p. 263, 2012. Cited 4 times in pages 49, 53, 61, and 62.

[89] H. F. Trotter, "On the product of semi-groups of operators," *Proceedings of the American Mathematical Society*, vol. 10, no. 4, 1959. Cited in page 59.

[90] M. Suzuki, "On the convergence of exponential operators- the zassenhaus formula, bch formula and systematic approximations," *Communication in Mathematical Physics*, vol. 57, p. 193, 1977. Cited in page 59.

[91] J. B. Anderson, "Quantum chemistry by random walk," *The Journal of Chemical Physics*, vol. 65, no. 10, 1976. Cited in page 62.

[92] P. J. Reynolds, D. M. Ceperley, B. J. Alder, and J. W. A. Lester, "Fixed-node quantum monte carlo for molecules," *The Journal of Chemical Physics*, vol. 77, p. 5593, 1982. Cited 2 times in pages 64 and 68.

[93] R. Ditchfield, W. J. Hehre, and J. A. Pople, "Self-consistent molecular-orbital methods. ix. an extended gaussian-type basis for molecularorbital studies of organic molecules," *The Journal of Chemical Physics*, vol. 54, p. 724, 1971. Cited in page 67.

[94] M. Frish, *Gaussian09*. Gaussian. Inc, 2004. Cited in page 67.

[95] T. B. Tai, N. M. Tam, and M. T. Nguyen, "The boron conundrum: the case of cationic clusters B_n^+ with $n = 2 - 20$," *Theoretical Chemistry Accounts*, vol. 131, p. 1241, 2012. Cited 35 times in pages 11, 12, 68, 70, 78, 79, 80, 81, 82, 83, 84, 86, 87, 88, 89, 90, 91, 92, 93, 94, 95, 96, 97, 98, 99, 100, 101, 102, 103, 104, 105, 106, 108, 114, and 115.

[96] R. Needs, M. Towler, N. Drummond, and P. Rios, "Continuum variational and diffusion quantum monte carlo calculations," *Journal of Physics: Condensed Matter*, vol. 22, p. 023201, 2010. Cited in page 68.

[97] N. D. Drummond and R. J. Needs, "Variance-minimization scheme for optimizing jastrow factors," *Physical Review B*, vol. 72, p. 085124, 2005. Cited in page 68.

[98] T. H. Dunning Jr., "Gaussian basis sets for use in correlated molecular calculations. i. the atoms boron through neon and hydrogen," *The Journal of Chemical Physics*, vol. 90, p. 1007, 1989. Cited in page 69.

[99] C. Filippi and C. J. Umrigar, "Multiconfiguration wave functions for quantum monte carlo calculations of first-row diatomic molecules," *The Journal of Chemical Physics*, vol. 105, pp. 213–226, 1996. Cited in page 70.

[100] S. J. Chakravorty, S. R. Gwaltney, and E. R. Davidson, "Ground-state correlation energies for atomic ions with 3 to 18 electrons," *Physical Review A.*, vol. 47, no. 5, 1993. Cited in page 70.

[101] M. W. Chase Jr., C. A. Davies, J. R. Dowuey Jr., D. J. Frmip, R. A. McDonald, and A. N. Syverud, "Janaf thermochemical tables," *Journal of Physical and Chemical Reference Data*, vol. 14, 1985. Cited 2 times in pages 70 and 114.

[102] J. C. Rienstra-Kiracofe, G. S. Tschumper, H. F. S. III, S. Nandi, and B. Ellison, "Atomic and molecular electron affinities: Photoelectron experiments and theoretical computations," *Chemical Reviews*, vol. 102, p. 231, 2002. Cited in page 71.

[103] P. O. Löwdin, "Correlation problem in manyelectron quantum mechanics i. review of different approaches and discussion of some current ideas," *Advances in Chemical Physics*, vol. 2, no. 207, 1959. Cited in page 75.

[104] A. Overhauser, *Anomalous Effects in Simple Metals*. John Wiley & Sons, 2011. Cited in page 76.

[105] J. Kruszewski and T. M. Krygowski, "Definition of aromaticity basing on the harmonic oscillator model," *Tetrahedron Letters*, no. 36, p. 3839, 1972. Cited in page 109.

[106] T. M. Krygowski, "Crystallographic studies of inter- and intramolecular interactions reflected in aromatic character of π-electron systems," *Journal of Chemical Information and Computer Sciences*, vol. 33, p. 70, 1993. Cited in page 109.

[107] E. Matito, M. Duran, and M. Solà, "The aromatic fluctuation index (FLU): A new aromaticity index based on electron delocalization," *The Journal of Chemical Physics*, vol. 122, p. 014109, 2005. Cited in page 109.

[108] P. Bultinck, R. Ponec, and S. V. Damme, "Multicenter bond indices as a new measure ofaromaticity in polycyclic aromatic hydrocarbons," *Journal of Physical Organic Chemistry*, vol. 18, p. 706, 2005. Cited in page 109.

[109] C. F. Matta and J. Hernández-Trujillo, "Bonding in polycyclic aromatic hydrocarbons in terms of the electron density and of electron delocalization," *The Journal of Physical Chemistry A*, vol. 107, p. 7496, 2003. Cited in page 109.

[110] M. K. Cyrański, "Energetic aspects of cyclic π-electron delocalization: Evaluation of the methods of estimating aromatic stabilization energies," *Chemical Reviews*, vol. 105, p. 3773, 2005. Cited in page 109.

[111] C.-G. Zhan, F. Zheng, and D. A. Dixon, "Electron affinities of Al_n clusters and multiple-fold aromaticity of the square Al_4^{2-} structure," *Journal of the American Chemical Society*, vol. 124, p. 14795, 2002. Cited in page 109.

[112] A. I. Boldyrev and A. E. Kuznetsov, "On the resonance energy in new all-metal aromatic molecules," *Inorganic Chemistry*, vol. 41, p. 532, 2002. Cited in page 109.

[113] E. Hückel, "Quantentheoretische beitrgge zum benzolproblem," *Zeitschrift für Physik*, vol. 70, p. 204, 1931. Cited in page 109.

[114] P. R. Schleyer, C. Maerker, A. Dransfeld, H. Jiao, and N. J. R. E. Hommes, "Nucleus-independent chemical shifts: A simple and efficient aromaticity probe," *Journal of the American Chemical Society*, vol. 118, p. 6317, 1996. Cited in page 109.

[115] M. Giambiagi, M. S. de Giambiagi, C. D. dos Santos Silva, and A. P. de Figueiredo, "Multicenter bond indices as a measure of aromaticity," *Physical Chemistry Chemical Physics*, vol. 2, p. 3381, 2000. Cited in page 109.

[116] P. Bultinck, M. Rafat, R. Ponec, B. Gheluwe, R. Carbó-Dorca, and P. Popelier, "Electron delocalization and aromaticity in linear polyacenes: Atoms in molecules multicenter delocalization index," *The Journal of Physical Chemistry*, vol. 110, p. 7642, 2006. Cited in page 109.

[117] J. Cioslowski, E. Matito, and M. Solà, "Properties of aromaticity indices based on the one-electron density matrix," *The Journal of Physical Chemistry A*, vol. 111, p. 6521, 2007. Cited in page 109.

[118] B. G. A. Brito, G.-Q. Hai, and L. Cândido, "Correlation effects on aromaticity of Be_3^{2-} cluster: A quantum monte carlo study," *Chemical Physics Letters*, vol. 586, p. 108, 2013. Cited 2 times in pages 109 and 112.

[119] B. G. A. Brito, G.-Q. Hai, J. N. T. Rabelo, and L. Cândido, "A quantum monte carlo study on electron correlation in all-metal aromatic clusters mAl_4 (m = Li, Na, K, Rb, Cu, Ag and Au)," *Physical Chemistry Chemical Physics*, vol. 16, p. 8639, 2014. Cited 2 times in pages 109 and 112.

[120] M. J. S. Dewar and C. de Llano, "Physical and inorganic chemistry," *Journal of the American Chemical Society*, vol. 91, no. 4, 1969. Cited 2 times in pages 109 and 113.

[121] R. G. Parr, R. A. Donnelly, M. Levy, and W. E. Palke, "Electronegativity: The density functional viewpoint," *The Journal of Chemical Physics*, vol. 68, p. 3801, 1978. Cited in page 111.

[122] R. G. Parr and R. G. Pearson, "Absolute hardness: Companion parameter to absolute electronegativity," *Journal of the American Chemical Society*, vol. 105, p. 7512, 1983. Cited in page 111.

[123] R. G. Parr, L. v. Szentpaly, and S. Liu, "Electrophilicity index," *Journal of the American Chemical Society*, vol. 121, pp. 1922–1924, 1999. Cited in page 111.

[124] L. Hanley, J. L. Witthen, and S. L. Anderson *The Journal of Physical Chemistry*, vol. 94, no. 2218, 1990. Cited in page 114.

[125] H. W. Jin and Q. S. Li, "Structure and stability of B_4, B_4^+ and B_4^- clusters," *Physical Chemistry Chemical Physics*, vol. 5, p. 1110, 2003. Cited in page 116.

[126] E. M. I. Moreira, B. G. A. Brito, J. H. Damasceno Jr., J. N. T. Rabelo, G.-Q. Hai, and L. Cândido, "Quantum monte carlo study of the electron binding energies and aromaticity of small neutral and charged boron clusters," *The Journal of Chemical Physics*, vol. 149, p. 214303, 2018. Cited in page 116.